Thesis for the Master's Degree in Chemistry

Hang T. T. Phan

Characterization of a Novel Thermoresponsive Polysaccharide Grafted with PNIPAAM.

60 study points

DEPARTMENT OF CHEMISTRY

Faculty of Mathematics
and Natural Sciences

UNIVERSITY OF OSLO

September / 2010

List of contents

☻ Acknowledgement ☻

This study was carried out at the Department of Chemistry, University of Oslo, in the period from January 2009 to August 2010. This project has been one of the most challenging for me since I started at the University. A lot of work has been done and many failures have taught me to be a better researcher. During my master time at the University of Oslo, it has been an honor for me to attending in two conferences; one in Spain 2009 and the last one in Vårmøte 2010 in Hønefoss. I could like to thank to the Chemistry department for giving me this opportunity. These conferences were a useful and informative experience for a master student.

First of all, I could like to thank to my principle supervisor Professor Dr. Bo Nyström who has been so kind to take me into his group and let me use many wonderful instruments in the group, and for writing publications about my results. Additionally, I want to express my deeply thanks to my second supervisor Dr. Anna-Lena Kjøniksen who has given me the inspiration, motivation and good advices. Even if she has 1000 things to do during a day, she was always taking her time to guide me throughout this study. It makes her becomes the most important person for me and she is the person who always gives me a hand every time I felt down.

Furthermore, I would like to thank The Polymer Research Group at the University in Oslo for being there and support me in several ways. It was many funny stories and good laughs we shared together during my grade. With you in our group, it keeps up my spirit to come to the University every day.

A special thank goes to Kaizheng who was making my interesting polymers and for helping me with my thesis. Special thanks also go to Loan T. T. Trinh who always give me many good advices and helped me when I'm stuck, and to Nodar, Atoosa and Ramón who has been there for me and supported me throughout my work.

Furthermore, I would like to say thanks to Trung Trinh and Le for their help with a fantastic Vietnamese abstract.

My gratitude to all faithful friends I have at the university and friends who are not belongs to the University to have been encouraged me to fulfill my grade. A special thank to my dear parents, sister and brother. They have shown me the values of education and thank you for your support and have faith in me. Without you I would not reach my goal.

Last but not least, a big thanks to my love for sympathetically listening to my problems during my grade and for being a strong support to me. I am so truly grateful that you are always beside me and take care of me. Thanks!

Oslo, August 2010

Hang Thuy Thi Phan

List of symbols and abbreviations

A_f	Amplitude of the fast mode
A_s	Amplitude of the slow mode
A_2	Second virial coefficient
B	Empirical factor
CP	Cloud point
d_f	Fractal dimension
D	Diffusive coefficient
D_m	Mutual diffusive coefficient
DLS	Dynamic light scattering
$g^1(q,t)$	First order electric field correlation function
$g^2(q,t)$	Measured homodyne intensity autocorrelation function
HEC	Hydroxyethylcellulose
Int1	Intensity along the shear axis
Int2	Intensity perpendicular to the shear axis
I_t	Transmitted light intensity
I_0	Incident light intensity
K	Kelvin
k	Boltzmann's constant
L	Light path length of the cuvette
LCST	Lower critical solution temperature
LS	Light scattering
MHEC	Modified hydroxyethylcellulose
M_n	Number average molecular weight
M_w	Weight average molecular weight
MS	Molar substitution degree
n	Refractive index
n_p	Refractive index of the particle
n_s	Refractive index of the solvent
n_{coup}	Coupling parameter
PNIPAAM	Poly(*N*-isopropylacrylamide)
PVCL	Poly(*N*-vinylcaprolactam)
q	Wave vektor

R_h	Hydrodynamic radius
$R_{h,f}$	Hydrodynamic radius for fast relaxation mode
$R_{h,s}$	Hydrodynamic radius for slow relaxation mode
R_g	Radius of gyration
S	Intensity signal from turbidity
SANS	Small angle neutron scattering
SDS	Sodium dodecyl sulphate
SLS	Static light scattering
T	Absolute temperature
t	Time
UCST	Upper critical solution temperature
wt %	Weight percent
α	Power law index ($\eta \propto \dot{\gamma}^{(\alpha-1)}$)
α_s	Power law exponent ($\tau_s^{-1} \propto q^{\alpha_s}$)
β	Stretch exponent
Γ	Gamma function
γ	Strain
$\dot{\gamma}$	Shear rate
η	Viscosity
η_s	Viscosity of solvent
η_0	Zero-shear viscosity
θ	Scattering angle
λ	Wavelength
ξ	Screening length
τ	Turbidity
τ_f	Fast relaxation time
τ_s	Slow relaxation time
τ_{se}	Effective slow relaxation time

Abstract

The uncharged temperature responsive polymer MHEC-*g*-PNIPAAM (modified hydroxyethylcellulose graft poly(*N*-isopropylacrylamide)), and its anionic analogue were characterized by the aid of dynamic light scattering (DLS), rheology, turbidity and rheo-small angle light scattering (rheo-SALS). The temperature sensitive PNIPAAM groups cause intramolecular associations in the system at elevated temperatures. At low concentrations (0.02 wt% - 0.5 wt%), DLS and turbidity was used to measure the complex interactions as the temperature was increased. The DLS data show that at low temperatures, the relaxation process is bimodal for all concentrations of the charged polymer, while above the lower critical solution temperature (LCST) only one mode has been observed. For the neutral polymer, a bimodal relaxation process has been detected up to 0.3 wt % below LCST. At higher polymer concentrations and above LCST only one mode is evident. The general feature for all polymer concentrations is the marked contraction of the polymer clusters at moderate temperatures, most visible at the LCST. After the LCST, the cluster sizes gradually increase for charged polymer while the neutral polymer gradually reduces the cluster sizes. The turbidity increases as the radius of the aggregates decrease.

Viscosity enhancements were observed for semidilute samples (0.5 wt%-5 wt%) around LCST. The light scattering pattern from rheo-SALS reveals that the system reorganize at elevated temperatures both in the presence and absence of shear forces. It is also shown that when a shear force is applied to the system, the neutral polymer has a random organization throughout the whole considered temperature region, while the charged polymer is anisotropic around LCST in the presence of shear forces.

Abstract in Vietnamese

Tóm Tắt

Polymer chịu nhiệt cách điện NHEC-g-PNIPAAM được tổng hợp từ hydroxyethylcellulose graft poly(N-isopropylacrylamide) và dẫn xuất anion NHEC-g-PNIPAAM được khảo sát bằng phương pháp động học tán sắc (DLS), lưu biến, độ đục và góc tán sắc nhỏ rheo (rheo-SALS). Nhóm cảm ứng nhiệt PNIPAAM được xem như là nguyên nhân dẫn đến sự tương tác nội phân tử khi tăng nhiệt độ. Ở khỏang nồng độ thấp của polymer từ 0.02 wt% - 0.5 %kl, DLS và độ đục được xử dụng để khảo sát mối tương tác phức tạp này khi có sự gia tăng nhiệt độ. Từ dữ liệu DLS cho thấy rằng quá trình duỗi mạch ở nhiệt độ thấp diễn ra theo đa cấu tử phức nhưng khi nhiệt độ vượt quá nhiệt độ tới hạn (LCST) thì cơ chế này xảy ra theo đơn cấu tử phức tại mọi nồng độ. Đối với polymer trung tính, đa cấu tử phức được được quan sát được ở nồng độ dưới 0.3 %kl và nhiệt độ dưới LCST, khi gia tăng nồng độ polymer và nhiệt độ trên LCST đơn cấu tử phức được tìm thấy. Một điều dễ dàng nhận thấy rằng quá trình co lại của phức polymer tại điểm LCST được tìm thấy ở mọi nồng độ tại khoàng nhiệt độ trung bình. Kích thước của phức tăng dần đối với polymer tích điện trong khi điều này ngược lại với polymer trung tính. Độ đục tăng khi bán kính của hạt kết tụ giàm dần.

Sự gia tăng độ nhớt được quan sát đối với những mẫu pha lõang môt phần với nồng độ trong khoảng 0.5 -5 %kl tại LCST. Phổ tán xạ ánh sáng từ rheo-SALS thể hiện rằng hệ thống tái cấu trúc khi nhiệt độ gia tăng trong cà hai trường hợp có sự hiện diện hay không có của lực ép. Điều này cũng được nhận thấy rằng khi lực ép được áp dụng trong hệ thống, polymer trung tính có sự sắp xếp ngẫu nhiên trong tòan bộ khoảng nhiệt độ khảo sát trong khi đó sự sắp xếp đẳng hướng dưới sự hiện diện của lực ép gần LCST được quan sát thấy ở polymer tích điện

1. Introduction

In recent years, many research groups have showed interest in thermoresponsive polymers copolymerized with hydrophibic/amphiphilic polymers. The basic challenge is to design model block and graft copolymer systems that will allow us to measure, compare and control the behaviour of various physical phenomena.[1] It has been shown that in aqueous solution, these copolymers which contain hydrophobic and hydrophilic parts, frequently build up core-shell like nanoparticles at elevated temperatures. The association in the core is due to hydrophobic interactions and the core is surrounded by a hydrophilic corona. If the thermosensitive block becomes more hydrophobic when heated, aqueous solutions of this type of copolymer is characterized by a microscopic phase separation upon heating, and the system exhibits a lower critical solution temperature (LCST).[2-4] This important physical phenomenon exhibited by aqueous solutions of thermosensitive polymers, has lead to different biomaterial utilizations, such as controlled drug delivery, tissue engineering, and other biomedical devices as well as improving new technologies .[5-10]

Earlier in this research group, Atoosa Maleki [11], Zheugjun Liu[12] and Noda Al-Manasir[13] have been working with dilute solutions of the hydrophilic polymer hydroxyethyl cellulose (HEC). They observed that HEC gave no intrachain contraction at quiescent conditions, but only multichain aggregation. When applying the cross-link agent, divinysulfone (DVS) or adding the surfactant sodium dodecyl sulphate (SDS), the growth of the aggregates start at earlier times and the viscosity increase. In this thesis, we are going to use the same HEC without using DVS or SDS as aggregation agent, instead a thermoresponsive side chain has been grafted to the polymer backbone.

Because of its interesting thermoresponsive behaviour, poly(*N*-isopropylacrylamide) (PNIPAAM)[8] has been grafted onto HEC. The primary aim of this work is to determine the physical behaviour of a neutral and a negative charged MHEC-*g*-PNIPAAM in aqueous solution. Furthermore, this polymer could be interesting for use in drug delivery systems, because it is thought to be harmless for use in the human body[1], other possible applications include enhanced oil recovery, viscosity enhancement etc.

1.1 Background

High molecular weight hydrophilic HEC grafted with PNIPAAM groups has not been studied previously. These is however a few publications regarding PNIPAAM groups grafted to carboxyethyl cellulose[14] , chitosan[15] or in block copolymer with poly(ethylene glycol) (PEG).[16-20] The research in the field of thermosensitive polymers has been mostly focused on PNIPAAM, but there are other *N*-substituted poly(acrylamides) which exhibit similar behaviour in aqueous solution too. Homopolymers of *N, N'*-diethylacrylamide, *N*-cyclopropylamcrylamide, and *N*-ethylacrylamide have been reported to display LCSTs in the 30-80 ^{o}C range.[3] Other temperature-responsive polymers[1] that also exbitit LCST behaviour are poly(*N*-vinylcaprolactam)(PVCL), elastin-like polypeptides (ELPs) and poly(2-isopropyl-2-oxazoline) (PIPOZ). All these temperature-responsive polymers have amide groups in common, see *Fig. 1* below, but the LCST differ with the amount of the molar mass and concentrations.[3,4,21-23] These amide groups are the main cause of the thermosensitivity of the polymers.[1]

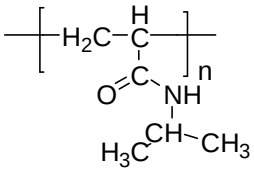

Poly(*N*-isopropylacrylamide)

PNIPAAM

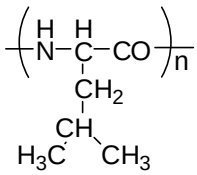

Elastin-like polypeptides

ELPs

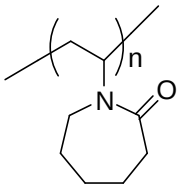

Poly(*N*-vinylcaprolactam)

PVCL

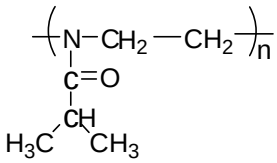

Poly(2-isopropyl-2-oxazoline)

PIPOZ

Figure 1. *Structures of some thermo-sensitive polymers.*

In order to understand the behaviour of HEC-*g*-PNIPAAM, we have used different experimental techniques such as light scattering, rheology and turbidimetry to gain

information about the thermoresponsive properties. The reason we use PNIPAAM in this investigation is because it is one of the most known and most stabile thermosensitive polymers and it is harmless too. In this research group, we have previously also worked with PVCL[24]. But in this work, NIPAAM is the first priority.

1.1.1 Cellulose

Figure 2. *A cotton tree which produce at least 90% cellulose*

Cellulose is a component of at least a third of advanced plants: 40-60% (in weight) of dry wood, and more than 90% of cotton (99.9% of purified cotton) and flax. Therefore, cellulose is unquestionably the most abundant naturally occurring renewable organic compound.[25]

Cellulose, also known as glycans, consist of D-glucose units linked by β-(1→ 4) glycosidic bonds, analogous of peptide bond in proteins. Glucose is known as monosaccharide or simple sugar, it has two stereoisomers. Only D-glucose is biologically active, and the mirror-image of this molecule is L-glucose, which cannot be metabolized by cells in the biochemical process known as glycolysis.

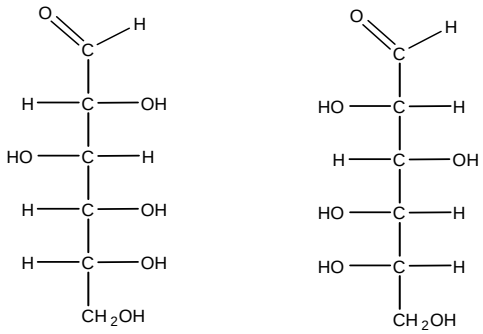

Figure 3. *Schematic presentation of D and L-glucose by Fischer projection*

When D-glucose is drawn as a Haworth projection or in the chair conformation, we can see that monosaccharides have two anomeric forms, α-glucose (true cellulose) and β-glucose, see *Fig. 4*. These two types are insoluble in water but dissolves in sodium hydroxide and they can be reacted in different ways with various chemicals to produce cellulose substances.[3]

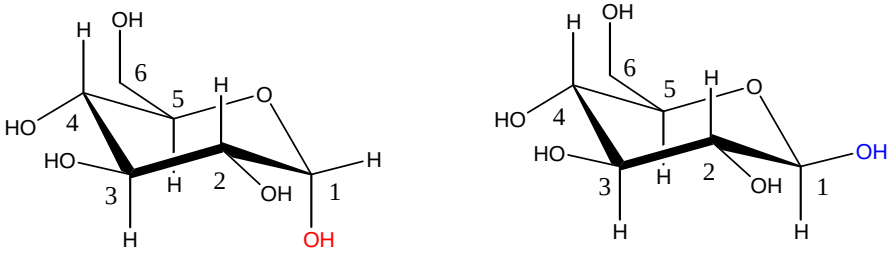

Figure 4. *Structure of α and β-glucose by chair conformation.*

By extension of α and β-glucose, we will get the polymers amylase and cellulose, respectively.

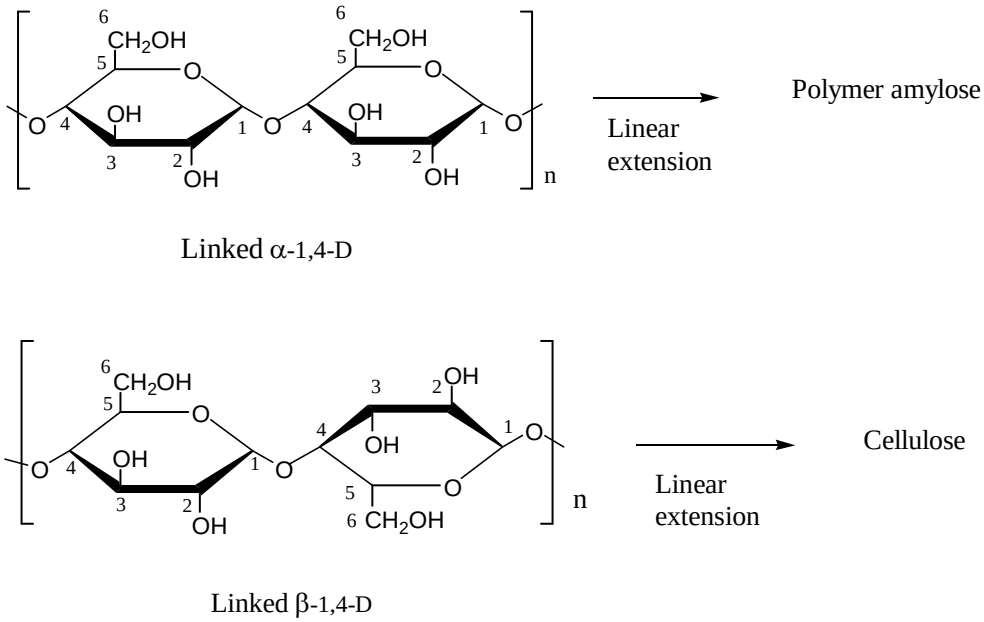

Figure 5. *Schematic representation of extended α and β-glucose by Haworth projection.*

When the cellulose molecule is extended, the highly cohesive, hydrogen bonded structure gives cellulose an exceptional strength by holding the chains firmly together side-by-side and forming fibers. Because of the high degree of organization and hydrogen bonding in the

crystalline regions, water cannot penetrate or disrupt these areas, and only strong alkali or certain organic solvents can dissolve this crystalline region.[26]

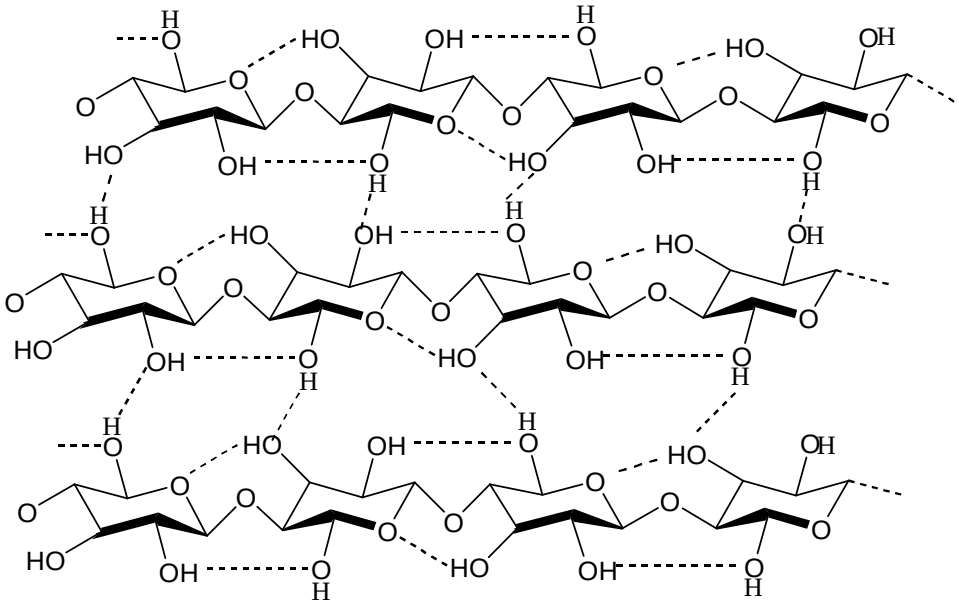

Figure 6. *Schematic sketch showing hydrogen bonds of cellulose strands*.

1.1.2 Cellulose Derivatives

Cellulose is as a non-ionic naturally occurring polymer material and it is favorable from the viewpoint of the environment, as it can be safely returned to the natural carbon cycle by simple decomposition. In addition cellulose is not toxic to living organisms, including humans.[27] Each of the cellulose units possesses hydroxyl groups at C-2, C-3 and C-6 positions rendering them capable of undergoing reactions with new functionalized side chains leading to derivatives with useful properties. The three hydroxyl groups can react to form cellulose ester or cellulose ether (-OR) bonds. See *Fig. 7 and 8* for some examples of commercial cellulose esters and ethers.[28]

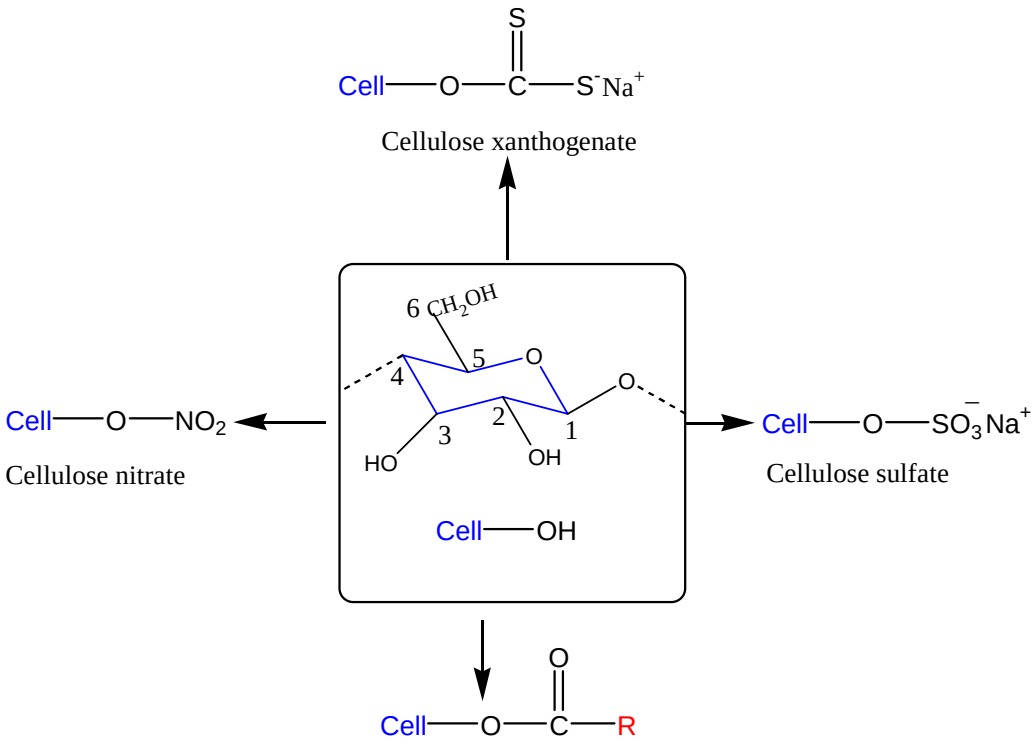

R= CH_3: Cellulose acetate (CA)

R= CH_3 or CH_2CH_3: Cellulose acetate pionate (CAP)

R= CH_3 or $CH_2CH_2CH_3$: Cellulose acetate butyrate (CAB)

Figure 7. *Examples of commercial cellulose esters*.[28]

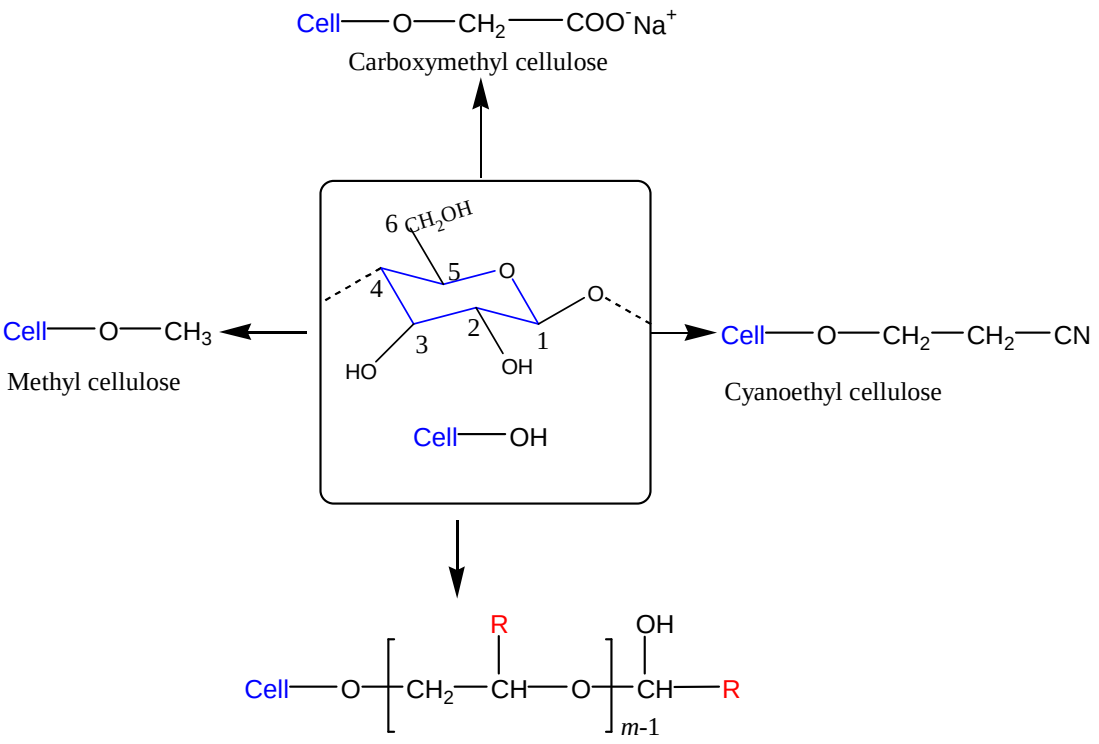

R= H: hydroxyethyl cellulose (HEC)

R= CH_3: Hydropropyl cellulose (HPC)

m = 1,2,3..

Figure 8. *Examples of commercial of cellulose ethers.*[28]

In this study, we used a cellulose ether derivate with hydroxyethyl groups[28,29], see *Fig. 9*. Hydroxyl groups have been replaced with hydroxyethyl groups. In the manufacturing process, purified cellulose is reacted with sodium hydroxide to produce swollen alkali cellulose. This alkali-treated cellulose is more reactive than cellulose. By reacting the alkali cellulose with ethylene oxide, a series of hydroxyethyl cellulose ether is produced. These hydroxyethyl groups prevent the formation of the crystalline structures which are formed in unmodified cellulose, thereby rendering the polymer water soluble.

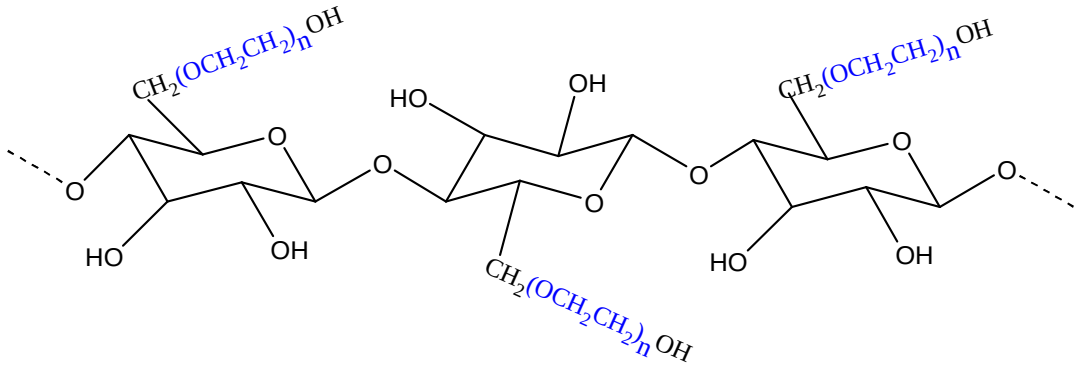

Figure 9. *Chemical structure of HEC.*

1.1.3 PNIPAAM

Since 1956, poly(*N*-isopropylakrylamide), PNIPAAM, has been appearing in the literature with increasing frequency. As *Fig. 10* illustrates, the number of publications concerning PNIPAAM is strongly increasing, especially over the past few years.

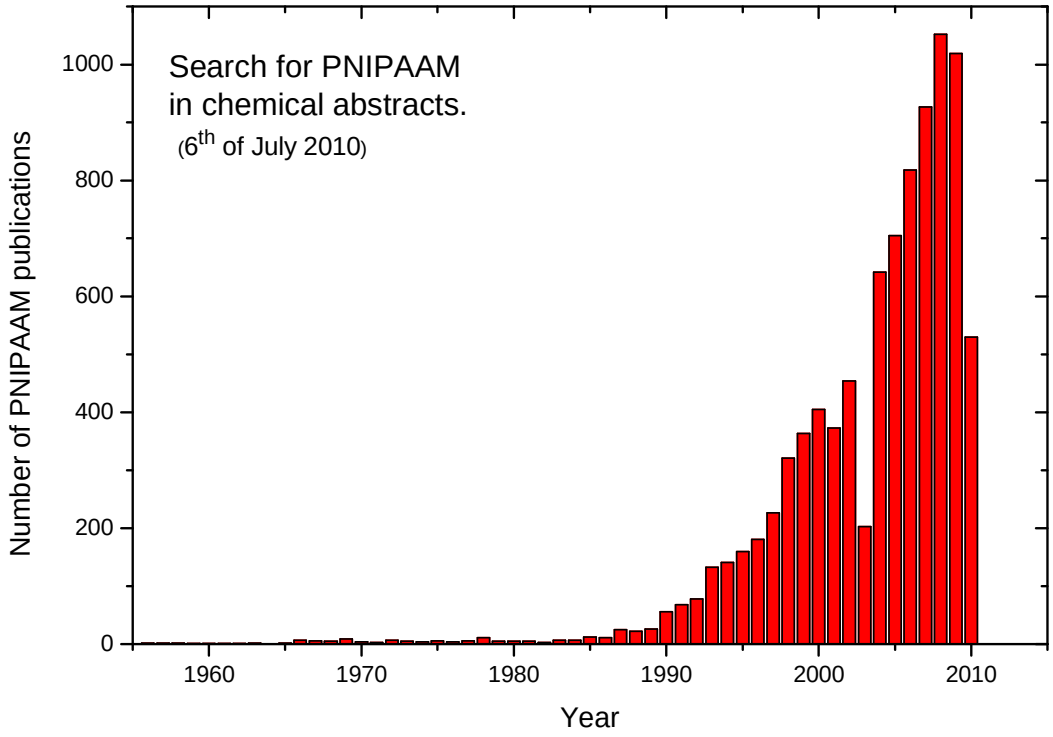

Figure 10. *Number of publications in CA concerning PNIPAAM.*

PNIPAAM exhibits interesting properties both as pure PNIPAAM polymers and as a component in block and graft copolymers and it has been used in many forms including single chains, macroscopic gels, microgels, latexes, thin films membranes, coatings, and fibbers. Moreover, a wide range of disciplines have examined PNIPAAM, encompassing chemistry, physics, pharmacy, biology, and photography.[8]

1.1.4 Thermoresponsive Properties of PNIPAAM

In most cases, when a macromolecule is heated up, it become more soluble or it has an upper-critical solution temperature (UCST). In other cases, it phase separate upon heating. That means it has a lower-critical solution temperature (LCST). This is caused by the changes in the polymer structure. As *Fig. 11* illustrate, at a low temperature, the polymer is hydrophilic and it is easily dissolved in water. The solution is transparent. When increasing the temperature, the polymer becomes hydrophobic, and since hydrophobic moities dislike water it will make self-assembly structures. With the naked eyes, you can see that the solution is turbid because of a microphase separation.

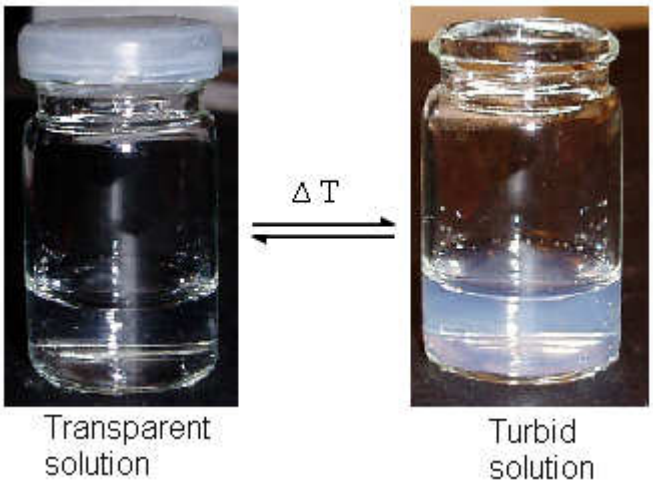

Figure 11. *An illustration of a transparent solution which is below LCST and above LCST which is turbid.*

This unusual effect appears because of hydrogen bonding between water molecules and amide residues of the PNIPAAM chains, see *Fig. 1*. When we increase the temperature, the effect of H-bonds is lessened, and as the bindings between the amide groups and water decreases and the polymers become more hydrophobic. This can be explained by introducing the Gibbs free energy: $\Delta G = \Delta H - T\Delta S$, where ΔH is dissolution enthalpy due to hydrogen bonds between water and amide groups and ΔS is entropic organisation of the sample. Since the free energy of dissolution is equal to $\Delta G = \Delta H - T\Delta S$, it can change from negative (favourable/miscible) to positive (unfavourable/turbid) as the temperature increases.[1] At low temperature, ΔH is small and ΔG is negative, while at higher temperatures ΔH increases and ΔG becomes positive.

1.2 Applications

Till now, we have discussed the chemical structure and the behaviour of HEC and PNIPAAM. In this section, we will have a closer look on the fields where we can use this combination of polymers together.

1.2.1 Drug delivery → encapsulation of drugs

Drug delivery is the method of controlling a pharmaceutical compound to achieve a therapeutic effect. Ideally, a drug delivery system should deliver the correct amount of drug to the site of action at the correct rate and timing, in order to maximize the desired therapeutic response. The most common methods of drug delivery are by injection and by oral delivery, but drugs can also be delivered by other routes such as suppositories, nasal sprays, eye-drops and topically. The oral sustained release route is the most convenient for many applications. The drug can be encapsulated by a polymer matrix and then released to the target area of the body. This technique can control the drug release over a period of time because of the chemical formulation. The advantage of using an injection is that many medications such as peptide and protein, antibody, vaccine and gene (based drugs), is badly suited for oral delivery, because they might degrade in the gastrointestinal tract and they are poorly absorbed in the digestive system.[30] Injections are also the best method for sustained release of a drug over an extended period of time (weeks or months). By encapsulating the drug in a harmless polymer that can release the drug in the desired fashion, improved drug delivery systems can be tailor-made for different purposes.

1.2.2 Enhanced oil recovery

Enhanced Oil Recovery (EOR) is a generic term for techniques for increasing the amount of crude oil that can be extracted from an oil field. It's difficult to gain a 100% crude oil just from one technique. Therefore, different techniques have been used to achieve EOR by gas injection, chemical injection, ultrasonic stimulation, microbial injection, or thermal recovery (which includes cyclic steam, steamflooding, and fireflooding). The most studied EOR field is by using chemical injection, and polymers are frequently used in EOR applications.[31-34] Polymers such as polyacrylamide and polysaccharides are often used in EOR.[35-38] Using a

polymer which is stable under pressure and high temperature and is available low cost are most desired. It should also be environmentally friendly. In polymer flooding, a polymer solution (preferable one which has a relatively high viscosity at low concentrations) is injected into the oil-well. The viscous solution presses the oil out in front of it, gaining higher oil yields.

1.2.3 Adsorption and detection of nanoparticles

Before 1960, many researchers were working with immunoassays, using radioactively-labeled antigens or antibodies to provide the signal which indicates whether a specific antigen or antibody is present in the sample. Radioimmunoassay was first described in a paper by Rosalyn S. Yalow and Solomon A. Berson published in 1960.[39] Because radioactivity poses a potential health threat, another method was sought. After 1960, instead of using a radioactive signal to detect the presence of an antibody or an antigen in the sample, enzyme-linking immunosorbent assay (ELISA) was used, which yields a colorimetric signal upon enzymatic cleavage of the chemiluminescent substrate.[40,41] However, this method has the limitation of detection in the picomolar analyte range. Later, fluorescence immunoassays, based on an alternative detection strategy where antibodies labelled with fluorophores (Rhodamine, Alexa fluor, FITC, etc.) are used as markers that provide high optical contrast and do not require an additional processing step.[42,43] Recently, the nano revolution has exhibited a growth of interest in nanotechnological disciplines. Noble metal nanoparticles display fascinating electronic and optical properties as a consequence of their dimensions and they may be easily synthesized from a wide range of materials.[44] The few conducted studies provide only scant insights into the interaction of nanosilver/ nanogold particles with the human body after entering via different portals.[45] Nanogold and nanosilver particles can be stabilized by anionic ligands such as citrate or lipoic acid[46] The biomolecules are often coupled through noncovalent electrostatic interaction. For instance, gold and silver nanoparticles, which are produced by the citrate method, have been functionalized with Immunoglobulin G (IgG) molecules at high pH values that are slightly above the isoelectric point of the citrate ligand [47] When coupling this gold (Au) or silver (Ag) particle onto the IgG, we may detect the surface composition as well as to elucidate the structural and geometric features at surfaces.[44] The best thing is that nanoparticles can either be coated by a polymer or it can be connected to the surface of a drug which is encapsulate by a polymer. Au and Ag nanoparticles are easily

detected by imaging techniques and the Au and Ag nanoparticles enable to monitor the signal where the drug takes place in human body.

1.2.4 Viscosity Enhancer

Viscosity enhancers show different viscosity improvement properties for many products. With the combination of different viscosity enhancers, the viscoelastic properties of a substance can be remarkably imported, and it may also reduce the cost. A viscosity enhancer agent is absolutely essential in common products like shampoo, personal care products, toothpaste, paint, etc. In personal care products, the viscosity can be controlled in many ways, but the most used method is by using the water soluble polymers such as cellulose derivatives, acrylates, natural gums, ethoxylates and related substances.[48]

2. Experimental Techniques

2.1 Turbidimetry

Turbidity is a measurement of the opaqueness of a sample and it characterize phase changes of the samples with high sensitivity and accuracy. By using a light beam, AlGaAs light, operating at 654 nm is focused on the solution that is placed onto a glass plate, which is coated with a thin metallic layer creating a very high reflectivity mirror, see *Fig.12* below. Directly above the applied sample, a detector continuously monitors the scattered intensity signal (S) from the sample. The instrument is interfaced to a PC, and the supplied software controls the operation of the turbidity meter and continuously collects data. In order to determine the turbidity (τ), the signal from turbidimeter has been compared with the turbidity determined from a spectrophotometer according to the equation:

$$\tau = \frac{1}{L} \cdot \ln\left(\frac{I_t}{I_0}\right) \qquad (1)$$

where L is the light path length of the cuvette, I_t is the transmitted light intensity, and I_0 is the incident light intensity. The relation between the calculated turbidity from the spectrophotometer experiments and the signal (*S*) from the cloud point (CL) analyzer is empirically found to be given by the relationship[24]

$$\tau = 9.0 \times 10^{-9} S^{3.751} \qquad (2)$$

All the data from the cloud point analyzer will be present in terms of turbidity.

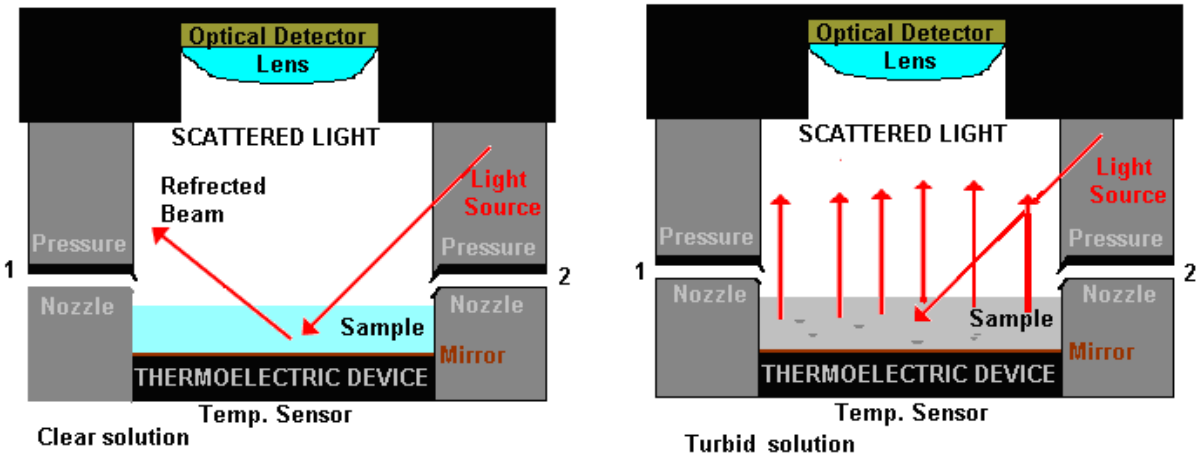

Figure 12. *A schematic picture of the turbidity meter chamber for a clear and a turbid sample*.

Fig. 12 illustrates how the cloud point analyzer is operating. There are two pressure nozzles in the chamber. This is used for circulation in the system where it removes the humidity from the air above the sample in order to avoid condensation on the lens. For a clear solution, very little of the refracted beam reaches the detector, giving a small signal with indicates a low turbidity in the system. When a turbid sample is measured, the sample scatters the light, and a large signal is detected. This signal can be transformed to turbidity results by using equation (2).

2.2 Light Scattering

Light scattering (LS) is one of the most powerful techniques we have in our research group. A principle sketch of the experimental setup of the LS is displayed in *Fig. 13*. There are two methods we can use, either static or dynamic light scattering. From static light scattering (SLS) measurements, we can determine the molecular weight (M_w), the radius of gyration (R_g) or the correlation length (ξ_g) the second Virial coefficient (A_2) and the fractal dimension (d_f). From dynamic light scattering (DLS) experiments we can measure the hydrodynamic radius (R_h) or correlation length (ξ_h) and their distribution. In addition the relaxation of chains and clusters in semidilute samples can be probed. It can also be used to probe the behavior of complex fluids such as concentrated polymer solutions. In this thesis, dynamic light scattering (DLS) has been used.

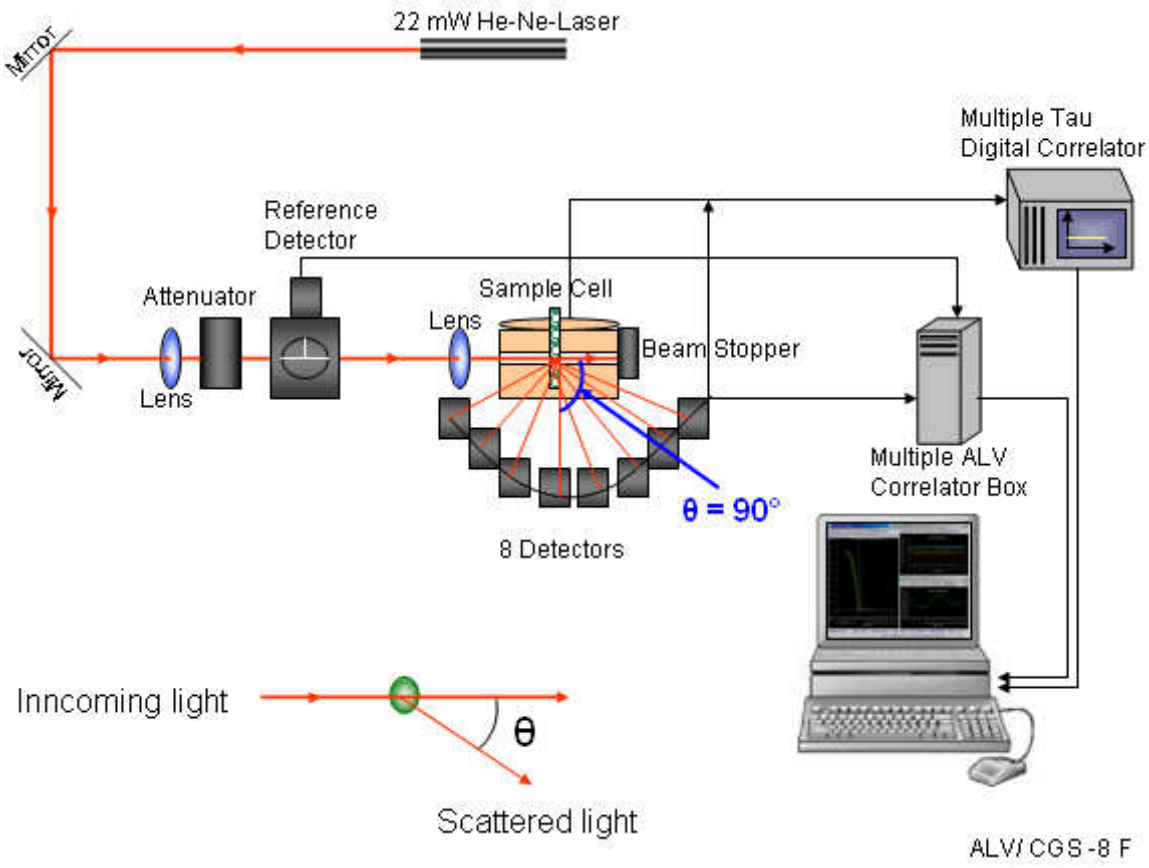

Figure 13. *A schematic picture of the light scattering with 8 detectors.*[49]

2.2.1 Dynamic Light Scattering

In DLS experiments, we measure the time average fluctuation of particles in the system. Here we can probe on a global or local scale by varying the wave vector (q). The experiments probe the system on a length scale that is the inverse of the q vector, which is given by

$$q = \frac{4\pi n}{\lambda} \cdot \sin\left(\frac{\theta}{2}\right) \qquad (3)$$

where n is the refractive index of the sample, λ is the wavelength of the incident light in vacuum, and θ is the scattering angle. The q vector can be changed by varying the scattering angle.

The concentration fluctuations in the sample can be converted into an intensity autocorrelation function $g^2(q,t)$ at different scattering angles. If the scattered field obeys Gaussian statistics, we can use the Siegert relation to determine the first-order electric field correlation function $g^1(q,t)$.

$$g^2(q,t) = 1 + B\left[g^1(q,t)\right]^2 \quad (4)$$

where B is an empirical factor. This empirical factor tells if we are in the ergodic or non-ergodic area. In an ergodic system, B should be between 0.6-1 and for a non-ergodic sample, B is lower than 0.6. The B value can also be below 0.6 if we have multiple scattering in the system.

The Siegert relation is only valid under ergodic conditions. In an ergodic system, the time average and the ensemble average is the same, i.e. the correlation functions are independent on the scattering position of the incident light in the sample. Normally, dilute solutions are always ergodic and gels are often, but not always, non-ergodic, because the chains cannot move freely in the gel, giving different conditions in the various microdomains of the sample. All DLS results in this thesis are observed to satisfy the condition for using the Siegert relation. It has also been observed that the decay of the correlation functions can be described by eq.(5)

$$g^1(t) = \exp\left[-(t/\tau_{se})^{\beta}\right] \quad (5)$$

where

τ_{se} is the effective slow relaxation time

β is the width of the distribution of relaxation times ($0 < \beta \leq 1$)

The mean relaxation time for the slow mode is given by

$$\tau_s = \frac{\tau_{se}}{\beta}\Gamma\left(\frac{1}{\beta}\right) \quad (6)$$

where Γ the gamma function. Eq. (5) has been used for the neutral polymer at concentrations 0.3 wt% and 0.5 wt%, and for all systems above the LCST of the polymer. Below the LCST for the charged polymer and at lower concentrations of the neutral polymer, the correlation functions have been fitted by a single exponential followed by a stretched exponential:

$$g^1(q,t) = A_f \exp\left[-t/\tau_f\right] + A_s \exp\left[-(t/\tau_{se})^{\beta}\right] \quad (7)$$

$$A_f + A_s = 1$$

A_f and A_s are the amplitudes for the fast and slow relaxation modes

τ_f is the mean relaxation time for the fast mode

τ_{se} is the effective slow relaxation time

β is the width of the distribution of relaxation times

To make sure that eq. 5 and eq.7 has been correctly selected, the goodness of the fitting procedure where scrutinized utilizing residual plots. As is displayed in *Fig. 14*, the residuals reveal how good the fitting of the correlation functions are. We notice that in *Fig. 14 a*, the fitting is not good with eq. 5 (one mode), but with eq. 7 (two mode) the fitting is much better. However, in *Fig. 14 b* the residuals shows that with eq. 7 the residuals are very close to zero, with little variation, i.e. a very good fit, while using eq. 5 the residuals vary a little more than with eq. 7, but they are much better than what was observed for eq. 7 in *Fig. 14 a*. To evaluate which of the equations we should use, we decided to take into account that A_f in eq. 7 is around 0.02 which is too low to gain reliable values for τ_f. We therefore decided to use eq.5 which employs fewer parameters. The very low values obtained for A_f in eq. 7 indicates that the number of small entities (unassociated polymer coils) in this sample is very low.

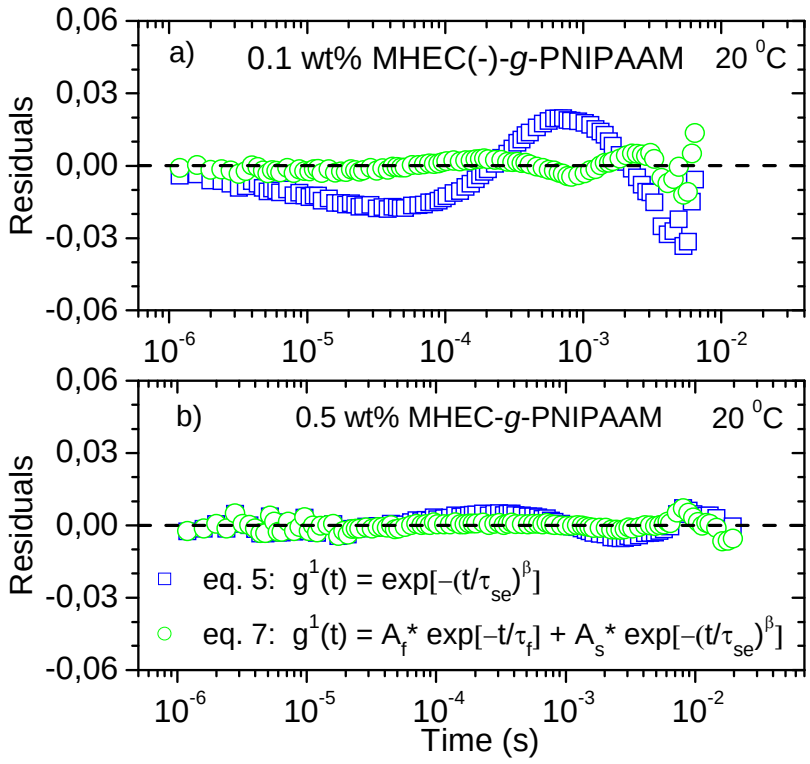

Figure 14. R*esidual plots fitting a typical correlation function with the aid of eq. 5 or eq. 7.*

Fig. 15 shows that above LCST, the correlation function which has been fitted with eq.5 gives a very nice residual plot. When we tried using eq. 7 to fit the same data, the errors of many of the fitting parameters were of the same magnitude as the fitted values, and often the fitting did not converge into stable values. In addition we also had problems with:

- A_f is too low, which give a high error in τ_f
- τ_f is too close to τ_s, indicating that we only have one mode.

Accordingly, the samples which were above LCST only exhibit one relaxation mode, and have been fitted with eq.5. Table 1 summarizes which equation that is used at the different conditions.

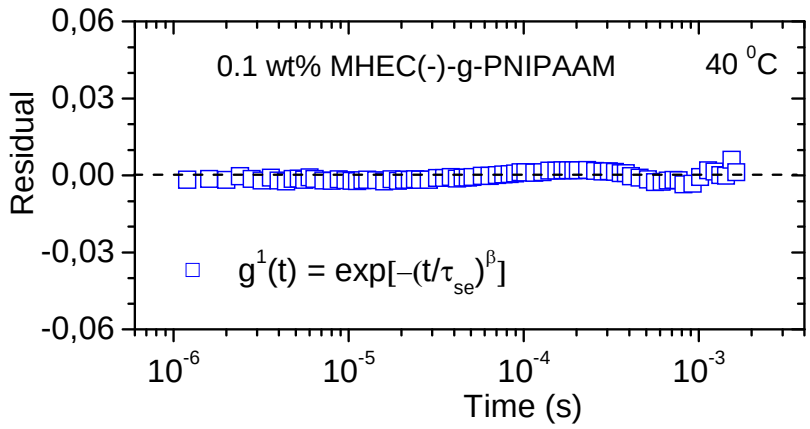

Figure 15. *The residual as verses time for a 0.1 wt% charged polymer above LCST by fitting with eq. 5.*

Table 1. A summarization of the conditions where eq.5 and eq.7 are used.

Polymer	Below LCST	Above LCST
Neutral (C < 0.3 wt%)	Eq. 7	Eq. 5
Neutral (C ≥ 0.3 wt%)	Eq. 5	Eq. 5
Charged (all concentrations)	Eq. 7	Eq. 5

In dilute solutions, such as the samples probed in this study, τ_f probes the movement of single polymer unimers or very small aggregates while τ_s probes larger aggregated clusters. When τ_f and τ_s is known, we can determine if the system is diffusive or not. In a diffusive system, the molecules can diffuse freely in the solution. Since the diffusion coefficient is a characteristic

of the sample, it should be independent of scattering angle. The mutual diffusion coefficient can be calculated by:

$$D_m = \frac{1}{\tau\ q^2} \qquad (8)$$

where τ is τ_f or τ_s.

Accordingly, for a diffusive mode: $\tau^{-1} \sim q^{\alpha}$ and the mode is diffusive when $\alpha = 2$. From the mutual diffusive coefficient, the hydrodynamic radius (R_h) can be determined by using the Stoke-Einstein equation:

$$R_h = \frac{kT}{6\pi\eta_s D_m} \qquad (9)$$

where k is Boltzmanns constant, T is the absolute temperature, and η_s is the solvent viscosity. In this thesis we have found that the fast mode is diffusive at all conditions. However, the slow relaxation mode is not always diffusive. Accordingly, we cannot calculate accurate R_h values from the slow mode. But an apparent R_h has been calculated from a scattering angle of 90^o. Anyway, it should be noted that these values are only a rough estimation of the sizes. Even though the correct values of R_h cannot be determined, the trends in the data will probably give a reasonable estimation of the behavior of the samples.

2.3 Rheology

Rheology is the study of the viscoelastic properties of a sample. A viscoelastic response appears when applying a stress to the sample. Normally, a solution shows both viscous and elastic behaviour. The elasticity is a reversible deformation and the viscous response is irreversible deformation. The reversible deformation is due to structure forms that can be reverted to its original configuration, while the viscous deformation is converted to the heat. From rheology techniques, we can determine the viscosity (η), zero shear viscosity (η_0) intrinsic viscosity [η], Huggins coefficient (k'), gel points, storage modulus (G') which represent to the pure elastic contribution, and the loss modulus (G'') which is the viscous contribution, etc. To determine these values, either steady shear or oscillatory shear measurements are used. In this thesis, steady shear experiments have been performed.

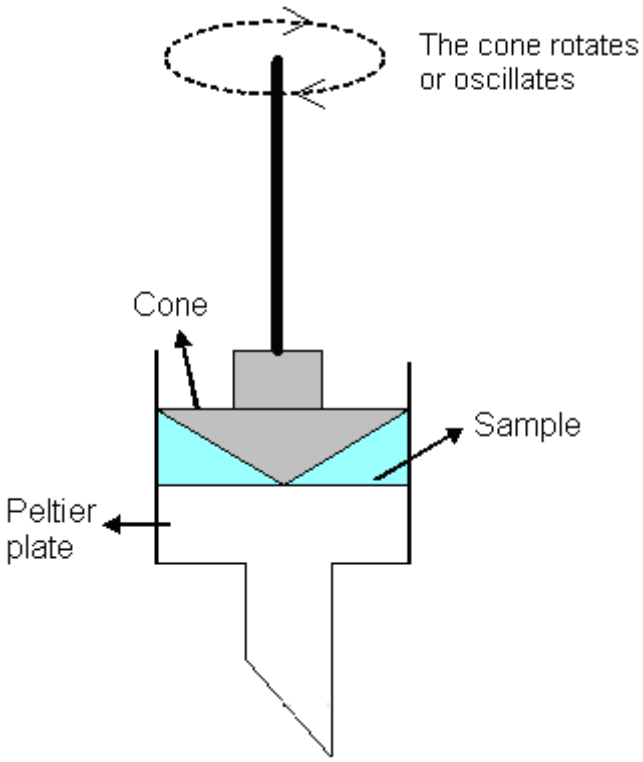

Figure 16. *A schematic picture of the rheometer*.

When we conduct rheological experiments, the cone is rotated/oscillated, and the resistance to this movement is measured and converted to the various viscoelastic parameters measured.

2.3.2 Steady shear

In steady shear measurements, the cone will rotate at a constant or at a different shear rates ($\dot{\gamma}$). The information we can gain from these experiments is how the viscosity varies with shear rate, the zero-shear viscosity, and where the Newtonian regime is. If the system is in the Newtonian region, it is shear rate independent, giving us a viscosity (η) that does not vary with the shear rate. In the non-Newtonian region, the system exhibit shears thickening, shear thinning or both in the same system. If shear thickening is observed, it is usually occur at low shear rates. This is caused by stretching and alignment of the polymer chains, giving rise to easier access for intermolecular associations. At high shear rates, polymer solutions usually exhibits shear thinning behaviour, because the associations are breaking up due to the high shear forces. The shear rate dependency of the viscosity can be calculated by eq. 10.

$$\eta \propto \dot{\gamma}^{(\alpha-1)} \qquad (10)$$

Power law index

- $\alpha < 1$ shear thinning system
- $\alpha = 1$ Newtonian system
- $\alpha > 1$ shear thickening system

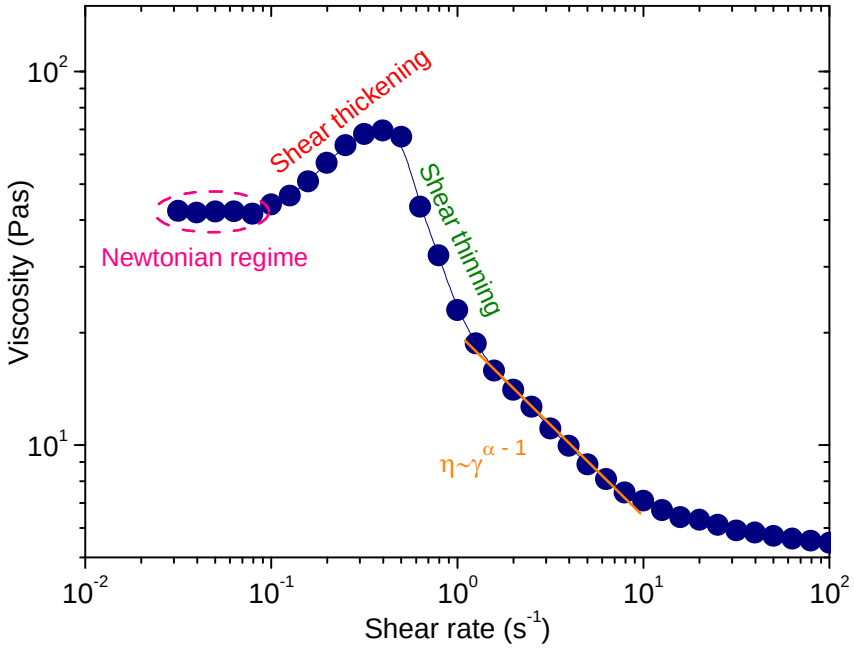

Figure 17. A*n illustration of the Newtonian regime, shear thickening and shear thinning.*

As is displayed in *Fig.17*, the Newtonian plateau is observed at very low shear rate. When the shear rate is increased then the shear thickening appears. This is caused by interaction, organization and alignment in the system when we apply the shear. At higher shear rates, the intermolecular association structures will be disrupted causing shear thinning.

2.4 Rheo-small- angle- light scattering

Rheo-SALS is a combination of rheology and small angle light scattering measurements. See *Fig.18* for an illustration of how this instrument is working.

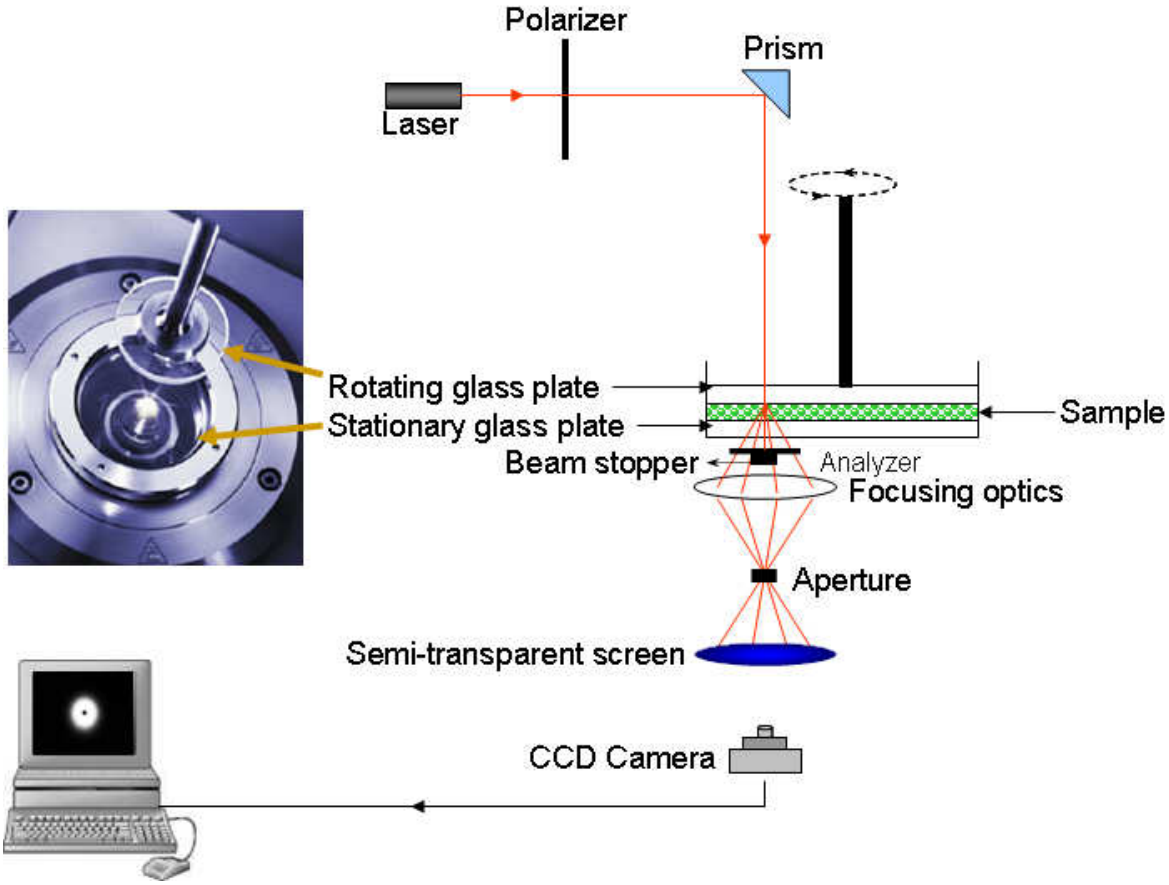

Figure 18. A schematic picture of the rheo-SALS.[49]

A detailed description at this instrumentation has been given elsewhere.[12,50] This type of technique can provide us with information about structural changes of cross-linked or aggregation complexes on a global dimensional scale under the influence of shear flow.[50] By this method the image of the sample will also reveal whether we have system which is oriented randomly, or if it is aligned in the shear directions.

2.4.3 Analysis of Rheo-SALS

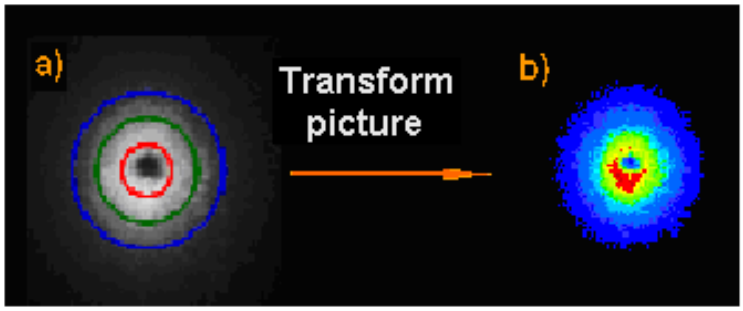

Figure 19. *Picture a) is a typical 2D scattering pattern, b) a transformed picture by using a homemade program.*

In *Fig. 19 a*, a 2D scattering pattern has been captured by a CCS camera at a given time. By taking into account the path of the scattered light, each distance from the centre of the scattering pattern (represented as a circle in *Fig. 19 a* can be related to a scattering angle, and transformed into a q-vector, see eq. 3. In the centre of the circle, q-values are low, and they increase as we move out from the centre. We are using a homemade program to calculate the average intensities at different q-values, and to transform the scattering pattern into a colour picture as illustrated in *Fig. 19 b.*

The scattering intensity can now be obtained roughly by observing the colour of the pattern. From the centre of the circle, red is the highest intensity scattering then yellow, green and the farthest outside is blue. The colour reveals if the system has a high amount of associations or not. If the middle of the centre is red, the system scatters strongly, indicating large association structures. The opposite is blue, which is typical for a system or no with few associations. The scattering intensity gradually decreases as the distance to the centre increases. For large aggregates, the overall scattering intensity increases and light can also be detected at higher scattering angles, giving rise to larger scattering patterns. In some cases, when applying a shear, we can either get a random association system (isotropic scatters pattern) or a system organized in the shear direction (anisotropic scatters pattern) as *Fig. 20 a and b* illustrate. In order to analyze the scattering intensity, we have to take into account the shear direction, and the scattering angles respectively. *Fig. 20 c and d* illustrate that the scatted intensity is the same in all directions for an isotropic sample, where the scattering moitres are randomly oriented. For a system which is aligned in the shear direction, anisotropy is observed, and the

scatted intensity along the shear axis (Int1) and perpendicular to the shear (Int2) differ significantly, see *Fig.20 d.*

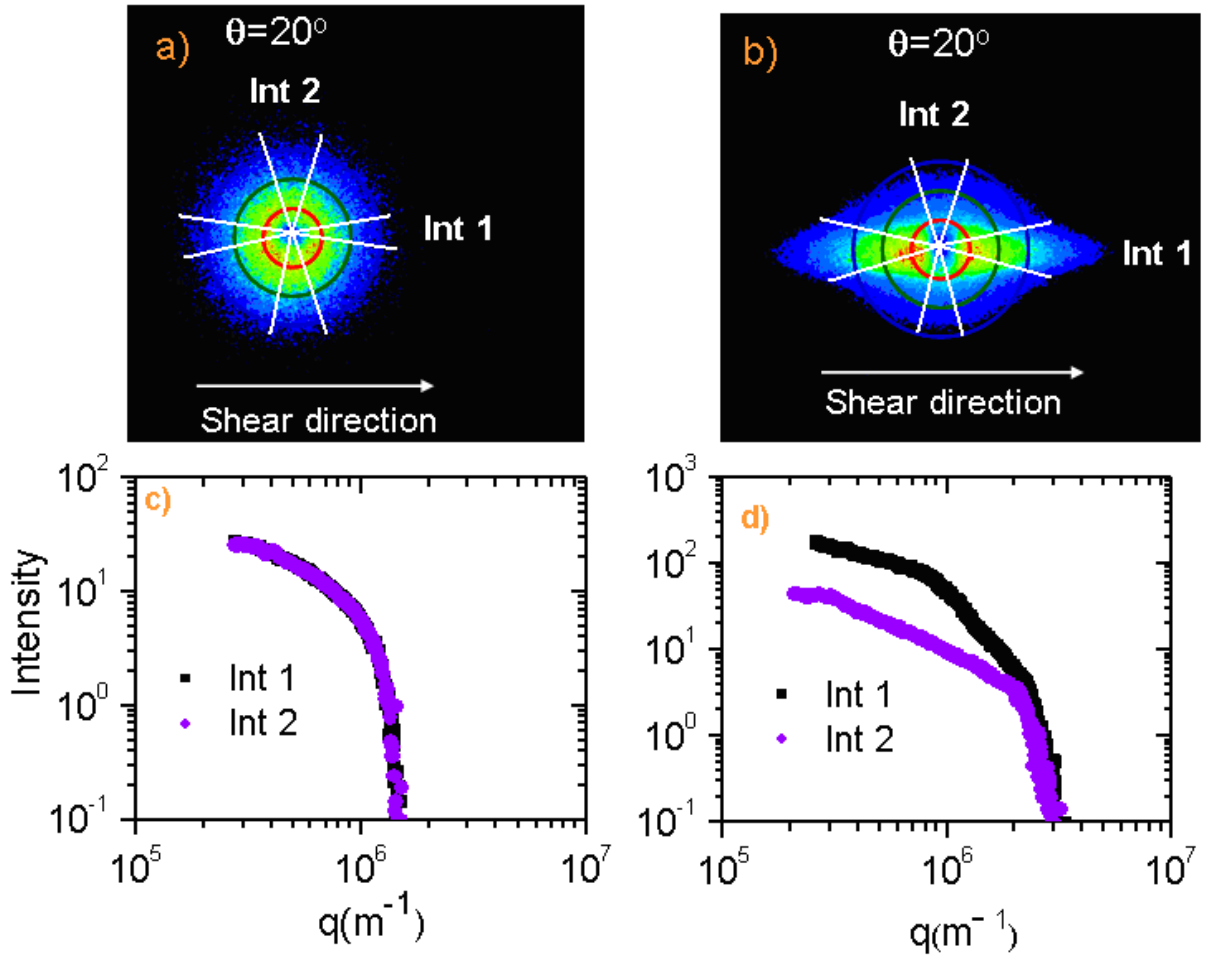

Figure 20. a) A *random organized scattering pattern which is an isotropic sample, b) an organized scattering pattern with shear direction which is anisotropic sample, c) and d) intensity as a function of q for the same systems.*

3. Experimental Section

In this study, low concentration (0.02-0.5 wt %) and high concentration (0.5-5.0 wt %) samples have been examined by different experimental techniques.

3.1 Materials

In this work, hydroxyethylcellulose (HEC) with commercial name Natrosol (250 GR(lot nr: V-1302), obtained from Hercules, Aqualon Division, was used as the starting precursor for the synthesis of HEC derivatives and its grafted products. (MHEC-*g*-PNIPAAM and MHEC(-)-*g*-PNIPAAM). The degree of substitution of hydroxyethyl groups per repeating anhydroglucose unit (AGU) for this HEC sample is 2.5 (given by the manufacturer), and the weight-average molecular weight was determined to be M_w = 400 000 by asymmetric flow field-flow fractionation (AFFFF).[51] To dry the polymer, it was first desiccated to remove absorbed moisture under vacuum dried. The other chemicals, 2-chloroethanol, cerium (IV) ammonium nitrate (CAN), nitric acid solution (1M) was purchased from Fluka and 3-chloro-2-hydroxy-1-propanesulfonic acid sodium salt from Aldrich were used as received. *N*-isopropylacrylamide (NIPAAM, Acros Organics) was recrystallized from a toluene/hexane mixture solvent and dried at room temperature in vacuum prior to use. Cellulase from trichoderma viride was purchased from Aldrich (5000 units/g). A regenerated cellulose membrane (Spectra/Por 6) with a molecular weight cutoff of 10 000 was purchased from Spectrum Laboratories and used for the dialysis process.

3.1.1 Modification of HEC

In order to acquire a grafted copolymer MHEC-g-PNIPAAM with good water solubility, hydroxyethylation of HEC was carried out to enhance the ethoxyl contents in HEC. Modified-hydroxyethlcellulose (MHEC) was prepared by the reaction of HEC with 2-chloroethanol in the present of NaOH solution.[52] MHEC was used as the precursor for the succeeding synthesis of the neutral and negative charged MHEC-*g*-PNIPAAM derivatives and the values of the MS hydroxyethyl groups will be higher than 2.5 due to the modification reaction.

3.1.2 Synthesis of MHEC- grafted-PNIPAAM

Graft polymerization of NIPAAM onto MHEC was carried out using cerium ammonium nitrate (CAN) as an initiator under an argon atmosphere at 30 ^{o}C following the method published by Wan et al with some modifications.[52] Redox reaction system of Ce(IV) with reducing agents (alcohols, aldehydes, ketones, acids, amines, thiols et al) in aqueous solution are well-know initiators for vinyl polymerization and homopolymers, block copolymers and graft copolymer can be easily prepared by this system.[53-55]

A certain amount of MHEC was dissolved into pre-degassed distilled water with gently magnetic stirring and argon bubbling for 1h. To this solution, a degassed cerium (IV) ammonium nitrate ($2\cdot10^{-3}$ M) in nitrite acid (1M) solution was added and stirred for another 10 min, and then, *N*-isopropylacrylamide monomer in degassed water was added and the polymerization was initiated. The polymerization was carried out at 30 ^{o}C for 10 hours under an argon atmosphere. After the polymerization was completed, the solution was diluted with cold water and neutralized with 1M NaOH aqueous. To remove unreacted monomer and cerium ions, the resulting mixture was dialyzed with repeated changes of fresh distilled deionized water by using regenerated cellulose with a molecular weight cut-off of about 10^4 (spectrum medical industries) as the dialyzing membrane for at least 2 weeks. The white solid collected by freeze drying was further extracted with cold methanol for 24 hrs to get rid of the PNIPAAM homopolymer. The MHEC-*g*-PNIPAAM product was finally dried under vacuum and kept at 4 ^{o}C.

3.1.3 Synthesis of MHEC(-)-g-PNIPAAM

MHEC was first mixed with isopropyl alcohol and a 48% aqueous solution of sodium hydroxide to prepare slurry. Thereafter sodium 3-chloro-2-hydroxypropanesulfonate in a 48% aqueous solution of sodium hydroxide was added, which resulted in the negative charged MHEC. [56-58] The degreed of substitution of the charged groups is ca 6.0 % analyzed by ^{1}H-NMR. MHEC(-) was then grafted with PNIPAAM using the same procedure as for the neural polymer.

A schematic representation of the preparation and the structure of MHEC(-)-g-PNIPAAM is shown in *Fig. 21*.

a)

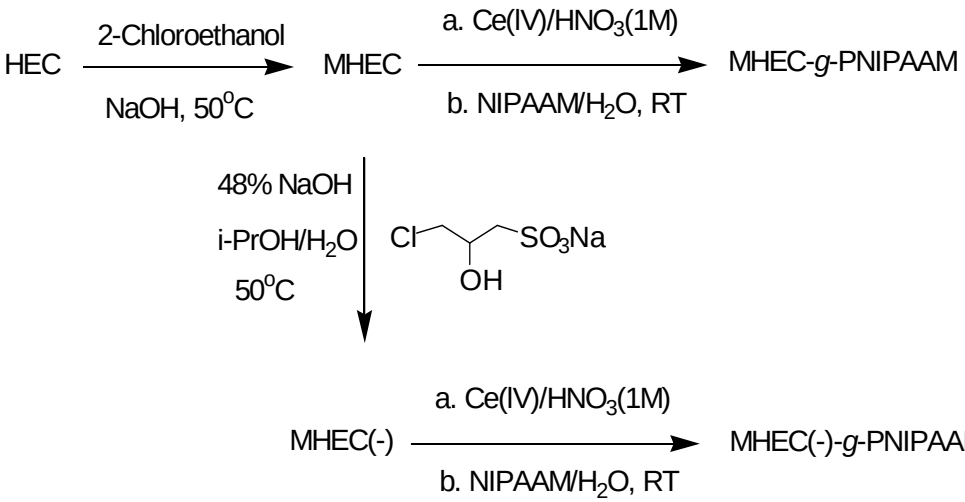

b)

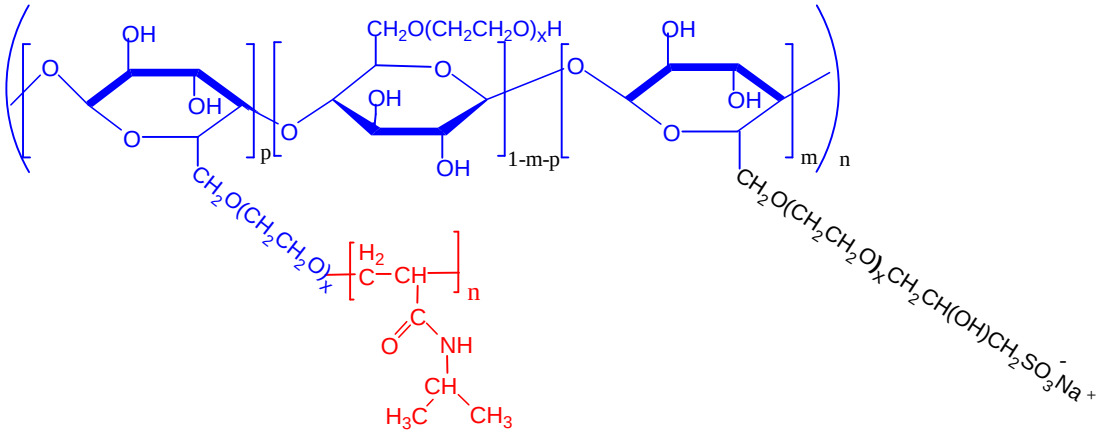

Figure 21. *a) Synthesizing procedure of the MHEC-g-PNIPAAM; b) schematic representation of the chemical structure of MHEC(-)-g-PNIPAAM(m=0.06) and MHEC-g-PNIPAAM (m=0).*

3.1.4 Characterization of MHEC-*g*-PNIPAAM and MHEC(-)-*g*-PNIPAAM

The chemical structure of the graft copolymers were ascertained by their ^{1}H NMR spectra with a Bruker AVANCE DPX 300 NMR spectrometer (Bruker Biospin, Fällanden, Switzerland), operating at 300.13 MHz at 25.0 ˚C by using heavy water (D_2O) as the solvent. The ^{1}H chemical shift in D_2O is referred to the residual HDO proton (δ = 4.70 ppm) in D_2O. MHEC and HEC show quite similar spectra but the ratio of the signals of the methylene proton at 3.3-3.4 ppm of MHEC is apparently larger than that of HEC due to the hydroxyethylation of HEC and increases the ethoxyl contents in HEC chain. *(Fig. 22)*.

In addition to the typical resonance peak of the HEC chain at 3.5-3.7 ppm, new characteristic signals of the poly(*N*-isopropylacrylamide) at 1.1 ppm (two methyl groups, -CH_3), 3.8 ppm(isopropylmethane groups, -CH-) and 1.5 ppm-2.0ppm (the main chain CH_2 and CH group of PNIPAM) appear in their proton spectra of graft derivatives indicated that NIPAAM monomer was successfully graft to the HEC chain *(Fig. 23)*.

All the syntheses procedures were carried out by Kaizheng Zhu.

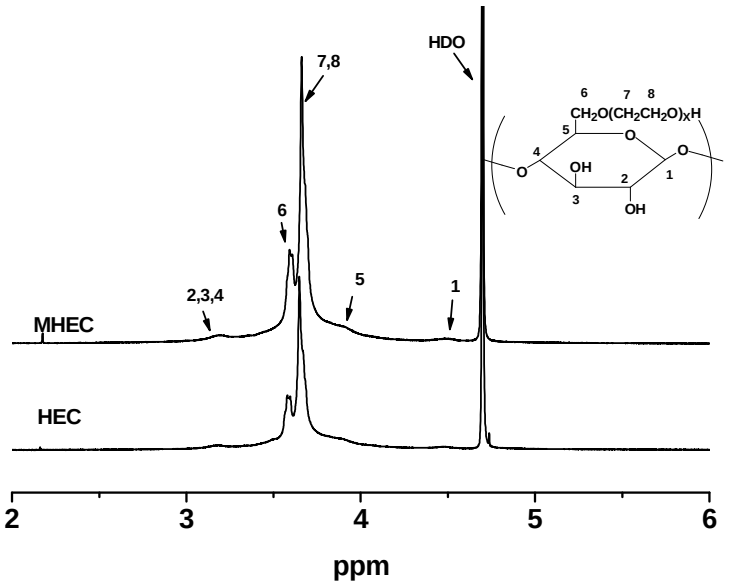

Figure 22. *^{1}H NMR Spectra of HEC and MHEC (300MHz, 25 ^{o}C, D_2O as the solvent).*

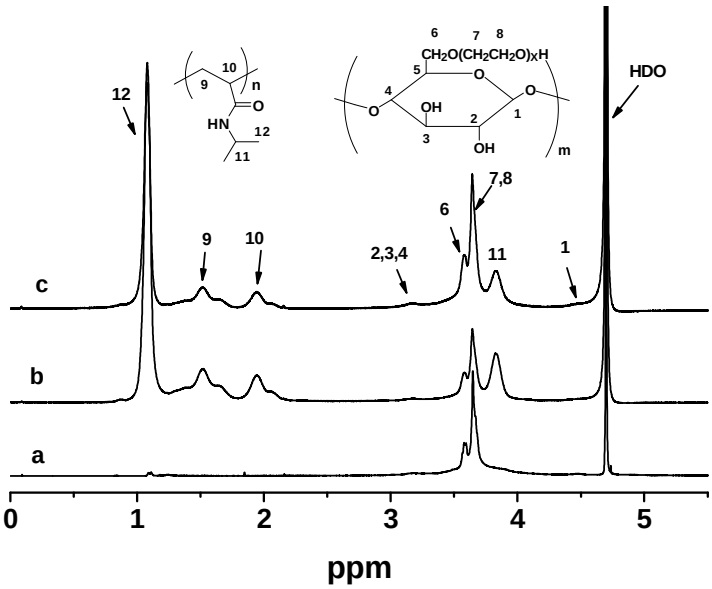

Figure 23. *^{1}H NMR Spectra of MHEC (a) and its graft derivatives: MHEC-g-PNIPAAM (b) and MHEC(-)-g-PNIPAAM (c) (300MHz, 25 ^{o}C, D_2O as the solvent).*

Elemental analysis

The chemical structure of the negatively charged polymer has one more reactive OH-group onto which the NIPAAM groups can be attached. Elementary analysis shows that we have more nitrogen for the negatively charged polymer than for the neutral polymer, see *table 2*. This elemental analysis does not show the amount of O and S. We have therefore sent both the neutral and charged polymer together with MHEC to a further elemental analysis which will give us C, H, O, N, and S, but unfortunately we do not have the results from this analysis yet. We have therefore tried to estimate the amount of PNIPAAM groups in the neutral polymer by assuming that the remaining 32.46 % of the sample is oxygen. Assuming that the sample contained some water which could not be removed, we found that MS of MHEC is about 5.6, and that there on average are about 3.6 NIPAAM groups and 3.7 water molecules per glucose unit. From ^{1}H NMR, Kaizheng Zhu found that this polymer contained 8.3 graft points per polymer backbone, and with a molecular weight of 400 000, this gives a length of the PNIPAAM substitutes of 213 NIPAAM units. However, when we try to do an analogous calculation for the charged polymer, we get very strange results (with negative values for the number of charges).[†] We are therefore waiting for the results from the new elemental analysis

[†] Anna-Lena helped me with these calculations.

before we can say anything certain about this sample, but it seems that the degree of substitution of NIPAAM units are larger for the charged sample, and in addition ^{1}H NMR show that this polymer contained a larger amount (12.3) of graft points per polymer backbone. This additional amount of PNIPAAM could be due to the extra reactive groups on the charged polymer.

Table 2. Results from elementary analyzes for nitrogen, carbon and hydrogen.

Name	Nitrogen	Carbon	Hydrogen
MHEC-g-PNPAAM	5.73 %	52.80 %	9.01%
MHEC(-)-g-PNPAAM	8.30 %	55.73 %	9.43 %

3.2 Samples preparation and instrument programmer

To make sure that all solutions are homogeneous, they were made and stirred for at least 1 day before the measurements. When the sample was not in use, they were kept in the fridge.

3.2.1 Turbidity Measurements

All solutions were carried out with a temperature increment with a heat rate of 0.2 ^{o}C/min and in the temperature interval 20 to 60^{o}C. For each measurement, 0.15 mL sample was used. To avoid evaporation of the solution at elevated temperatures, the sample surface is covered with 0.15 mL of highly transparent silicon oil. The density of the oil is lower than the sample and it will float on the top of the sample. The instrument is calibrated using this silicone oil, so it will not affect the calculated turbidity values. The same cooling rate of the samples was also checked to reveal possible hysteresis effects. There is a small hysteresis effect when the sample is cooled down again. However, in this thesis, only heating curves are reported.

3.2.2 Rheology

Steady shear measurements were performed using a Paar-Physica MCR 300 rheometer with a cone-and plate geometry, with a cone angle of 1^{o} and a diameter of 75 mm. The instrument was programmed to do a temperature scan from 20 to 60 ^{o}C. The first measurement was

started at 20 ^{o}C and the temperature was increased in steps of 5 ^{o}C until 60 ^{o}C was reached. Between each measurment, the sample was left to equilibrate for 30 minutes to ensure that the sample was stabilized at the correct temperature. The shear rate was varied from 10^{-3} s^{-1} to 1000 s^{-1} for each scan. A 2.6 mL sample were introduces onto the plate, and to prevent evaporation of the solvent, the free surface of the sample was always covered with a thin layer of low-viscosity silicone oil. This silicone oil will not give any significant effect on the viscoelastic response.

3.2.3 Rheo-SALS

Fixed shear rates were used in the rheo-SALS experiments. For each concentration, measurement were carried out at 4 constant shear rates (0 s^{-1}, 1 s^{-1} , 10 s^{-1} and 100 s^{-1}). Each measurement was conducted, using a temperature scan from 20 to 60 ^{o}C with a heating rate of 0.2^{o}C/min. The sample volume was 1.2 mL, and to prevent evaporation of the solvent, the free surface of the sample was always covered with a thin layer of low-viscosity silicone oil. When applying the sample, great care was taken to avoid bubbles in the system, and to ensure that the amount of oil covering the sample was not too large. If the oil enters the incoming light beam, this will affect the detected scattering pattern and induce artifacts in the scattered light. It is also important to cover the instrument with a black cloth before starting the experiment, to avoid light from the surroundings to influence the scattering patterns.

3.2.4 Dynamic Light Scattering (DLS)

All samples were made one day in advance, and were filtrated with a 5 µm millipore filter into clean 10 mm NMR tubes. The tube was set to rest for about 2 hour before measurements were commenced. This is to ensure that any air bubbles created during filtration process has disappeared. Tubes which are not measured same day were kept in the fridge and used the day after. It has been shown that after measurements with a temperature scan from 20 to 60 ^{o}C with a heating rate of 0.2 ^{o}C/min, and subsequently cooling down again to 20 ^{o}C, the same cluster site as before was observed. For samples where two relaxation modes were observed at low temperatures, two modes were also revealed after the heating cycle. This indicates that once the unimers has been absorbed into an aggregate, some of them can easily be released

from the association complexes at low temperature. This system appears to be mostly reversible and it is also reproducible when remeasuring it some days later.

Salt preparation

Salt solutions where prepared at the desired salt concentrations, and the polymer was dissolved in the salt containing solvent. Otherwise, the same preparation method as was described above has been used.

4. Results and discussion

Results are presented in two sections: low concentration and high concentration. In this way, the presentation of the results should be easy to follow.

4.1 Turbidity

Before discussing the different concentration regions, a brief overview of the turbidity results for the whole concentration range is presented. *Fig. 24* displays the turbidity results for both polymers at a heating rate at 0.2 ^{o}C/min. As can be seen, there is a clear transition in the turbidity curves around 29-33 ^{o}C, depending on polymer concentration. In view of these aspects, the cloud point (CP) can be determined by observing the starting point of the steep increase in turbidity. The CP is the point at which a definite lack of clarity, cloudiness, appears in the solution, which is due to the microphase separation. Note that the turbidity is affected by the number of particles, the sizes of the particles and also by the compactness of the particles (changes in the differences between the refractive index of the particle and the refractive index of the solvent). As can be seen from *Fig. 24*, the turbidity increases with increasing concentration. This effect is mostly due to the increased number of particles in the system. The reason for the transition in the turbidity curves will be discussed in more detail below.

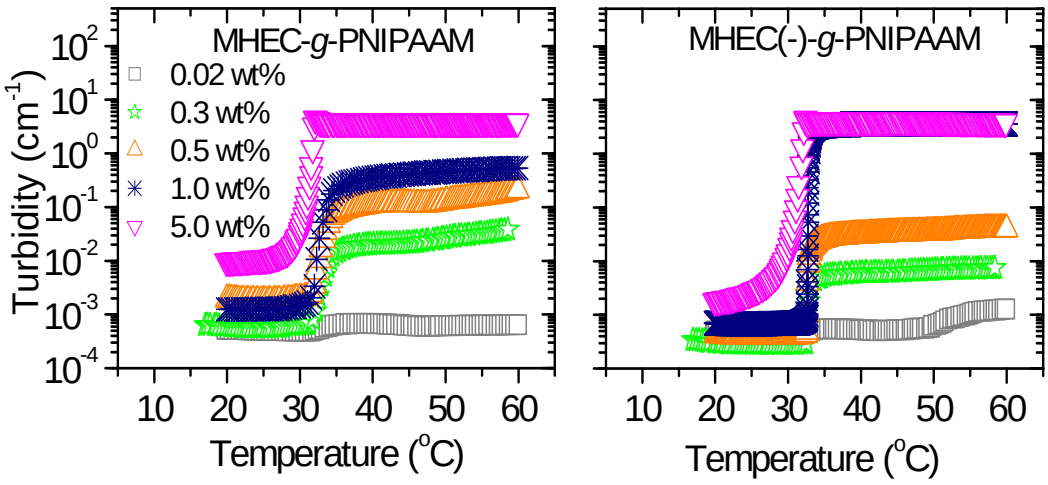

Figure 24. *Temperature dependency of the turbidity during heating (0.2 ^{o}C/min) for the neutral and charged polymer at different polymer concentrations.*

Fig.25 shows the concentration dependency of the CP for both polymers. The CP occurs earlier for higher concentrations, which is due to the increasing the number of particles, which leads to enhanced associative interactions in the system. The CP for the charged polymer is higher than for the neutral polymer, this is caused by the repulsive electrostatic forces which cause the clusters to swell and which also reduce the amount of aggregation. It is interesting to note that while the CP for the charged polymer decreases nearly lineally with increasing concentration, the neutral polymer exhibits a much sharper decline at low concentrations, followed by a more moderate change at higher concentrations, the cause of this will be discussed below.

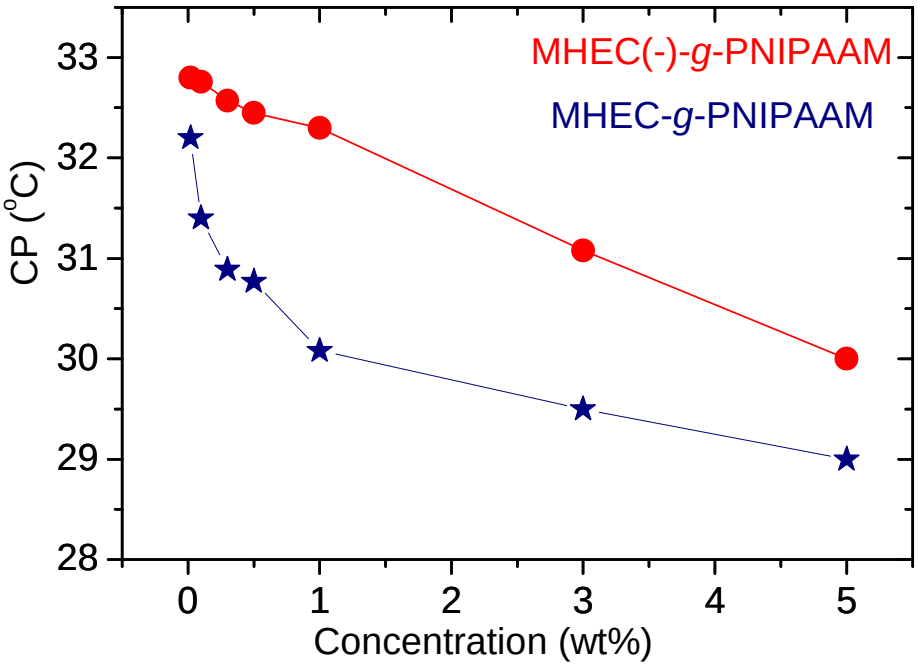

Figure 25. *Effect of polymer concentration on the cloud point for the neutral and charged polymers.*

4.2 Low Concentrations (0.02 wt% - 0.5 wt%)

4.2.1 Turbidimetry

In the beginning of the discussion section, the turbidity results were briefly introduced. In this section, the turbidity results at low polymer concentrations will be discussed in more detail. *Fig. 26* displays the heating curves (0.2 ^{o}C/min) of the turbidity for the neutral and negatively charged polymers. It is obvious that the solutions become more turbid after 30 ^{o}C, which is close to the region where PNIPAAM become much more hydrophobic at its LCST. The turbidity increase with increasing the concentration. Even at low temperatures, the turbidity has different starts values for the neutral polymer. This is due to an increase in the number of particles in the system, and in addition associations occur easier at higher concentrations since the polymer chains are closer to each other. The turbidity differences are more pronounced at elevated the temperatures, where the compactness of the clusters in the system dominates. This effect will be discussed in more detail in the DLS part below.

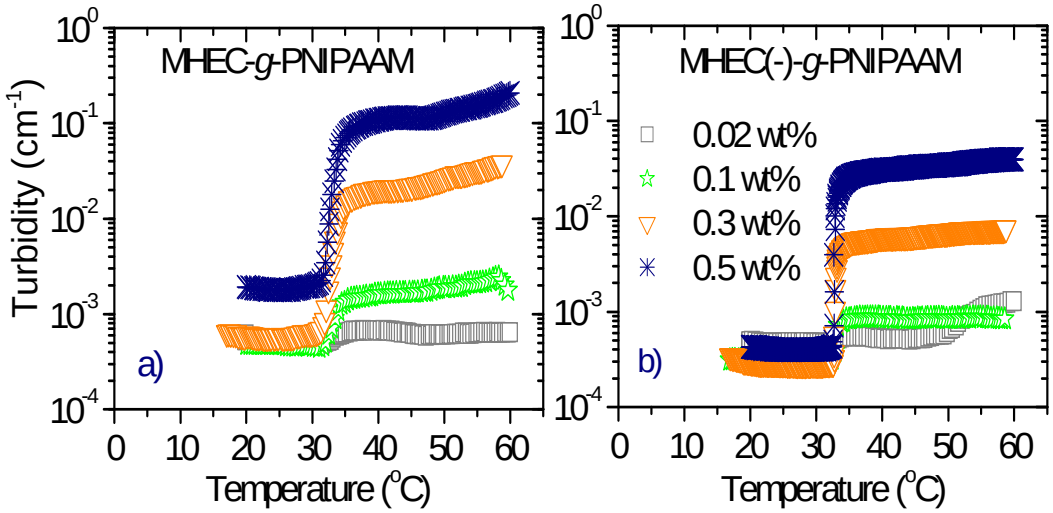

Figure 26. *Temperature dependence of the turbidity at different concentration for a) the neutral polymer and b) the negatively charged polymer.*

For the charged polymer, the cloud point decrease and the turbidity increase with increasing concentration, analogous to what was observed for the neutral polymer. However, at temperatures below the LCST, the turbidity is low even at 0.5 wt%, and the concentration dependency of the turbidity is only evident after the LCST. This is probably due to the negative charges in the system, which make the polymer coils more expanded, giving rise to a lower turbidity. This illustrates that the incoming light is scattered less for the negative charged polymer than for the neutral polymer. The repulsive electrostatic interactions counteract the hydrophobic attractive forces, leading to less contraction of the particles and a reduced tendency to form aggregates. This give rise to higher CP for the charged system and also a reduced concentration dependency of the CP compared with the neutral polymer.

The CP in *Fig. 27* presents a significantly decrease when increasing the concentration, again illustrating the enhanced interactions at higher polymer concentrations.

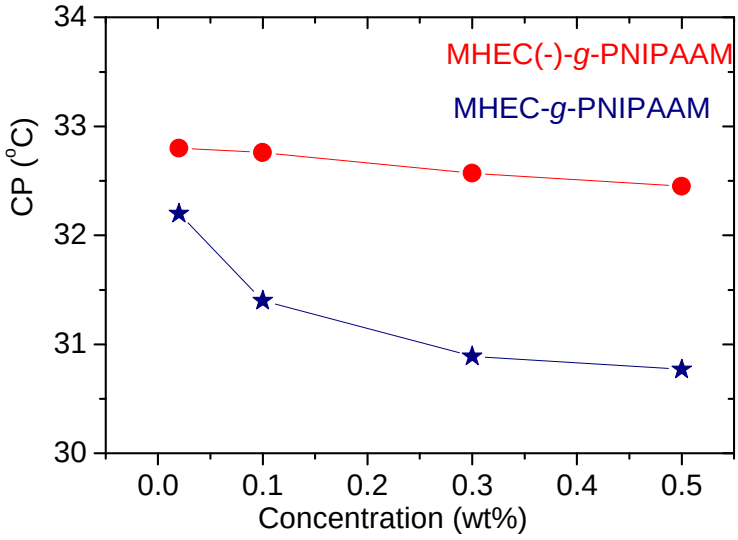

Figure 27. *Effect of polymer concentration on the cloud point for the neutral and charged polymers.*

To compare the turbidity between the neutral and the charged polymers, the turbidity for 0.3 wt % neutral- and charged polymer is displayed in *Fig. 28*. The neutral polymer clearly has a higher turbidity than the charged polymer over the whole temperature region. As mentioned above, this is due to the differences in compactness of the polymer coils. Negative charges in the structure make the polymer coil more expanded and thereby less turbid.

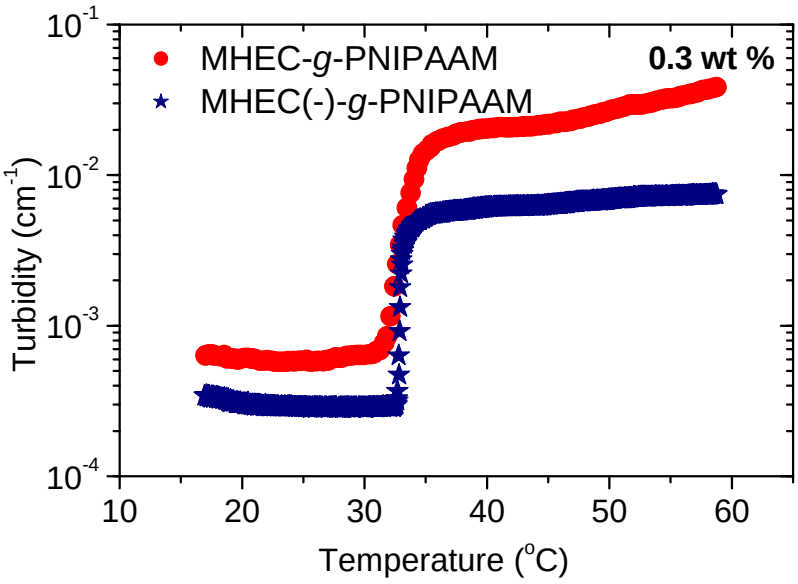

Figure 28. *A comparison of the turbidity for 0.3 wt% neutral- and charged polymer.*

4.2.2 DLS

As mentioned earlier, all the hydrodynamic radii have been analyzed at a scattering angle of 90° and the fast mode is always diffusive ($\tau_f \sim q^{-2}$). For the slow mode, since the system is not always diffusive, the apparent hydrodynamic radii at 90° have been used. *Table 3* display the q-dependency (with 3 standard deviations) together with 2/ β according to the coupling model of Ngai [59], α_s and 2/ β should be equal, and the coupling parameter n_{coup} ($\beta = 1-n_{coup}$) is a direct measure of the coupling strength between the moities probed by the slow relaxation mode and its complex environment. The coupling parameter is close to one if the strength of the interaction between the polymer chains is high. According to the coupling model of Ngai, the fast mode (τ_0) is diffusive, and the q-dependency of the slow mode can be expressed as:

$$\tau_s^*(q) = \left[t_c^{-n} \times \tau_0(q)\right]^{1/(1-n)} \sim q^{-2/(1-n)} \sim q^{-2/\beta} \qquad (11)$$

Table 3. The q-dependency of the slow relaxation mode compared with 2/ β according to the coupling model of Ngai.

Neutral polymer

Temp.	0.02 wt%		0.1 wt%		0.3 wt%		0.5 wt%	
(^{o}C)	α_s	2/β	α_s	2/β	α_s	2/β	α_s	2/β
25	2.2 ± 0.2	2.3	2.3 ± 0.3	2.3	2.4 ± 0.1	2.5	2.3 ± 0.5	2.5
30	2.2 ± 0.3	2.3	2.3 ± 0.2	2.3	2.4 ± 0.2	2.5	2.3 ± 0.2	2.5
40	2.4 ± 0.1	2.1	2.1 ± 0.1	2.1	2.1 ± 0.1	2.2	2.2 ± 0.1	2.3

Negativly charged polymer

Temp.	0.02 wt%		0.1 wt%		0.3 wt%		0.5 wt%	
(^{o}C)	α_s	2/β	α_s	2/β	α_s	2/β	α_s	2/β
25	2.5 ± 0.5	2.5	2.2 ± 0.3	2.5	2.7 ± 0.5	2.8	2.8 ± 0.2	2.8
30	2.7± 0.4	2.6	2.5 ± 0.4	2.5	2.5± 0.6	2.6	2.8 ± 0.2	2.7
40	2.1± 0.1	2.1	2.1 ± 0.1	2.2	2.1 ± 0.1	2.2	2.1 ± 0.1	2.3

As is shown in *table 3*, the agreement between α_s and 2/ β is reasonably good. Indeed, α_s is lying between 2 and 2.8. For most of the systems, $\alpha_s > 2$ at low temperatures and then it decreases towards 2 at temperatures above LCST. This suggests that there are stronger couplings in the system at low temperatures, and that the particles above LCST do not experience strong coupling effects.

The time evolution of the normalized correlation functions for different concentrations of the neutral polymer has been display in *Fig. 29*. To take into account trivial changes of the solvent viscosity with temperature, the correlation function data have been plotted against the

quantity tT/η_s (where T is the absolute temperature and η_s is the solvent viscosity). All the correlation functions are shifted toward shorter times as the temperature is increased, indicating that the sizes decrease. The correlation functions have been fitted with eq. 5 and 7. Even though it is not always evident from just looking at the correlation functions, the analysis of the correlation functions where eq. 7 was used clearly exhibit a bimodal distribution, see section 2.2.1 and the discussion regarding *Fig. 14 and 15*. The fast mode portrays the diffusion behaviour of molecularly dispersed polymer unimers or small clusters, whereas the slow mode depicts motions of large aggregates, i.e., there are two different sizes in the system. A small amount of the polymer is present as unimers and the rest is in the form of large clusters.

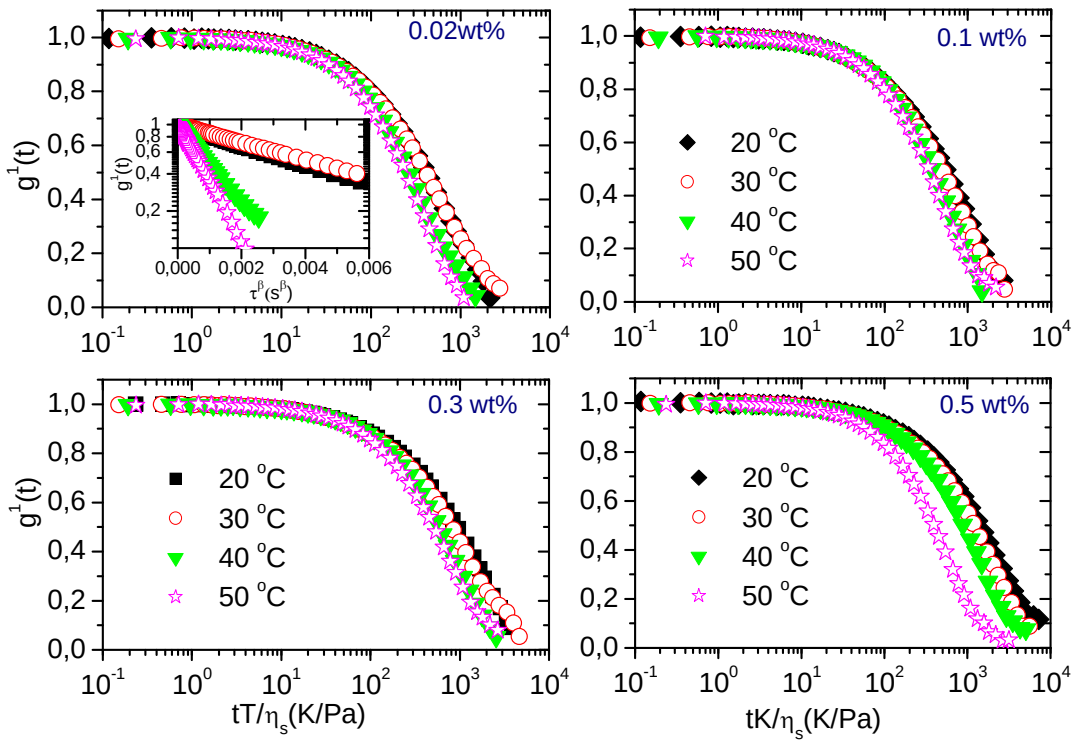

Figure 29. *Plot of the first- order electric field correlation function vs. the quantity tT/η_s (trivial changes of the solvent viscosity with temperature are thereby accounted for) at a scattering angle of 90° for 0.02 wt%, 0.1 wt%, 0.3 wt% and 0.5 wt% MHEC-g-PNIPAAM. The correlation functions have been fitted with eq. 5 and 7 depending on the sample conditions, see table 1. The inset plot demonstrates the stretched exponential character of the correlation function at long times.*

To further scrutinize the goodness of the fitting procedure, the inset plot in *Fig. 29* shows semi-logarithmic plots of $g^1(t)$ as a function of t^β. This type of plot reveals a straight line at longer times provided that the fitted exponent β is correct and therefore indicated how well the correlation function has been fitted. As can be seen from the figure, the lines are all straight at longer times. All other correlation functions have also revealed good fits with this kind of plots.

For the charged polymer, normalized correlation function data for 0.1 wt% aqueous solutions at various temperatures has been displayed in *Fig. 30*. The correlation function goes toward shorter times at elevated the temperatures, but the correlation function at 50 ^oC is shifted toward longer times. The same effect has also been observed for the other concentrations. This illustrates the temperature-induced growth of association complexes at high temperatures. During the fitting process all the correlation functions exhibit a bimodal relaxation process at low temperatures. The goodness of fitting procedure where utilized using a residual plot as in *Fig. 14 and 15*. In addition, the inset plot in *Fig. 30* shows that the correlation functions are well described by straight lines.

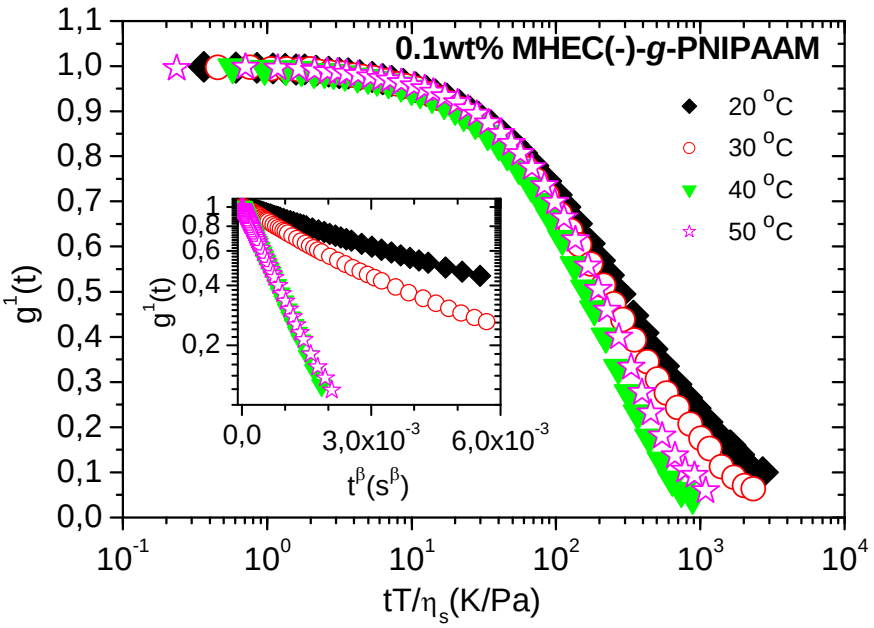

Figure 30. *First- order field correlation function (at a scattering angle of 90^o) vs. the quantity tT/ η_s (trivial changes of the solvent viscosity with temperature are thereby accounted for) for 0.1 wt% of the negative charged polymer. The inset plot demonstrates the stretched exponential character of the correlation functions at long times.*

The hydrodynamic radii of the fast ($R_{h,f}$) and the slow ($R_{h,s}$) relaxation mode are depicted in *Fig. 31*. $R_{h,f}$ and $R_{h,s}$ have been calculated from eq. 9 and represents the unimers and large clusters, respectively. We should remember that the slow mode is not always diffusive, and that therefore $R_{h,s}$ is only an apparent size. At an early stage (before the transition region), the size of the unimers is independent of the concentration, but on the other hand, the cluster sizes grow as the concentration is raised. It is interesting to note that before the transition state, $R_{h,s}$ is slightly decreasing with increasing temperature and then the sizes collapse very fast at a temperature around 33 to 35 ^{o}C. This can be explained by the presence of the PNIPAAM side chain. As the temperature increases, the PNIPAAM side chains become more hydrophobic. This results in a competition between aggregation and contraction in the system.

For the two lowest polymer concentrations, the transition region is dominated by the contraction, and around 33-35 ^{o}C there is a rapid decrease in aggregate size, followed by a continuing slow decay at even higher temperatures. The abrupt decline in aggregate sizes is also observed for the higher polymer concentrations, but for those systems, this stage is followed by a subsequent increase aggregate site before the radius decrease again at elevated temperatures. This behaviour clearly illustrates that there is a competition between smaller aggregate sizes caused by a contraction of the existing aggregates and increasing aggregate sizes due to enhanced aggregation. After the maximum, most of the hydrophobic PNIPAAM groups are located in the core of the aggregates, and the surfaces of the particles are covered by a protecting hydrophilic HEC layer. The hydrophobic PNIPAAM groups located in the core of the aggregates results in a contraction of the clusters.

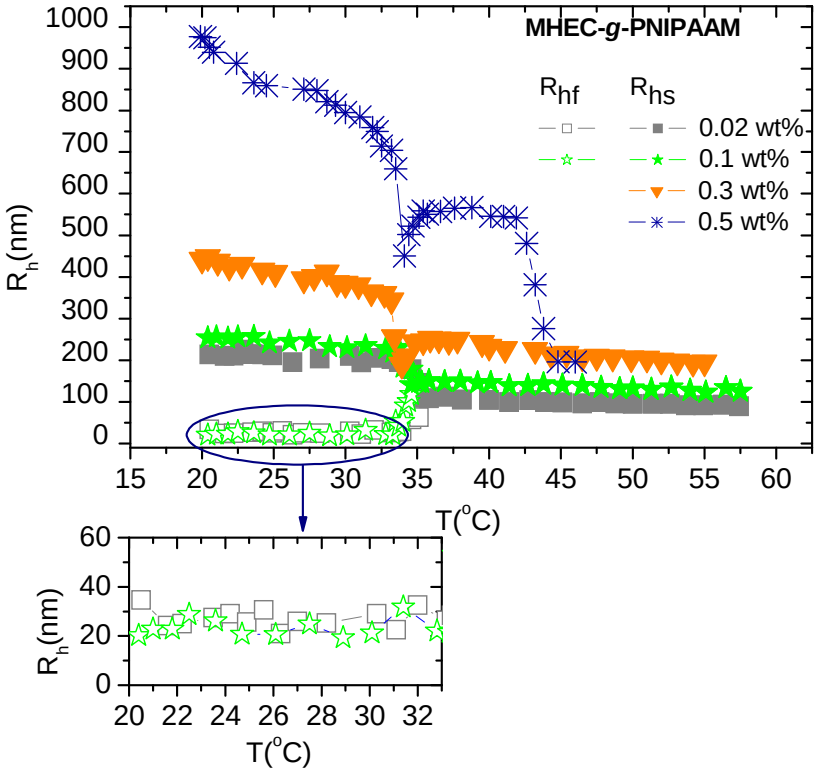

Figure 31.*Temperature dependencies of the apparent hydrodynamic radii determined from the fast relaxation time ($R_{h,f}$) and the slow relaxation time ($R_{h,s}$) through the stoke Einstein relationship for neutral polymer at different concentrations.*

Fig. 32, display the hydrodynamic radii for charged polymer, the general feature for all polymer concentrations is the marked contraction of the polymer clusters at moderate temperatures. At low temperatures before the transition state, a bimodal size distribution has been observed for all the considered concentrations (0.02 wt% to 0.5 wt%). $R_{h,f}$ is independent of concentration while $R_{h,s}$ is concentration dependent. As can be seen from *Fig. 32*, $R_{h,s}$ gradually decrease until the temperature is around 34 ^{o}C, then an abruptly decline of the sizes is observed. Unlike the neutral polymer in *Fig. 31*, no maximum is observed for the charged polymer. This is due to the repulsive forces between the negative charged groups which reduce the tendency of the polymers to form aggregates. After the transition state, the cluster sizes gradually increase of because high temperatures, the attractive forces overcome the repulsive electrostatic interactions and aggregation is observed.

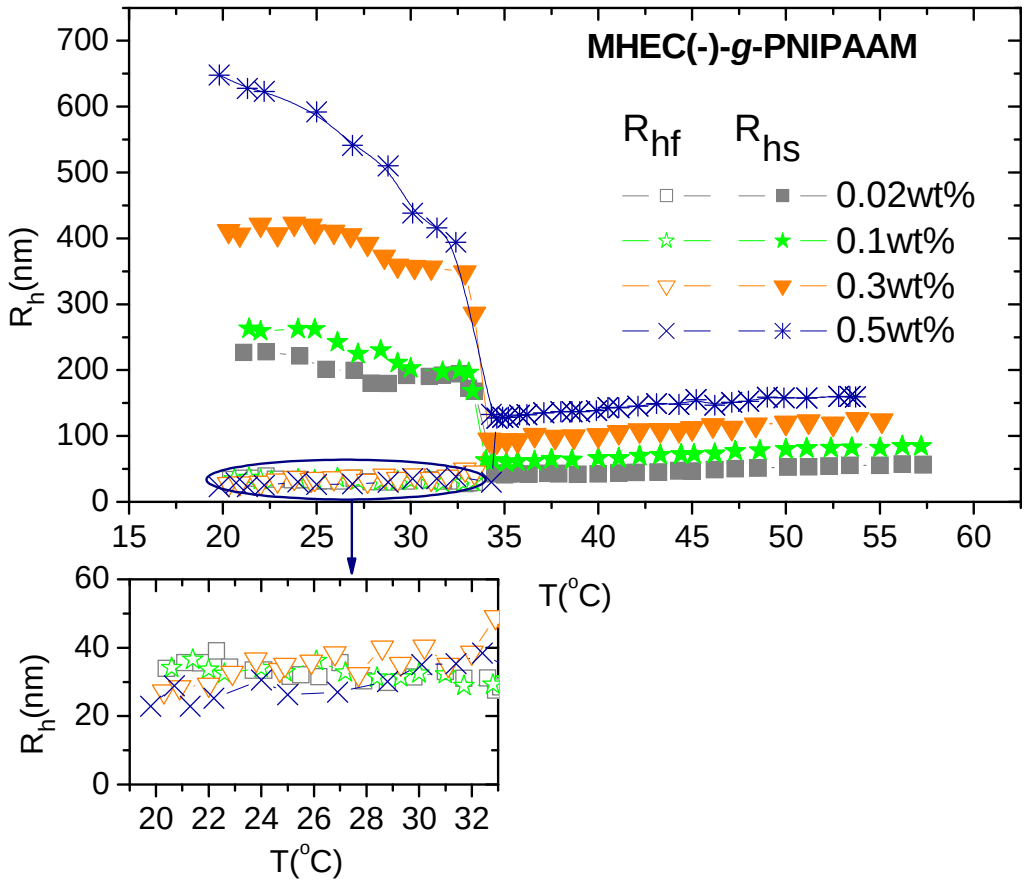

Figure 32. *Temperature dependencies of the apparent hydrodynamic radius ($R_{h,s}$ and $R_{h,f}$), calculated through the Stoke Einstein relation for different concentrations of the negatively charged polymer.*

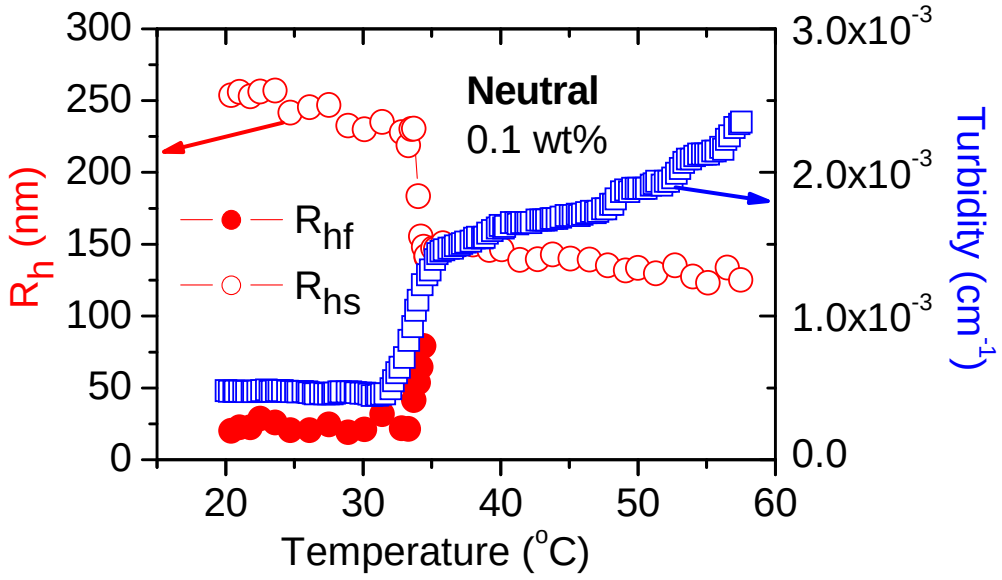

Figure 33. *A comparison of the turbidity and the hydrodynamic radius for the neutral polymer.*

Fig. 33 displays a direct comparison of the DLS data with the turbidity results for 0.1 wt% of the neutral polymer. The turbidity increase as the radius of the aggregates decrease. As mentioned earlier, we have a competition between contraction and aggregation in this system. This explains why at the transition state, the sizes first decrease then they increase a little bit before it falls off again. The factors that affect the turbidity are:

- Particle size
- Number of particles
- Particle compactness (the ratio between the refractive index of the particle and the refractive index of the solvent: n_p/n_s.)

In the transition region, the particles aggregate, i.e., the number of particles decreases. In addition the size of the particles is reduced. Both this factors should reduce the overall turbidity, and therefore the enhanced turbidity values must be due to the formation of more compact particles. This effect has been observed before for PNIPAAM microgelsl.[60]

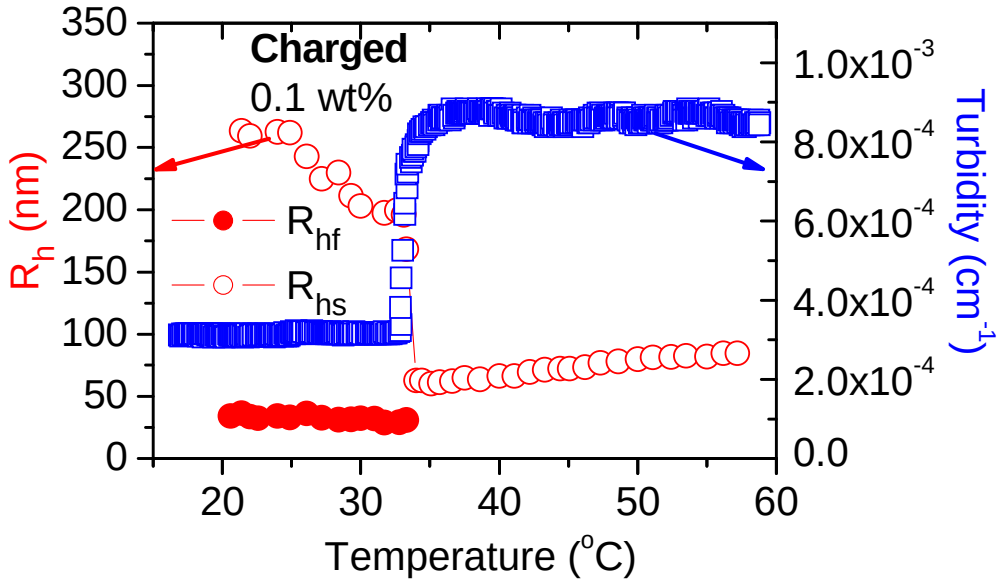

Figure 34. *A comparison of the turbidity and the hydrodynamic radius for the charged polymer.*

For the charged polymer, a comparison of the DLS data with the turbidity results for 0.1 wt.% samples is displayed in *Fig. 34*. The turbidity increases as the radius decrease, suggesting that the compactness of the particles is causing the turbidity transition for this system also. As mentioned earlier regarding *Fig. 33*, the enhanced turbidity values observed for more compact particles is due to the changes in the ratio between the refractive index of the particle and the refractive index of the solvent: n_p/n_s. When this ratio increases, the turbidity of the sample goes up. Particles that are very swollen in the solvent consist mainly of solvent and n_p/n_s is close to unity, while compact particles have a high local concentration of polymer giving higher values of n_p/n_s. When the polymers contract, the differences in refractive index between the solvent and the aggregates increase, and the turbidity goes up. The charged polymer is more swollen due to the electrostatic interactions, and therefore the turbidity is lower than for the neutral polymer. At elevated temperatures, the neutral polymer continues to contract, and hence the turbidity increases. The repulsive forces inhibit further contraction of the charged polymer, and the turbidity flattens out at elevated temperatures. The turbidity transition for the charged polymer is much sharper than what is observed for the neutral polymer. This is probably caused by the competition between contraction and aggregation in the neutral polymer giving rise to a more gradual transition.

The correlation functions for the charges and neutral polymers at a low and a high temperature is displayed in *Fig. 35*. A progressive slowing down of the relaxation process as the concentration increases is observed, confirming that $R_{h,s}$ increase with the concentration. This information fit nicely with what is observed in *Fig. 31 and 32.*

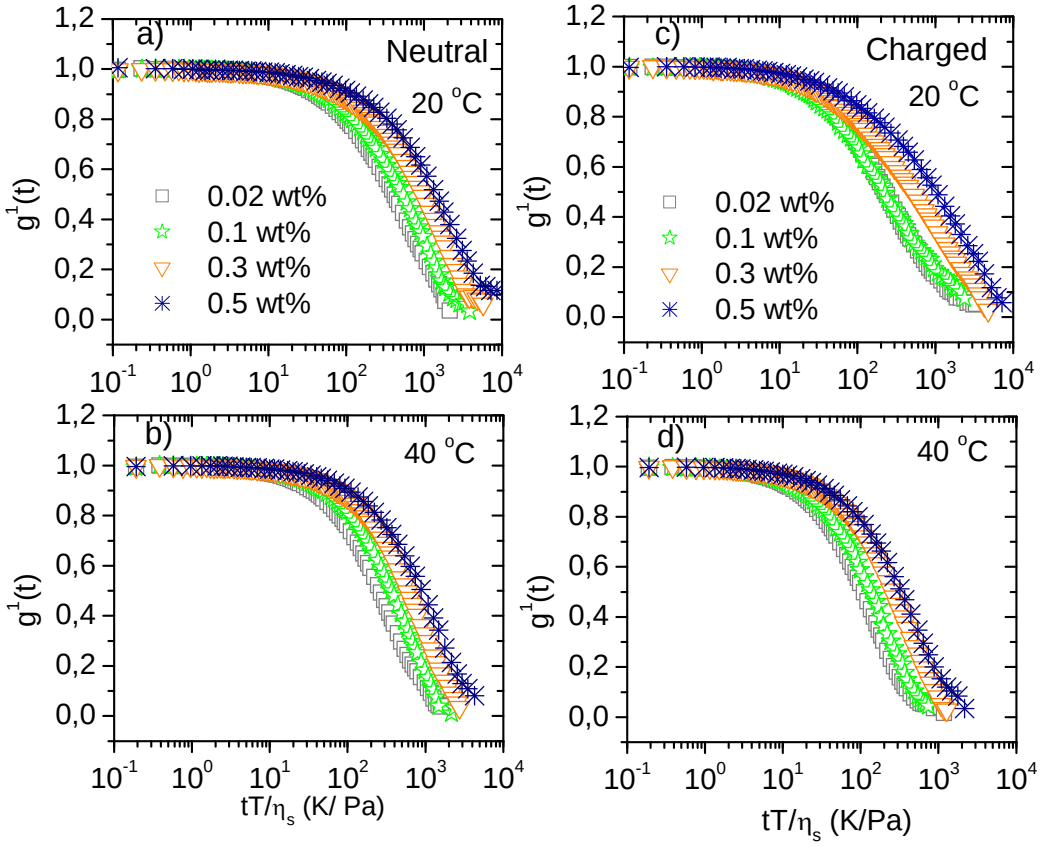

Figure 35. *Plot of the first-order electric field correlation function versus tT/η_s at a scattering angle of 90^o for different concentrations at temperature 20 ^{o}C and 40 ^{o} where a) and b) display the neutral polymer and c) and d) the charged polymer.*

The ratio between the amplitudes of the slow and the fast mode is displayed in *Fig. 36 and 37*. In *Fig. 36* it can be seen that the slow mode for the neutral polymer is more dominant for the 0.1 wt% sample than for 0.02 wt%. This is due to the amount of polymer present in the sample. When adding more polymers to the system, the average distance between the polymer chains is smaller and they will aggregate easier. Accordingly, the number of unimers will be diminished at higher concentrations, and the number of unimers is much lower for 0.1 wt% than for 0.02 wt%. At the transition state, A_s/ A_f decreases, indicating that the number of

aggregates decreases due to interaggregate associations. At even higher temperatures the slow relaxation mode dominates the whole system. Suggesting that at this stage none or very few, single molecular coils are left in the sample. The data in *Fig. 36* is quite noisy since the amplitude of the fast mode is small.

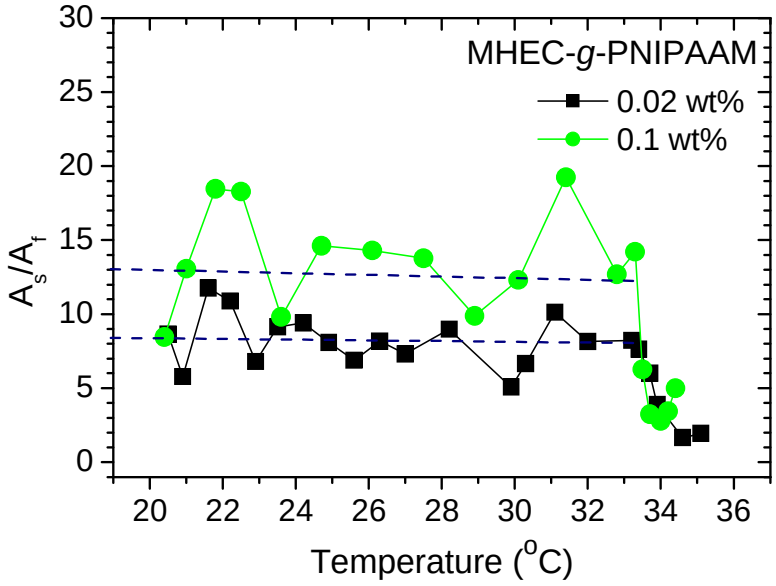

Figure 36. *Amplitudes A_s/ A_f as function of temperature for concentration 0.02 wt% and 0.1 wt% neutral polymer. The dashed line represents an average in the region before the ratio start to decrease.*

On the other hand, in *Fig.37* an interesting trend for charged polymer is observed. Again, the clusters are more dominating as the concentration is increasing. As is shown in the inset plot in *Fig. 37*, at a concentration of 0.5 wt%, the values of A_f is around 0.1 and it is barely possible to extract the fast relaxation mode from the correlation functions. The amplitude of the fast mode increases with the temperature. This could be due to the decreased sizes of the large aggregates, see *Fig. 32*, which makes the slow mode less dominant.

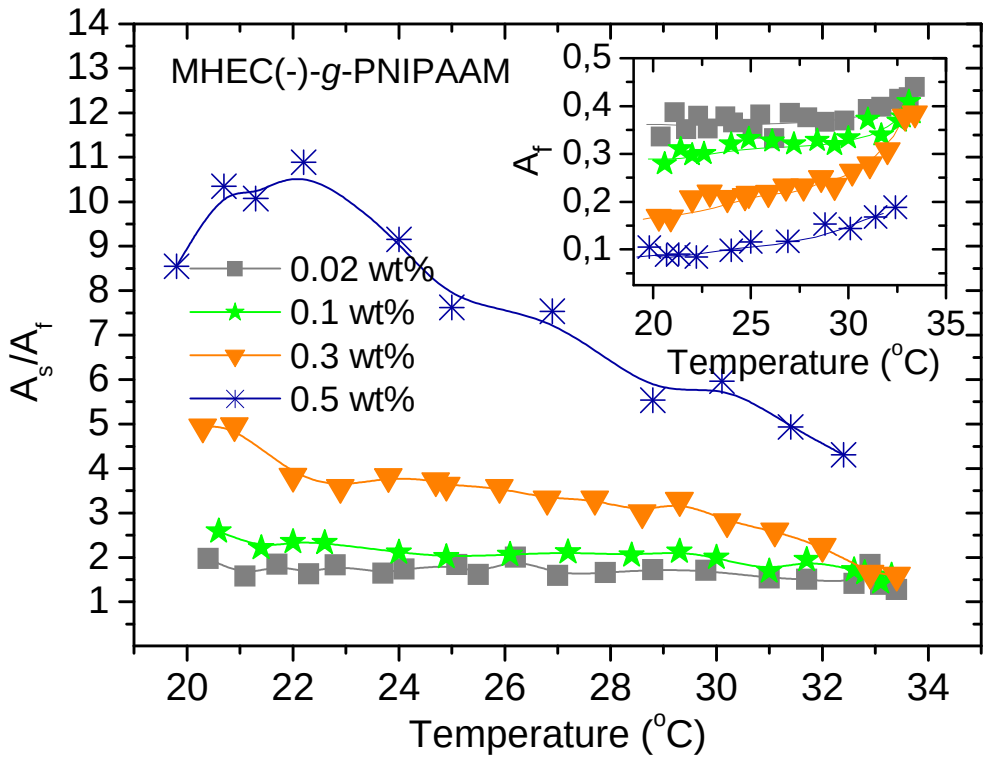

Figure 37. *Amplitudes A_s / A_f as function of temperature for different negative charged polymer concentrations.*

In *Fig.38* the general trend of stretched exponential (β) gives the information about the distribution of relaxation times for the slow mode. If β = 1, the sizes are monodisperse and when β decrease, this indicates that the size distribution become wider. As mentioned earlier that β can also be used to calculate the as coupling parameter in Ngai's coupling model.

For the neutral polymer in *Fig. 38 a*, β ~ 0.87 at low temperatures for 0.02 and 0.1 wt%. At the higher concentrations (0.3 and 0.5 wt%), β ~ 0.8; the size distribution is wider because with more polymer present, it is easier to form aggregates of different sizes. The distribution is smaller after the transition state, β ~ 0.92. This shows that the size distribution is nearly monodisperse, indicating that particles of a uniform size are formed after the transition region. This effect has also been observed for other thermoresponsive polymers.[61] For the charged polymer in *Fig. 38 b*, the distribution at low temperatures increases with the polymer concentrations and it is also lower than for the neutral polymer. The negative charges it

prevents the polymer coils from aggregating. Therefore the size distribution is less homogeneous than what was observed for the neutral polymer. We should note that HEC itself is very polydisperse, and in order to give a small size distribution, there should be an optimal aggregate size that is thermodynamically favorable in the system. At high temperatures β are nearly 0.97 for the lowest concentration which is very close to one, indicating a monodisperse size distribution. Afterwards, β decrease as the concentration increase. This is due to an increased tendency to form aggregates when more polymers is present in the system, in this case some polymers may aggregate faster than others and the sizes will vary more than for the dilute solutions. As the polymer concentration is increased, the effect of the electrostatic repulsions is diminished both because of a screening out of some of the charges by counterions and by the enhanced hydrophobic interactions at higher polymer concentrations.

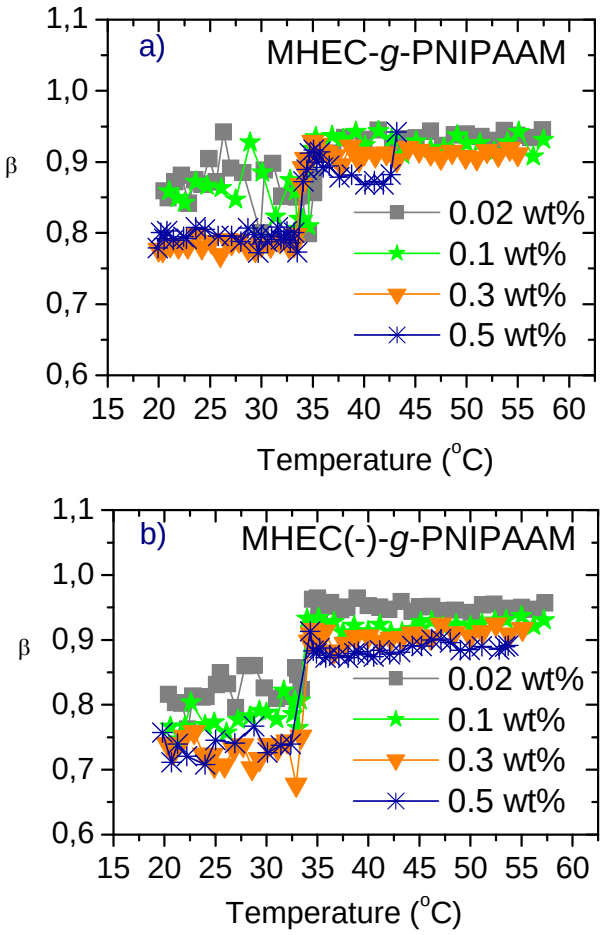

Figure 38. *Plot of the stretched exponential for the slow mode as a function of temperature for different concentrations. A) neutral polymer and B) negatively charged polymer.*

A schematic illustration of the effects of the temperature induced aggregation and contraction of the polymer clusters in a dilute solution of the charged and neutral polymers is depicted in *Fig. 39*. In the presence of associative side chains sticking out from the aggregate, the particles has the possibility to aggregate with other cluster until there is no more side chains left on the outside of the aggregate. Then the polymer coil is fully protected by a hydrophilic corona. Since the charged polymer had electrostatic repulsive forces, this repulsive force must be overcome before they can make associations. The illustration is based on the hydrodynamic radii in *Fig.31 and 32*. For the neutral polymer a competition between aggregation and contraction is observed around LCST, followed by a gradual decrease in aggregate size as they continue to contract. For the charged polymer, the repulsive electrostatic forces prevent aggregation and contraction dominates around LCST. At high temperatures, the attractive forces are more dominant and aggregation is observed.

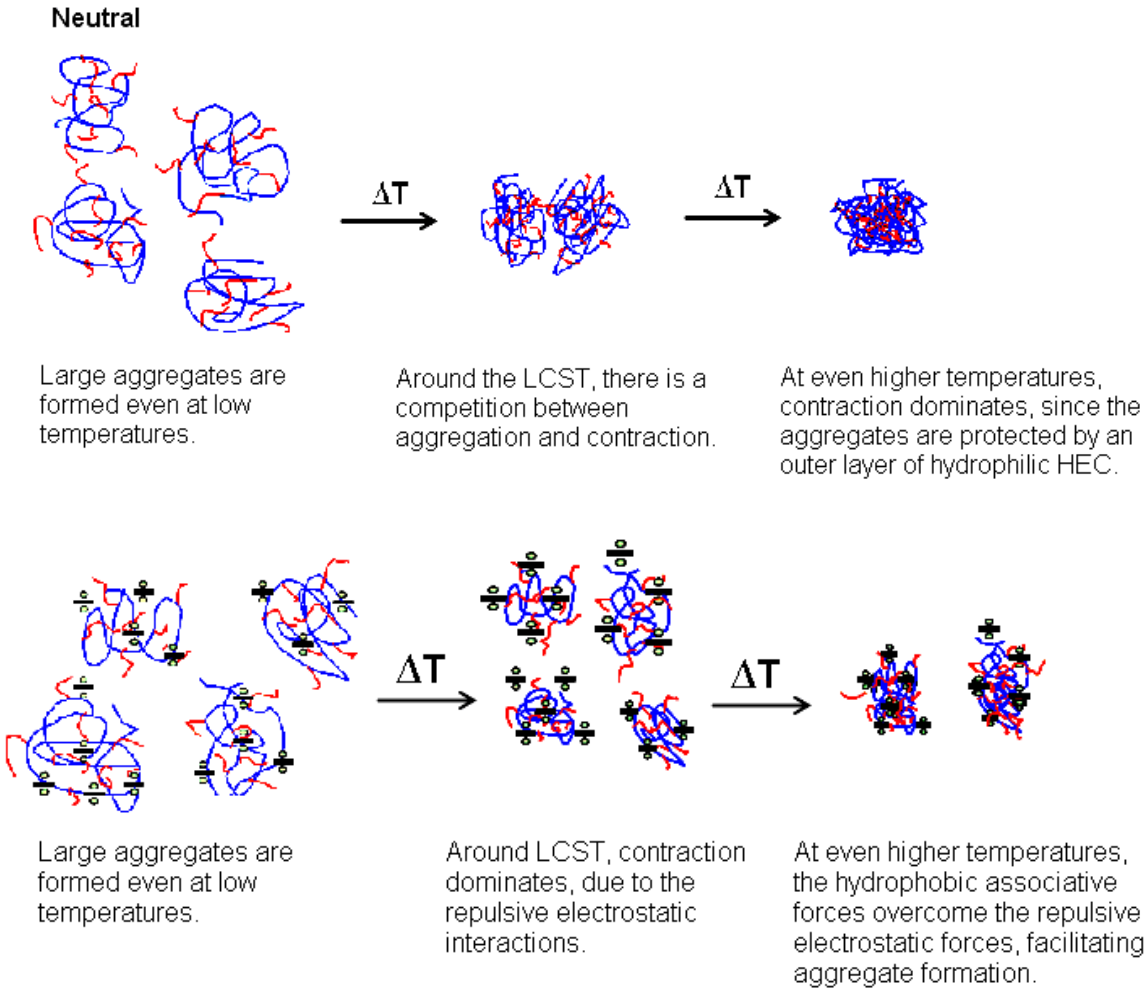

Figure 39. *Schematic illustration of the effect of temperature inducted aggregation.*

4.2.3 Salt induced aggregation

In order to see the effect of the screening out of the electrostatic interactions, salt (NaCl) was added to the system. With the aid of turbidity and DLS, we can study its behavior and see if there are any differences. The effect of salt addition on the turbidity of the two polymers is displayed in *Fig. 40*. The same transition in the turbidity around LCST is observed when salt is added in the system, but the turbidity values are generally much higher in the presence of salt. The effect of salt addition is especially strong for the charged polymer at elevated temperatures, where is assumes much higher values than what is observed in the absence of salt. Interestingly, the turbidity values are even higher than what is observed for the neutral polymer either in the absence or presence of salt. In order to explain this behavior, we need to examine the DLS data, and this effect will be discussed in more detail in the DLS part below.

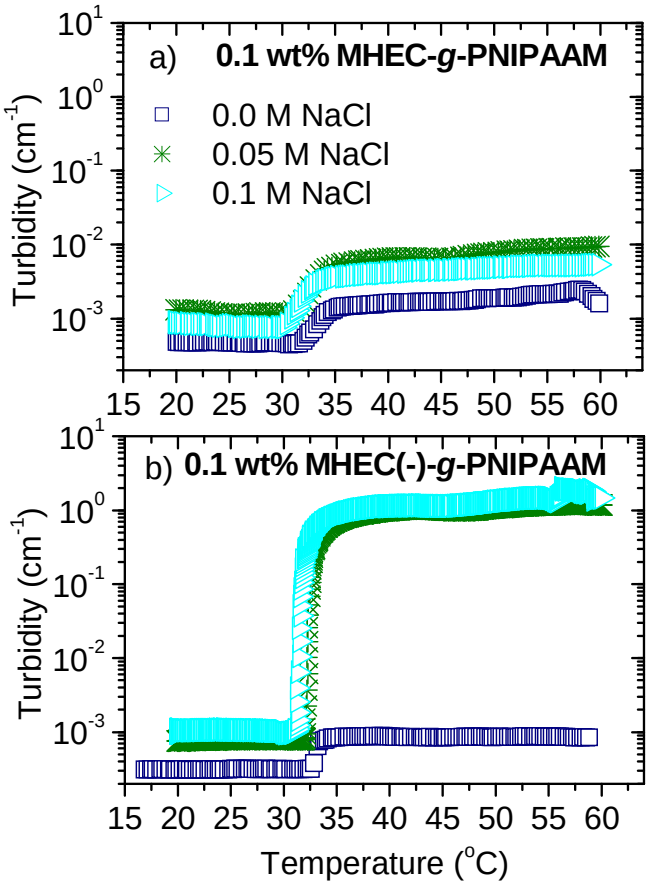

Figure 40. *The effect of salt addition on the temperature dependence of the turbidity at a polymer concentration of 0.1 wt% of a) the neutral polymer and b)the negatively charged polymer.*

Before we start to examine the DLS result, we should remember that $R_{h,s}$ is only an estimate because this mode is not diffusive even at low temperatures. This can be seen in *Fig. 41* for 0.1 wt% of the charged polymer with and without salt. If the system is diffusive, the normalized correlation function at different scattering angles should collapse on each other. Since most of the correlation functions are separated at longer times, this indicates that the slow mode is not diffusive. The same behavior has been observed for the neutral polymer.

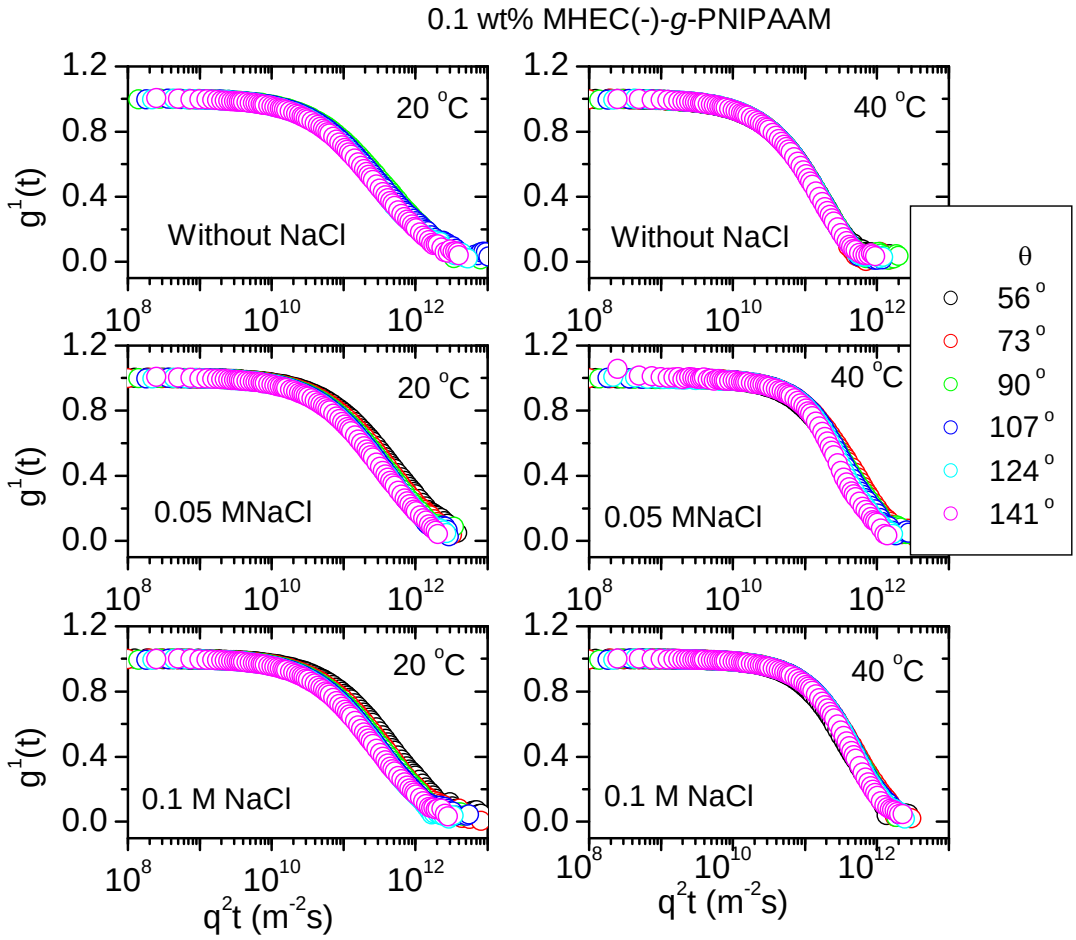

Figure 41. *Plot of first-order electric field correlation function as a function of q^2t for different salt concentrations and at 20 °C and 40 °C for 0.1 wt% of the charged polymer.*

The effect of salt on R_h for the two polymers is displayed in *Fig. 42*. As expected the effect of salt addition on the neutral polymer enhance the tendency to form large aggregates. Salt induces poorer thermodynamic conditions for the polymer (salting out effect) which induce larger polymer aggregates. On the other hand at low temperatures, the charged polymer is not significantly affected by the addition of salt. This is surprising since one would expect that

adding salt would screen out the electrostatic repulsions in the system and thereby cause the charged polymer to behave as the neutral polymer. At least, when 0.1 M NaCl is present one would expect that all charges is screened out. The reason could be that the charged groups on the polymer could render the polymer more hydrophilic even when most of the charges have been screened out. This counteracts the salting-out effect and could cause better thermodynamic conditions. Around the transition region, the neutral polymer exhibits the same trends as the solution without salt. This is reasonable, because the system only experiences generally poorer thermodynamic conditions in the whole temperature range. For the charged polymer, aggregation dominates at the transition state and at higher temperatures the sizes slightly decrease because contraction dominates at elevated temperatures. Thereafter, the solution scatters too much (multiple scattering) and the correlation functions could not be analyzed at temperatures above 45 ^{o}C. The domination of aggregate formation in the transition region, and the following contraction suggest that the charges have been screened out.

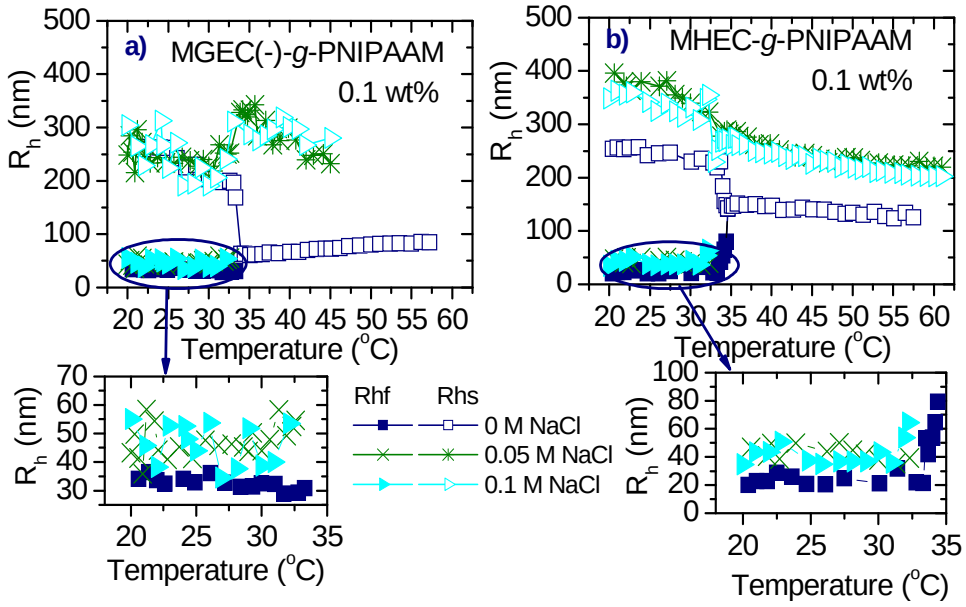

Figure 42. *Temperature dependencies of the apparent hydrodynamic radius ($R_{h,s}$ and $R_{h,f}$), for different salt concentrations, a) the negatively charged polymer and b) the neutral polymer.*

In order to elucidate the differences between the charged and the neutral polymers in the presence of salt, the hydrodynamic radii and the turbidity of both polymers have been compared in *Fig. 43*. At low temperature, the aggregates of the charged polymer are smaller

than what is observed for the neutral polymer, and it also has a lower turbidity. This indicates that even when the charged groups are screened out, they contribute to better thermodynamic conditions preventing the sample from forming large aggregates at low temperatures. However, at elevated temperatures the charged polymer creates larger aggregates than the neutral polymer. In addition the turbidity for the charged polymer is much higher, indicating that the aggregates are very compact compared to what is observed for the neutral polymer. This enhanced tendency to form large compact aggregates at elevated temperatures could be caused by the larger substitution degree of PNIPAAM on the charged polymer, making it much more hydrophobic at high temperatures.

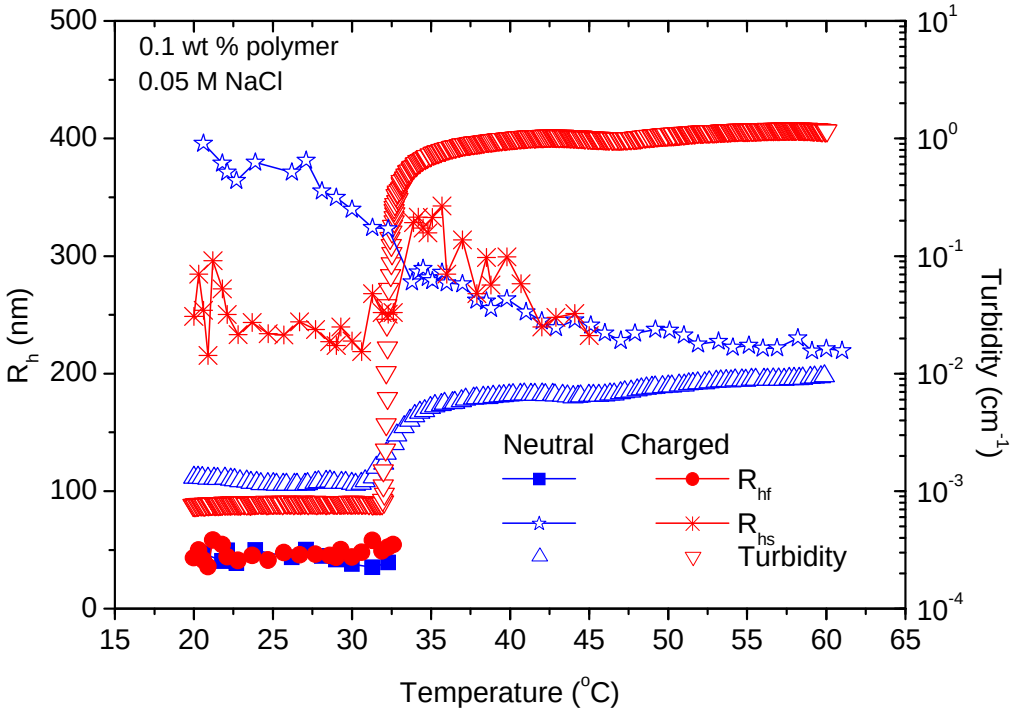

Figure 43. *Temperature dependencies of the apparent hydrodynamic radius ($R_{h,s}$ and $R_{h,f}$),and the turbidity for the neutral and the negatively charged polymer in the presence of 0.05 M NaCl.*

4.3 High Concentrations (0.5 wt% - 5 wt%)

4.3.1 Turbidimetry

Fig. 44 displays the heating curves (0.2 ^{o}C/min) of the turbidity for the neutral and negative charged polymers. It is obvious that the turbidity increases as the concentration increase at the transition state. As mentioned earlier in section 4.2.2 for the dilute regime, the turbidity is dependent on the number of particles, the size of the particles, and the compactness of the particles (change in n_p/n_s). Analogous to this, the turbidity of an associative semidilute solution is affected by the size, number and compactness of aggregated microdomains in the sample. In the concentration range 1.0 wt% to 5 wt% for the negatively charged polymer and 3-5 wt% for the neutral polymer, the sharp upturn of the turbidity curve at elevated temperatures reflects the formation of intermolecular associations causing local inhomogenittes in the system. For the two highest polymer concentrations, a peak is evident in the turbidity curves, before they flatten out at elevated temperatures. This reflects the interplay between the number, size and compactness of the association structures. The upturn is caused by the formation of compact association structures and at the top of the peak, a downturn before the curves flatted out suggest that either the number of associated microdomains are reduced because several associative clusters are combining together, or that the size of the associated microdomains is decreasing because of a contraction. Otherwise, the turbidity at elevated temperatures is high for 1 wt% for the charged polymer while for the neutral polymer the concentration has to be increased to 3 wt% before the samples becomes visibility turbid at high temperatures. This is surprising since repulsive negative charges should reduce the potential to form associations in the system. However, the more expanded conformation of a charged polymer might increase the overlap concentration which suggests that at 1.0 wt% the charged sample is further into the semidilute regime than the neutral sample, causing it to behave more like the higher concentrations.

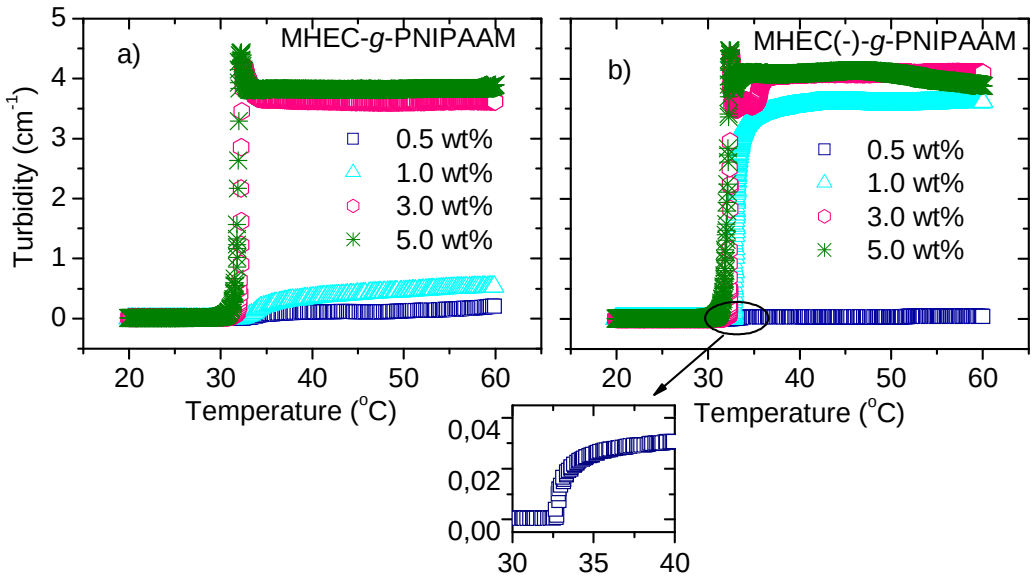

Figure 44. *Temperature dependence of the turbidity for different concentration of a) neutral and b) negatively charged polymer.*

The cloud point in *Fig. 45* is higher for the negatively charged polymer than for the neutral polymer. This is due to the electrostatic repulsion between the charged groups, which counteract the associative interactions.

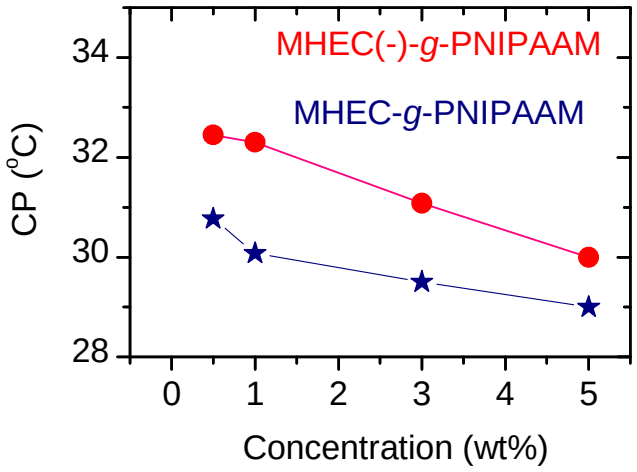

Figure 45. *Effect of polymer concentration on the cloud point for the neutral and charged polymers.*

4.3.2 Rheology

Fig. 46 and 47 demonstrates the effect of shear rate on the measured viscosity for solutions of the neutral and charged polymers. By plotting the quantity η/η_s (η is the complex viscosity and η_s is the solvent viscosity) against the temperature, trivial changes of the solvent viscosity with the temperature have been taken into account. These viscosity curves illustrate the viscosities as a function of increasing shear rate. When the subsequent high to low shear rates was measured, no significant hysteresis effects were detected. Therefore, only the up-ramp curves will be presented and discussed below.

The viscosity measurements for the neutral polymer solutions are displayed in *Fig 46*. At the temperatures 20 ^{o}C and 30 ^{o}C, the viscosity is low and nearly shear rate independent over the considered shear-rate region. The concentrations 0.5 wt% and 1.0 wt%, is particularly flat indicating that there are no or low interactions between polymer chains. The 3 wt% and 5wt% sample exhibit some shear thinning effects at high shear rates. This suggests that the network is disrupted. For the 5 wt% sample, shear thickening is observed at 35 ^{o}C in the low shear region, followed by shear thinning at higher shear rates. The former effect signalizes a shear-induced reorganization of the association network, probably due to stretching and alignment of the chains, thereby facilitating the formation of more intermolecular junctions. The progressive increase in viscosity as the temperature rises is related to the large association structures caused by hydrophobic interactions. Even at high polymer concentrations and high molecular weights, the network will rearrange back to its original configuration. The drop in the viscosity at high temperatures for the low concentrations shows that the association complexes are breaking up. For the lowest concentrations, the viscosity is highest at 35 ^{o}C, and at higher temperatures the viscosity of the samples is reduced. This is probably due to the formation of a fragmented network, where the strong association forces at elevated temperatures causes the formation of fragmented associated clusters. At higher polymer concentrations, the high amount of polymer present in the system prevent the network from forming separate fragments, and an interconnected network is formed. This causes enhanced viscosity values at elevated temperatures.

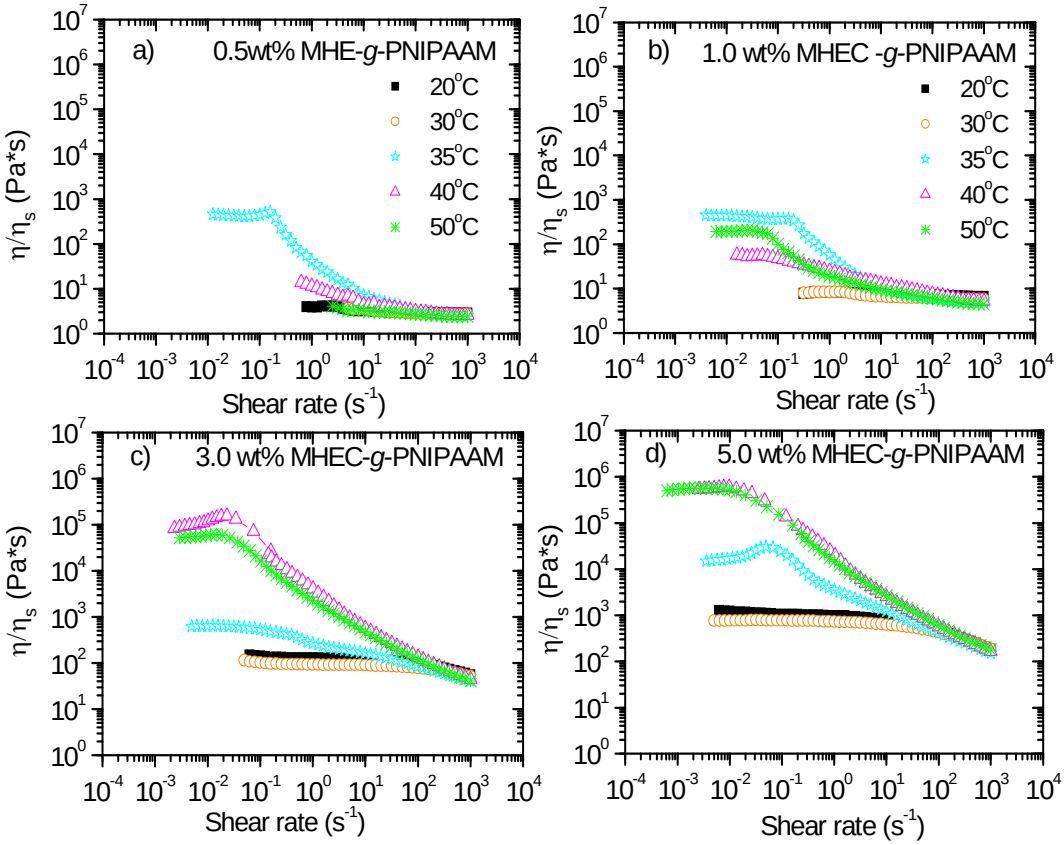

Figure 46. *Shear-rate dependencies of the reduced viscosity for different neutral polymer concentrations at the temperatures indicated.*

In *Fig. 47* a similar behaviour has been revealed for the charged polymer. The shear thickening behaviour is also appeared for this polymer, but it occurs at 30 °C instead of 35 °C as for the neutral polymer. The highest concentration which can be measure for this polymer is 1.0 wt%. At 3 wt% and 5 wt% the measurement could not be conducted over the whole temperature region, because the polymer samples expanded out of the measuring system when the temperature was above 30 °C. This effect could be caused by the repulsive forces between the negative charges, which are enhanced by the applied shear forces. Therefore the 3 wt% and 5 wt% samples have not been shown in *Fig. 47*, but the zero-shear rates for the temperatures that could be measured have been showed in *Fig. 48 b*.

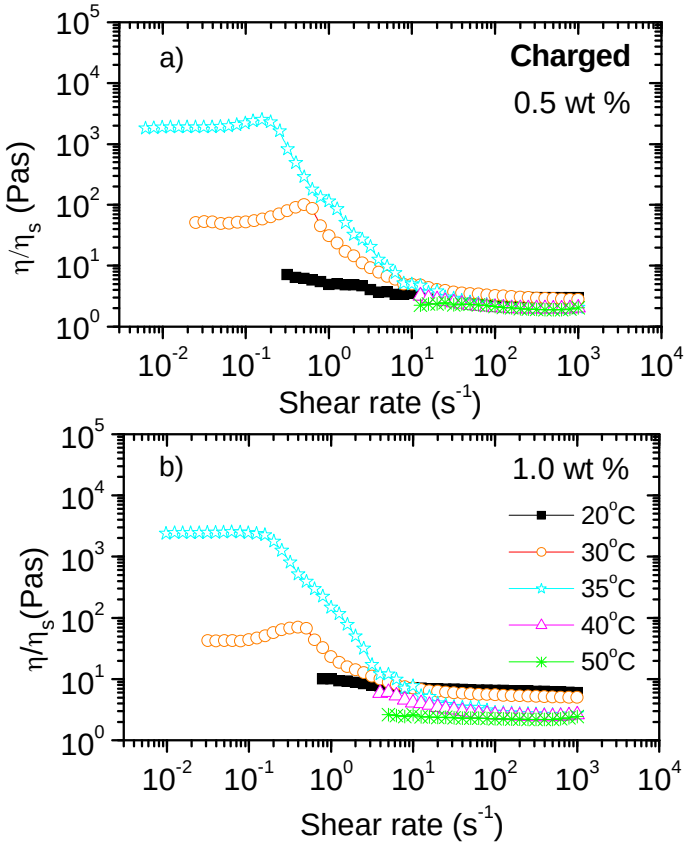

Figure 47. *Shear-rate dependencies of the reduced viscosity for 0.5 wt% and 1.0 wt% solutions of the charged polymer at the indicated temperatures.*

Fig. 48 shows the zero-shear viscosity plotted as a function of temperature for all the investigated polymers. As is evident for the 0.5 wt% and 1.0 wt% samples, the viscosity values goes through a maximum which is located at 35 ^{o}C for both polymers, but which has much higher amplitude for the charged polymer. The higher values indicate that the connectivity is better for the charged polymer. The viscosity decreases at elevated temperatures indicate a fragmentation of the network. By using eq. 10, the power law index for shear thinning at 35 ^{o}C is found to be nearly -1 for the neutral polymer while the negatively charged polymer has a value nearly -1.5 for 0.5 wt% and 1 wt%. This means that when we introduce negative charges, each cluster will swell and the PNIPAAM side chains can easily associate with other side chains and an interconnected network will form. This could be the reason for the higher zero-shear viscosity peak for the negative charged polymer than neutral polymer at the same concentration. The disrupting of the network appear very

rapidly at a certainly shear rate because the attached negatively charged groups makes the associating network slightly weaker than without charges.

At higher concentrations, only the neutral polymer gave a complete temperature scan. The zero-shear viscosity is almost flat at lower temperatures before it increases and then flatted out at 40 ^{o}C. The idea could be that at low temperatures, none or few hydrophobic interactions are present just entanglements in the system. At the transition state, three factors are contributing to the viscosity values:

- The hydrophobic associations
- Entanglements
- High polymer concentration.

The combination of these three factors keeps the connectivity in the network giving rise to the high viscosity values at high temperatures. For the charged polymer at low temperatures, the zero-shear viscosity increase as the concentration increase.

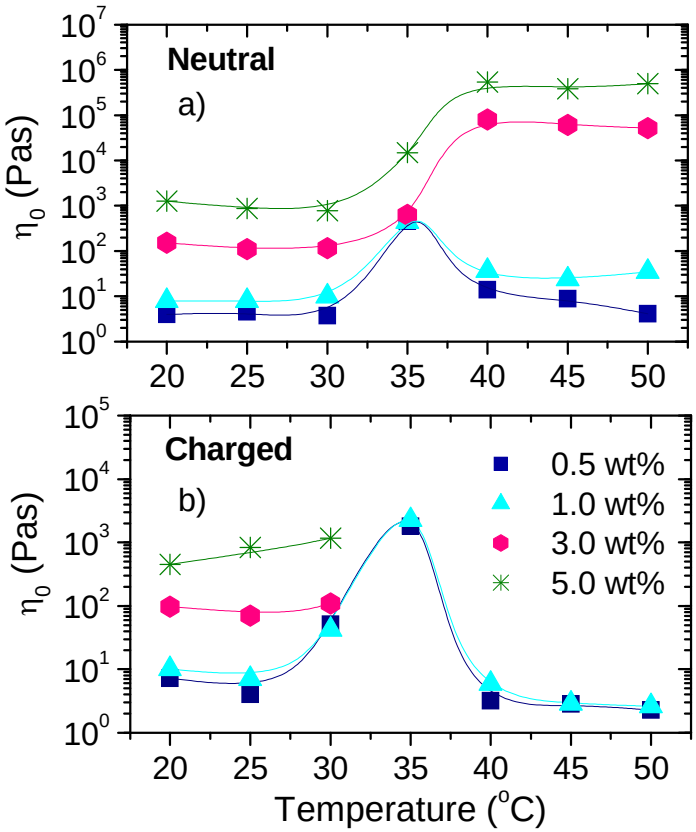

Figure 48. *Zero-shear viscosity as a function of temperature for a) the neutral polymer and b) the negatively charged polymer.*

4.3.3 Rheo-SALS

Fig. 49 and 50 show typical SALS patterns obtained from 1 wt% and 3 wt% solutions at different temperatures and shear rates. The 2D colour images reveal that the scattered intensity increase as the temperature is raised. This behaviour substantiates the hypothesis launched above that huge interchain complexes are formed at high temperatures. The images in *Fig. 49 and 50* indicate how the association structures changes during the temperature scan. We can not gain an exact explanation for what happen in the system from these pictures alone, but in combination with additional information such as the rheological data and the intensity vs temperature. We can obtain a more through understanding of the system.

In *Fig.49* the scattering patterns with no shear rate and at $\dot{\gamma} = 1\ s^{-1}$ for 1 wt% and 3 wt% of the neutral polymer is displayed. We observe that for both concentrations the scattering intensity is higher when shear is applied. With zero shear, we measure at quiescent conditions and see if the intensity increase or decrease at elevated temperatures. We observe that the intensity increase with temperature when no shear forces have been applied. This is reasonable because of the enhanced hydrophobic interaction in the system at high temperatures, which make intrachain associations that influence the network structure. When a constant shear ($1\ s^{-1}$) is applied, the chains are forced in contact with each other and the network is reorganized, promoting the growth of association structures in this system, giving more intense scattering patterns. With 3 wt%, the scattering patterns are larger than for 1 wt% because the presence of more polymer in the system which also contribute to more associations and an overall higher scattering intensity. Factors that can influence the scattering patterns are:

- Concentration
- Size and shape of structures in the sample
- Homogeneous/heterogeneous network
- Compactness of structures (n_p/n_s)
- Bubbles in the picture and other artifacts

Fig. 49 revealed that the system is a randomly organized because of that the pictures are isotropic in all directions and also at all temperatures. This effect has also been observed at higher shear rates ($10\ s^{-1}$ and $100\ s^{-1}$) and concentrations (5 wt%), see appendix. For the highest shear rates, some of the systems exhibit an orientation in the opposite direction of the shear. This might be due to turbulence in the system.

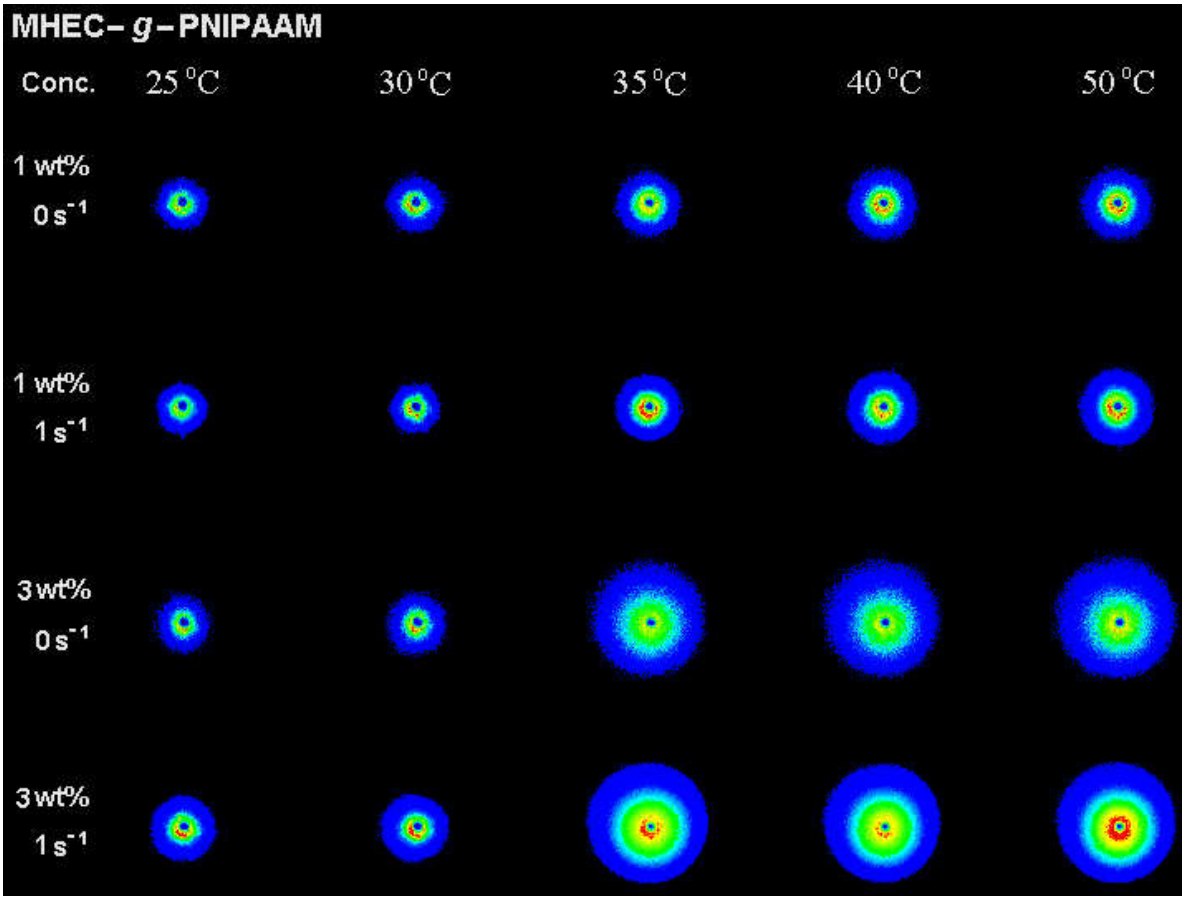

Figure 49. *2D SALS patterns of 1.0 wt% and 3.0 wt% solutions of the neutral polymer at different temperatures at the shear rates indicated.*

Fig. 50 illustrates the scattering patterns for the charged polymer. It shows the same trend as for the neutral polymer with regards to the effect of shear. The scattering patterns are larger with an overall higher intensity when the temperature or the concentration is increased. Note that at 33 ^{o}C in the presence of shear forces for the 3 wt% sample, the scattered intensity profile exhibits an anisotropic pattern with an elliptical image. This type of feature is due to the charged groups which repel each other causing a reorganization of the polymer chains which aligned themselves in the shear direction. When increasing the temperature, the elliptical image goes towards a circular pattern again. The random direction of the association structures dominates again. The same effect has been observed for 10 and 100 s^{-1} and also for the 5 wt% sample, see appendix. With the 1 wt% sample, the elliptical pattern did not appear even at high shear rates. All these effects will be discussed in more detail below. We are going to look at the rheology and the intensity verses temperatures to see why the neutral and charged polymer is behaving so differently.

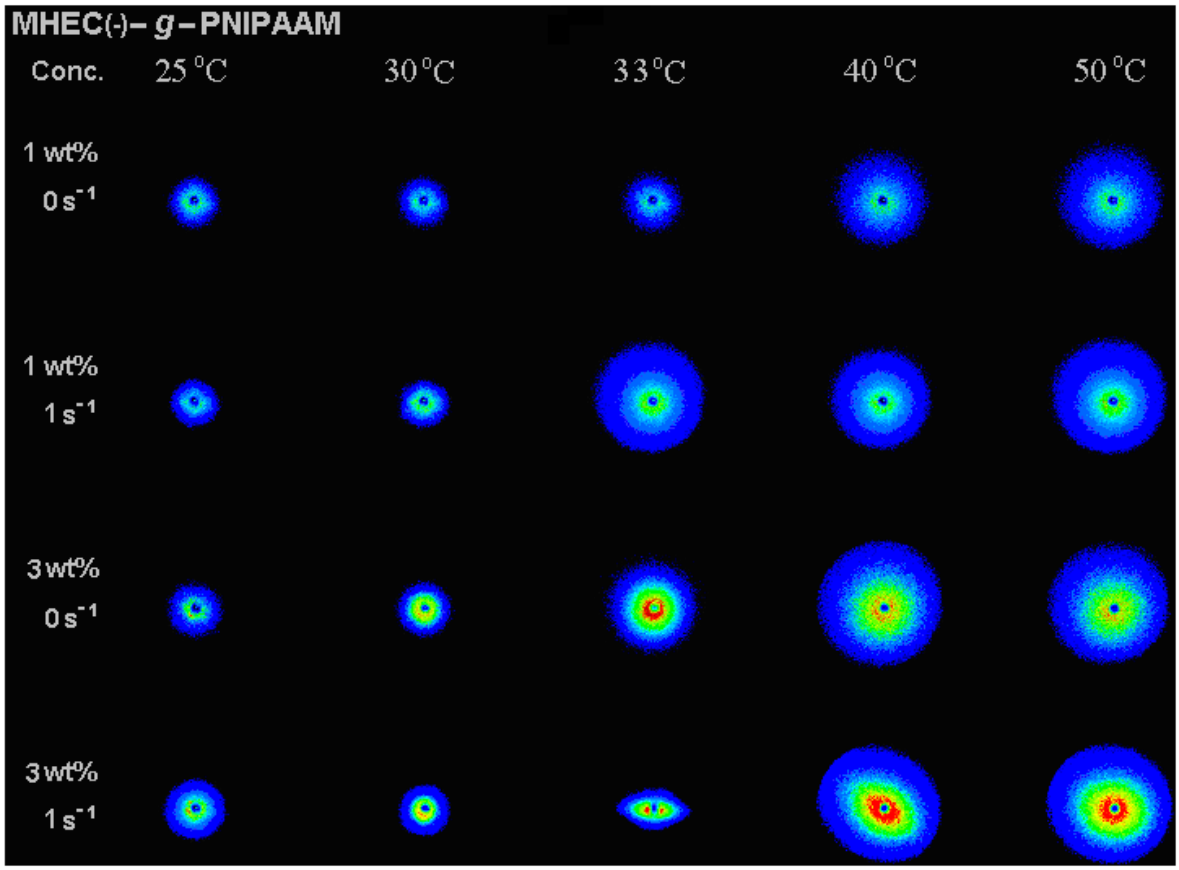

Figure 50. *2D SALS patterns of 1.0 wt% and 3.0 wt% solutions of the charged polymer at different temperatures at the shear rates indicated.*

The average intensity around the whole circle as a function of temperature for different concentrations the shear rates of the neutral polymer has been shown in *Fig. 51*. The same scale has been used for each of the plots. At intermediate temperatures, a peak in the intensity curves is observed. The intensity peak amplitude is higher as the concentration is increased. At higher concentrations, the peak is followed by a sharp decrease in intensity while this effect is more moderate at lower concentrations. This is due to more associations in the system when more polymer chains are added. An explanation for the observed peak is that first, the intensity is raised as association structures are formed in the system. Then it decrease because the network is becoming more heterogeneous with large associated structures, but also with a more open structure (ξ increase) at high temperatures, small compact association regions and large open spaces characterizes the polymer network, giving rise to the decreased intensity values. When increasing the shear rate, the intensity also increase as can be seen in *Fig. 49*. Since the intensity reveals how much the sample scatter, it can clearly be seen that at low temperatures, the intensity is low and slowly increases to the maximum. After the transition state at around 35 ^{o}C, the curves slightly decrease and flatten out. A closer look at

the intensity plots compares with what is observed for the pictures. The pictures do not change much from 25 °C till 30 °C, and because the pictures are similar to each other when T > 40 °C, the curves are also flat. At 35 °C, the picture is similar to the two latest pictures, suggesting that maximum interaction has been reached after the transition state. Anyway, the images and intensity plots just give an overview of how the system behaves. The intensity increase with shear rate has also been revealed from images; they scatter more.

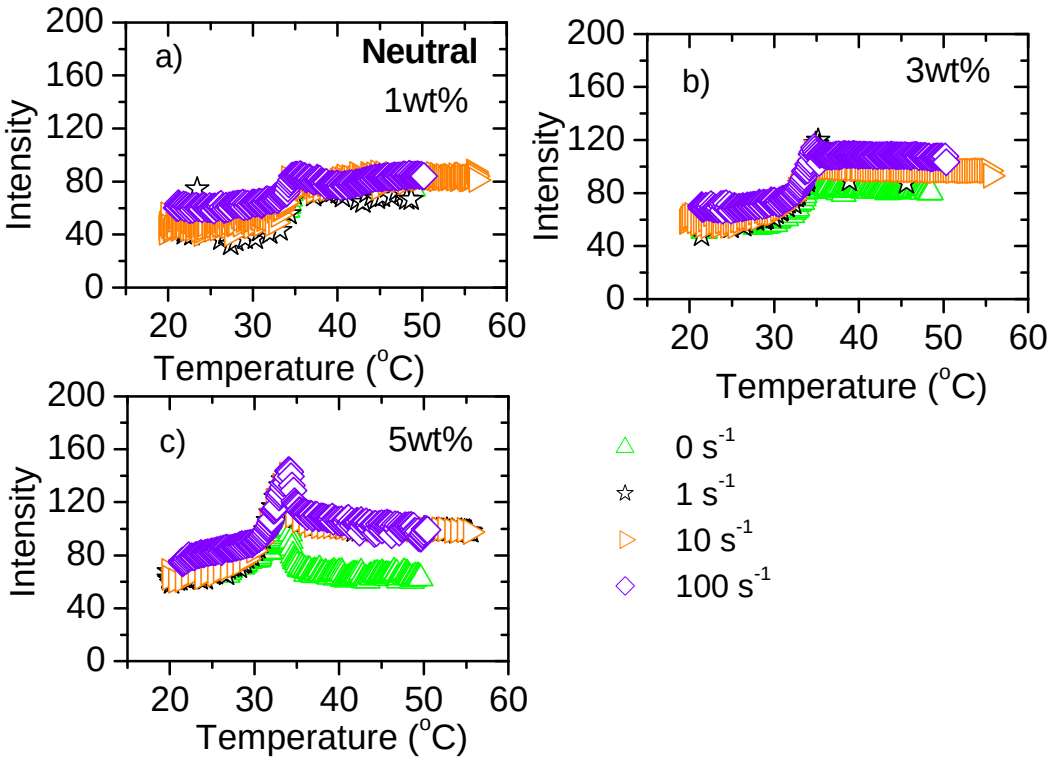

Figure 51. *The average intensity as a function of temperature for the neutral polymer a) 1 wt%, b) 3 wt% and c) 5 wt% at different shear rates.*

A closer look at *Fig. 52*, at a shear rate of 0 s^{-1} for different concentrations of the neutral polymer reveals an interesting trend. At low temperatures the intensity raises with the polymer concentration, as expected. Interestingly, for 5 wt% after the transition state, the intensity decrease markedly, and at high temperatures it is lower than what is observed for 1 wt% and 3 wt%. Since the intensity top of 5 wt% is highest and it decrease most, this indicate that a huge reorganization of the polymer network is taking place around the transition region. The resulting network at high temperatures is probably a heterogeneous network with large open spaces in between the polymers associated clusters giving rise to a decrease in the intensity.

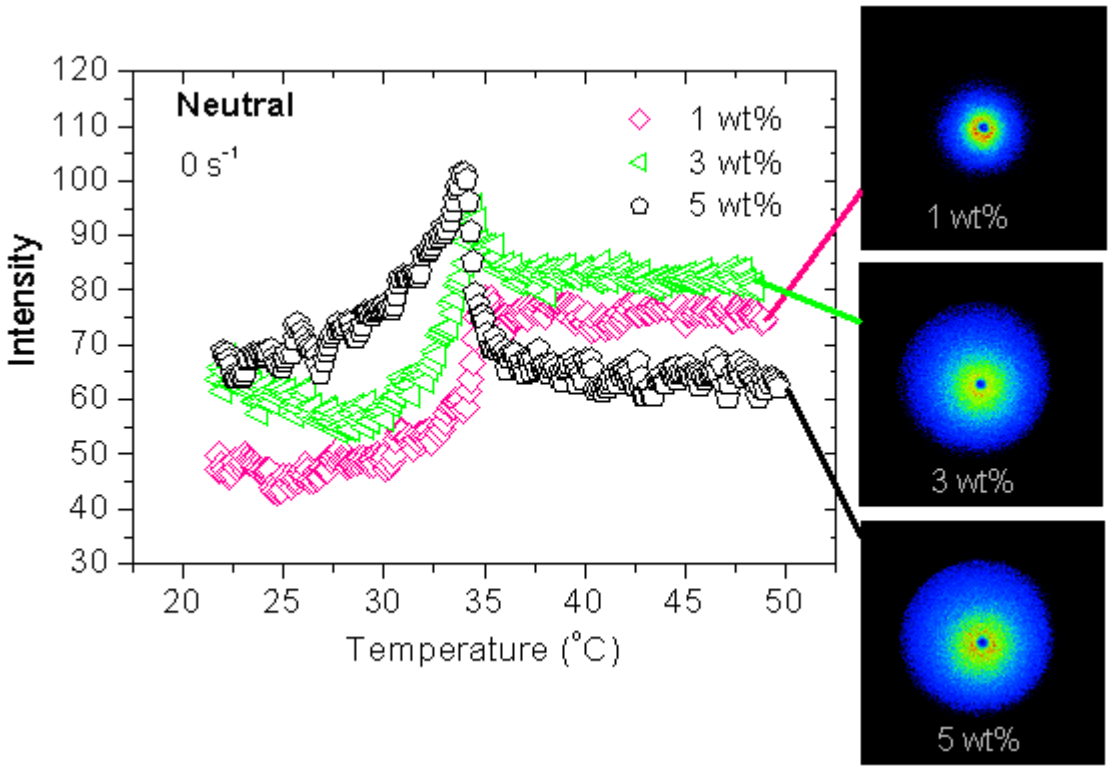

Figure 52. *The average intensity as a function of temperature for zero shear rate with different concentrations.*

Even though the average scattered intensity at low q-values (*Fig. 52*) is lower for 5 wt% than for the other concentrations and the scattering pattern is much larger than for 1 wt%, indicating a higher scattering intensity at larger q-values. Since higher q-values probes smaller structures, this suggest that there are more large structures in the system at low concentrations, while at high concentrations, a large amount of smaller structures are present.

As for the neutral polymer, an intensity peak is evident as intermediate temperatures, although the peak amplitude is even higher for the charged polymer, see *Fig. 53*.

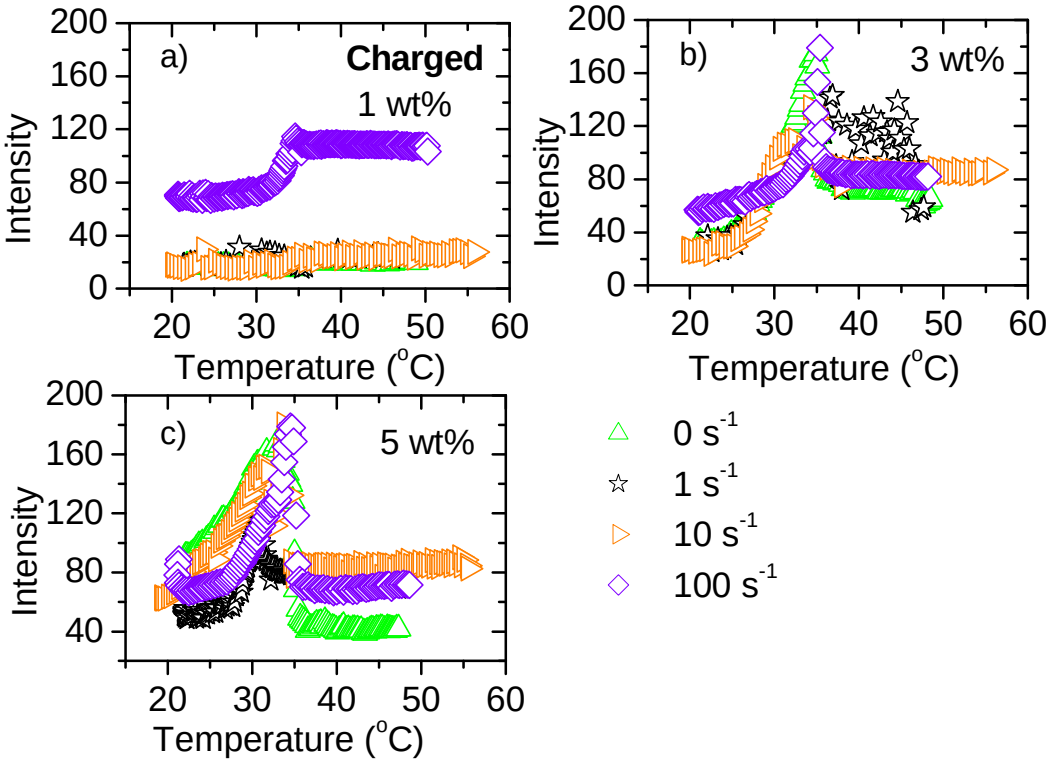

Figure 53. *The average intensity as a function of temperature for the charged polymer a) 1 wt%, b) 3 wt% and c) 5 wt% at different shear rates.*

The average intensity at zero shear rate for different concentrations is compared in *Fig. 54*. As for the neutral polymer, the intensity goes through a peak at intermediate temperatures, followed by an intensity decrease that is greatest for the highest polymer concentration. The compactness will increase even more because of the negative charges. A negative charge causes the chains to repulse each other and make the structure more open, more than it does with the neutral polymer. This causes higher peak amplitudes for the charged polymer compared with the neutral one.

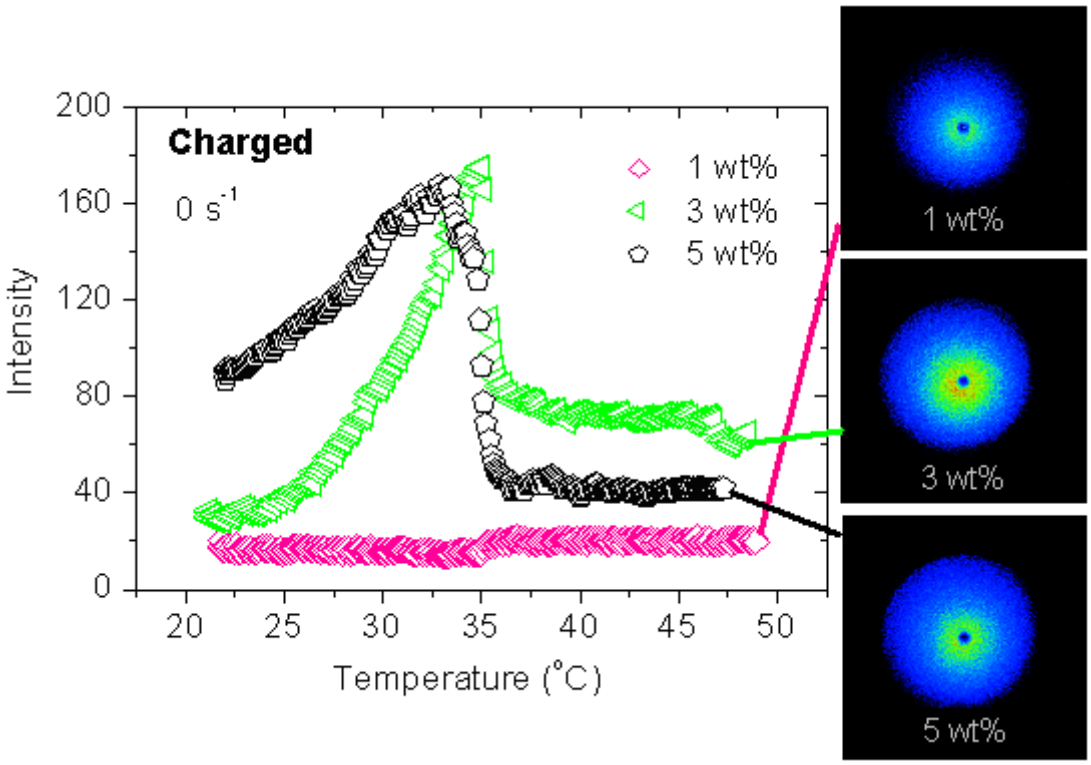

Fig. 54 *The average intensity as a function of temperature for zero shear rate with different concentrations.*

A comparison of the neutral and the charged polymer has been shown in *Fig. 55*. As can be seen, the peak of the charged polymer is sharper, higher in amplitude and also the intensity at high temperatures decrease much more than for the neutral polymer. This effect must be due to the repulsive electricity forces facilitating the formation of a more open structure giving rise to the drop in the intensity values.

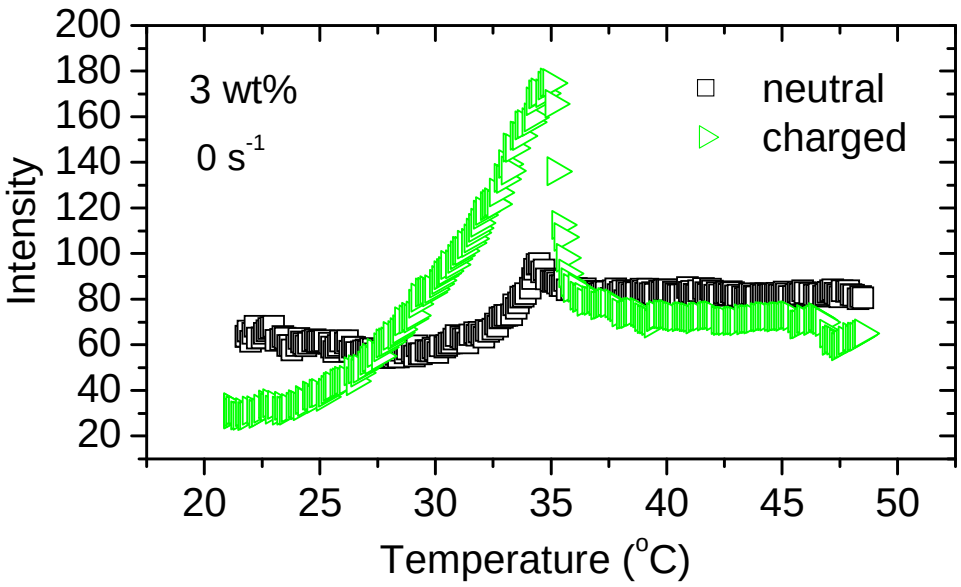

Figure 55. *Comparison between charged and neutral polymers for zero shear rate of the 3 wt% sample.*

4.3.3.1 Rheology

Viscosity values from rheo-SALS are displayed in *Fig. 56 and 57* for the neutral and charged polymers obtained from fixed concentrations and fixed shear rates. In *Fig. 56*, the viscosity is strongly shear-rate dependent. The more shears that is applied, the lower the viscosity. This is because when applying a stress on the solution, the force will disrupt the entanglements and hydrophobic associations. The plot also shows that as the concentration is increased, a sharp transition state is revealed when the temperature is increased. Even at high shear rates, the viscosity increases at elevated temperatures, even though the effect is much diminished compared to low shear rates. Note that for the 1 wt% sample at 1 s^{-1} the viscosity values are very unstable throughout the experiment, suggesting a competition between the building up of associations and the disruption of these association structures in the systems.

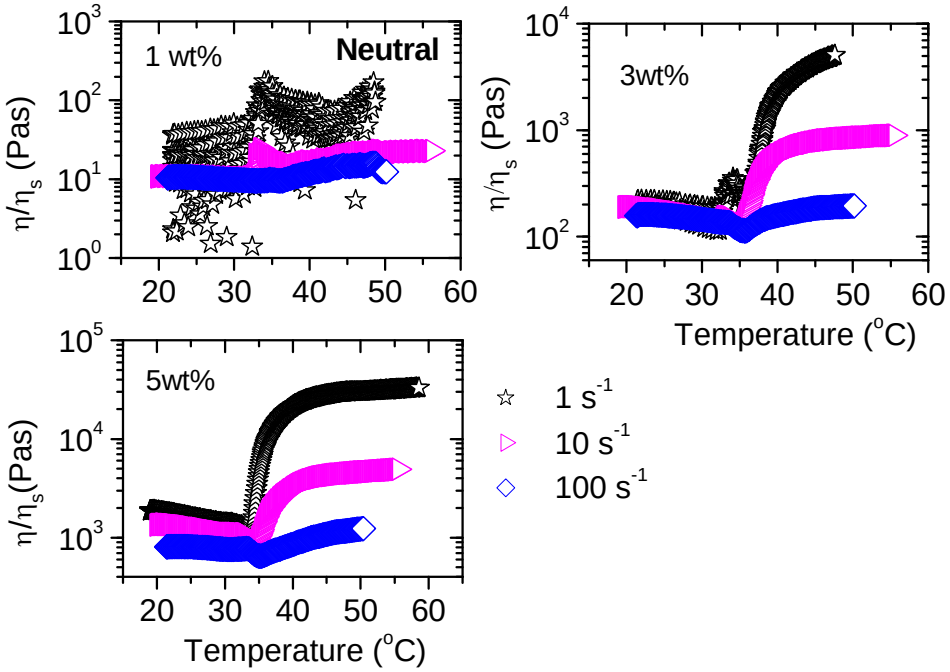

Figure 56. *Plot of viscosity as a function of temperature for different shear rates of the neutral polymer. a) 1 wt%, b) 3 wt% and c) 5 wt%. Heating rate was 0.2 °C/min.*

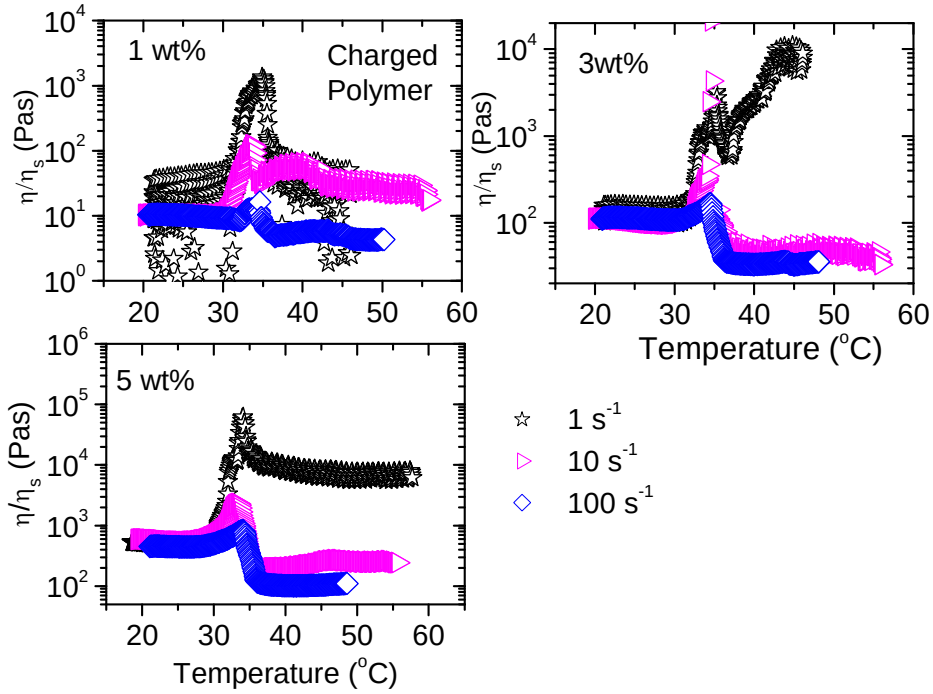

Figure 57. *Plot of the viscosity as a function of temperature for different shear rates of the charged polymer. a) 1 wt%, b) 3 wt% and c) 5 wt%. Heating rate was 0.2 C°/min.*

In *Fig 57* the reduced viscosity for different concentrations of the charged polymer is displayed as a function of temperature. Before LCST, the viscosity is fairly constant. At LCST, a sharp up-turn peak followed by a fast viscosity decrease is clearly seen with increasing temperature. Thereafter, the curves flatted out again, and the values for the highest shear rates at high temperatures are even lower than what was observed at 25 ^{o}C. This is totally opposite from what was observed for the neutral polymer when applying a shear, especially for 3 and 5 wt%. While the aggregation causes the neutral polymer to build up an interconnected network at high temperatures, the charged polymer seem to lose its connectivity when the sample is heated leading to the formation of a fragmented network. This effect is evident even at low shear rates, and as expected higher shear rates amplify the break-down of the network structure. An explanation for the opposite behaviour of the charged polymer is the electrostatic repulsion forces, preventing the building up of an interconnected network. When increasing the shear rate, the peaks reduce and so do the viscosity after the transition state. Again, this behaviour occurs because of the repulsive electrostatic forces and also because of the higher shear breaking up the hydrophobic interaction in the system. The anisotropy observed in *Fig. 50* in the transition region seems to be connected with the disruption of the network and the formation of a fragmented network. During this process, the aggregated structures aligned themselves in the shear direction, and anisotropy is observed.

In *Fig. 58*, different polymer concentrations of the charged and neutral polymer have been plotted at 1 s^{-1}. The small plots are an enlargement of the transition region for 1 wt% and 3 wt%. For the neutral polymer in *Fig. 58 a*, the small plot has a little peak at 34 ^{o}C. Indicating the formation of hydrophobic interaggregate complexes at that temperature. The peaks for the 1 wt% sample break up and then flatten out, suggesting that the connectivity is too low to produce an interconnected network. At 3 wt%, the peak decrease then increase again at higher temperatures. The grafted PNIPAAM groups facilitate the building up of association structures as the temperature increase. The highest concentration (5 wt%) gives the highest upturn in the viscosity since more associations are building up around the transition state because more polymer are present in the sample, giving the network a stronger connectivity. A short glance back to the images of the neutral polymer in *Fig. 49*, illustrates that this explanation is in agreement with the 1 s^{-1} images. More intensive scattering has been observed as the concentration increase and also the scattering patterns increase in size with concentration. In *Fig. 58 b*, the reduced viscosity at a shear rate of 1 s^{-1} has been displayed at

different concentrations of the charged polymer. As is shown, the viscosity increase as the concentration is raised and also the amplitude of the peak is highest for the 5 wt% sample. The same trend has also been observed at other shear rates. This shows that with the highest concentration, the contribution of hydrophobic associations and entanglements is strong at the LCST. After the transition state, the viscosity values are nearly as low as the viscosity at 20 ^{o}C. This is due to loss of in connectivity in the network. The breaking up is facilitated by the repulsive charges in the system, which prevents the chains from coming in contact and forming a network. As seen in *Fig. 50*, all images are clearly red in the middle above LCST when shear is applied, except for the 1 wt% sample which has a blue colour (little association). This means that even though the viscosity is low, the images display high intensity (red colour in the middle), large association structures is present in the sample after breaking up the connectivity. This means that while the connectivity is breaking up, a fragmented network is formed and the systems reorganize its structure, with a high amount of associations in the system.

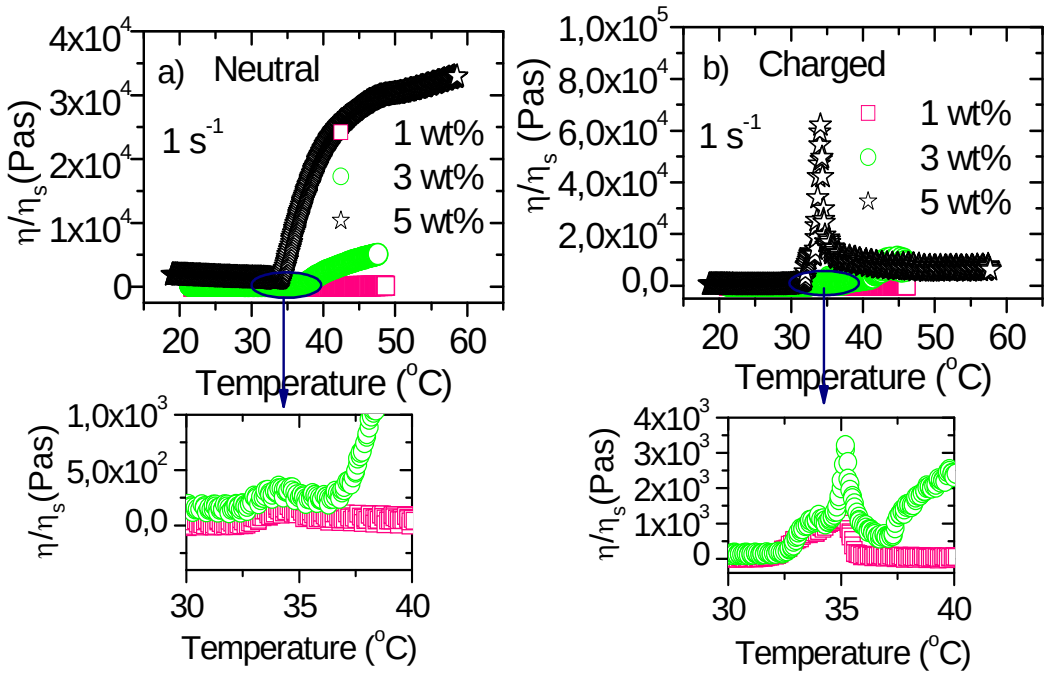

Figure 58. *Plot of viscosity as a function s of temperature for different concentrations of neutral and charged polymer for 1 s^{-1}. a) neutral polymer b) charged polymer.*

A briefly summary of the viscosity as a function of temperature compared with the light scattering pattern is displayed in *Fig. 59.*

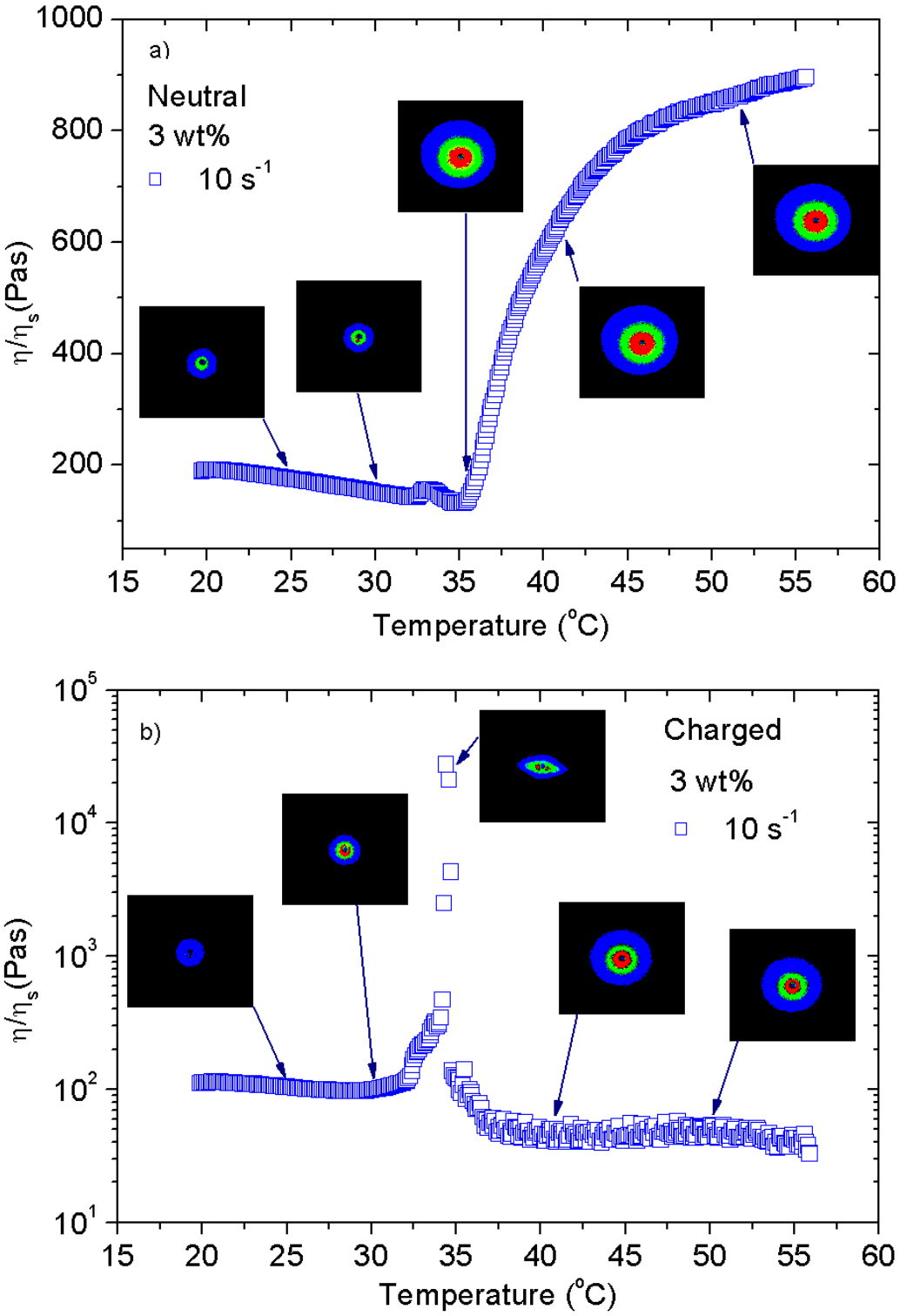

Figure 59. *Evolution of shear viscosity and SALS patterns at a shear rate of 10 s^{-1} and a) is for the neutral and b) for the charged polymer.*

For the neutral polymer (*Fig. 59 a*) the intensity of the scattering pattern increase markedly at the same time as the upturn in the viscosity values. For this system the scattering patterns remain isotropic at all temperatures. Even though the viscosity of the charged system (*Fig. 59 b*) is lower at 50 ^{o}C than at 25 ^{o}C, the sample scatters much more intensely at high temperatures, indicating the formation of large association structures, but the loss of connectivity between them at elevated temperatures. In the transition region, where the viscosity goes through a maximum, the scattering pattering are anisotropic, indicating an alignment of the cluster is around the paint where the connectivity is lost.

In *Fig. 60*, an illustration of how the intensity in two directions behave when the system is randomly organized (isotropic) and when it is organized in the shear direction (anisotropic). The average intensity vs temperature has been calculated as shown in *Fig 20*. Int1 is the intensity in the shear direction and Int2 perpendicular to the shear direction.

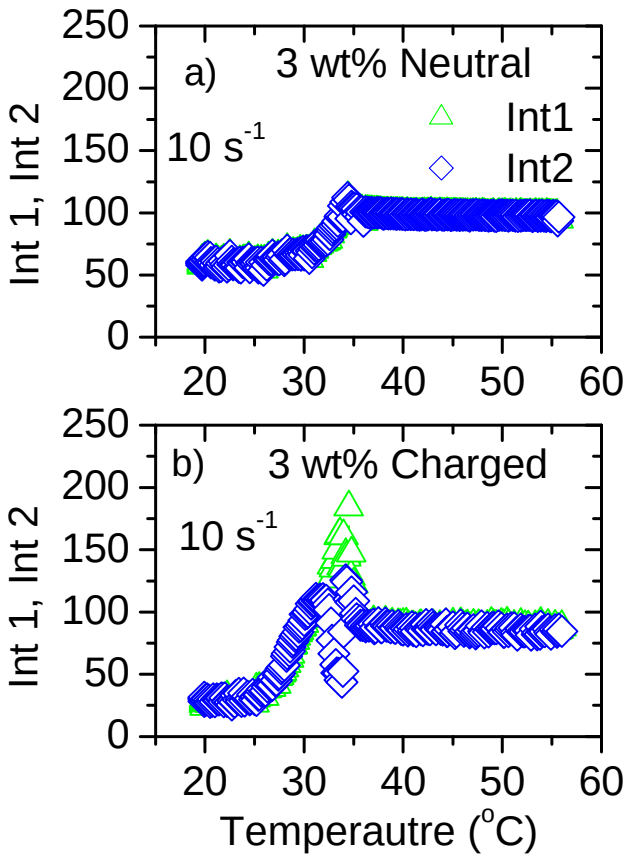

Figure 60. *Int1 and Int2 as a function of temperature for 3 wt% with 10 shear rate. a) is neutral polymer, b) charged polymer.*

For the neutral polymer, the intensity in the shear direction and perpendicular to the shear direction is the same, illustrations that we have isotropic conditions. The two intensities for the charged polymer deviates from each other in the transition region but not at high and low temperatures, indicating that this system is anisotropic, but only during the transition state.

5. Conclusions

In this work, some novel and interesting information about the intramolecular and intermolecular associations in dilute aqueous solutions of neutral and charged hydroxyethycellulose grafted with poly(N-isopropylacrylamide) has been found. With the aid of DLS and turbidity, it was observed that the effect of temperature influenced the polymer clusters to contract above LCST. DLS results at quiescent conditions reveal intrachain contraction and aggregation at LCST and above LCST, contraction is dominating for the neutral polymer. However, the contraction dominates for the charged polymers at LCST while some aggregation appears above LCST. The growth of the hydrodynamic radii increases as the concentrations increase. It has also been shown that the sizes of the unimers are independent on polymer concentration, but above LCST, no detectable amount of unimers is present in the system. It is thought that the unimers merges with the bigger aggregates. Indeed, the turbidity increases as the hydrodynamic radii decrease. This phenomenon is caused by the contraction of the particles causing the ratio between the refractive index of the particle and the refractive index of the solvent (n_p/n_s) to increase.

In order to see the effect of the screening out of the electrostatic interactions, salt (NaCl) was added to the system. The effect of salt is different for the charged polymer compared with the neutral polymer. As expected, the effect of salt addition (poorer thermodynamic conditions) on the neutral polymer enhances the tendency to form large aggregates. Surprisingly for the charged polymer, one would expect that adding salt would screen out the electrostatic repulsions in the system and thereby cause the charged polymers to behave as the neutral polymer. However, the results show that before LCST the charged polymer radii is the same as without salt addition, but at LCST a great upturn in R_h is observed, suggesting the formation of large aggregates.

Rheology results at increasing shear rates show that the polymer chains will come close to each other through the shear forces and the chains will reorganize. At a temperature of 35^{o}C for the neutral polymer, the PNIPAAM side chains will come in contact with each other and gradually large aggregates will be build-up via hydrophobic intramolecular associations. Shear thickening is observed in the low shear region followed by shear thinning at higher shear rates. The commencement and magnitude of the shear thickening is depending on polymer concentration and temperature. For the charged polymer, the same behaviour has

been observed, but shear thickening appear already at 30 ^{o}C. The highest concentration which can be measured for this polymer is 1.0 wt%, because the polymer samples expanded out of the measuring system when the temperature was above 30 ^{o}C. When increasing the temperature, the zero-shear viscosity goes through a maximum for 0.5 and 1.0 wt% for both the charged and the neutral polymers. At higher polymer concentrations, the zero-shear viscosity of neutral polymer increases and then flattens out at elevated temperatures.

The results from rheo-SALS experiments disclosed that with a temperature gradient at a fixed shear rates, the viscosity behave differently for the neutral and charged polymers. For the neutral polymer, above LCST, gradually association structures is building up as the temperature increase, especially at concentrations above 3 wt%, one can clearly see the upturn ramp. For the charged polymer, a peak in the viscosity curve appears around LCST, followed by a decreased viscosity that flattens out at high temperatures. When comparing the viscosity behaviour with the light scattering images, we observe that the neutral polymer form an associated interconnected network at high temperatures while the charged polymer form a fragmented structure where the association structures have lost their connectivity. The SALS images also show that the charged polymer shows an anisotropic behaviour at LCST in the presence of shear forces while neutral polymer gave isotropic images throughout all the considered temperatures, shear rates and concentrations.

5.1 Directions for further Works

This work shows that by changing the temperature, the hydrodynamic radii have been reduced to a size around 75 nm to 250 nm (above LCST) which is favourable for the use in drug delivery systems. When using the rheology with concentration above 1 wt%, the effect of the negative charged polymer gave an interesting behaviour. It expanded and when using rheo-SALS, the viscosity decrease above LCST which could be interesting to mix with another polymer (for instance an opposite charged one). This technique will give lower viscosity then what it could be when for instance using neutral polymer. It will also be interesting to study the adsorption and detection on nanoparticles, because the effect of a thermosensitive polymer can affect the adsorption rate when increasing the temperature. Another application such as in enhanced oil recovery technique, stable and low radii sizes above LCST could be interesting too.

6. Appendix

Rheo-SALS Scatter patterns

	25 °C	30 °C	35 °C	40 °C	50 °C
MHEC-gP 1wt% 0 s^{-1}	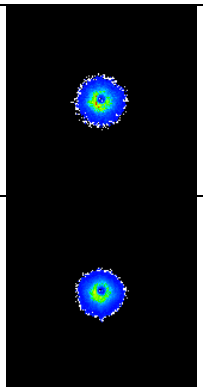	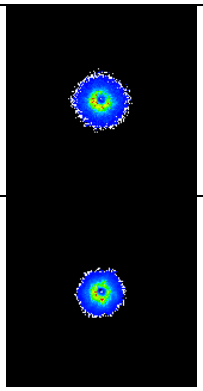	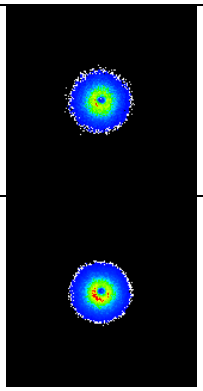	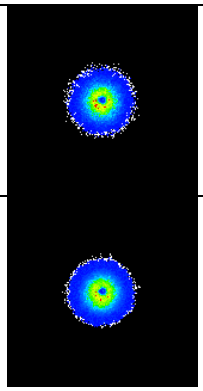	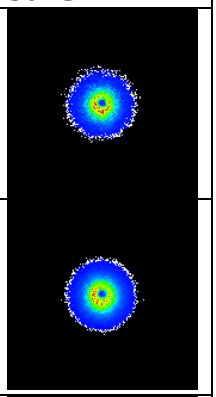
MHEC-gP 1wt% 1 s^{-1}					
MHEC-gP 1wt% 10 s^{-1}					
MHEC-gP 1wt% 100 s^{-1}					

	25 °C	30 °C	35 °C	40 °C	50 °C
MHEC-gP 3wt% 0 s^{-1}	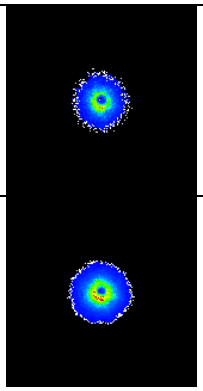	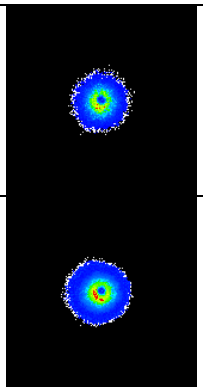	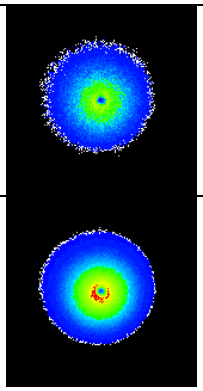	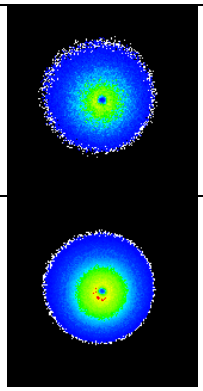	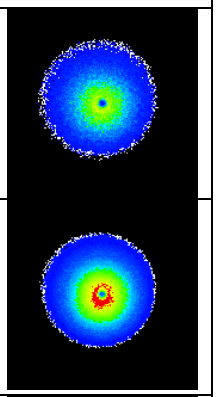
MHEC-gP 3wt% 1 s^{-1}					
MHEC-gP 3wt% 10 s^{-1}					

MHEC-gP 3wt% 100 s^{-1}	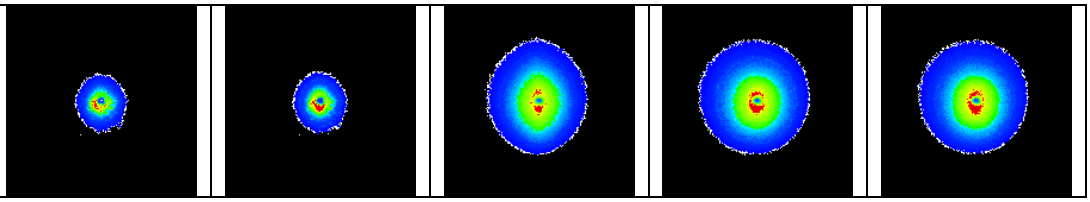

	25°C	30 °C	35 °C	40 °C	50 °C
MHEC-gP 5wt% 0 s^{-1}	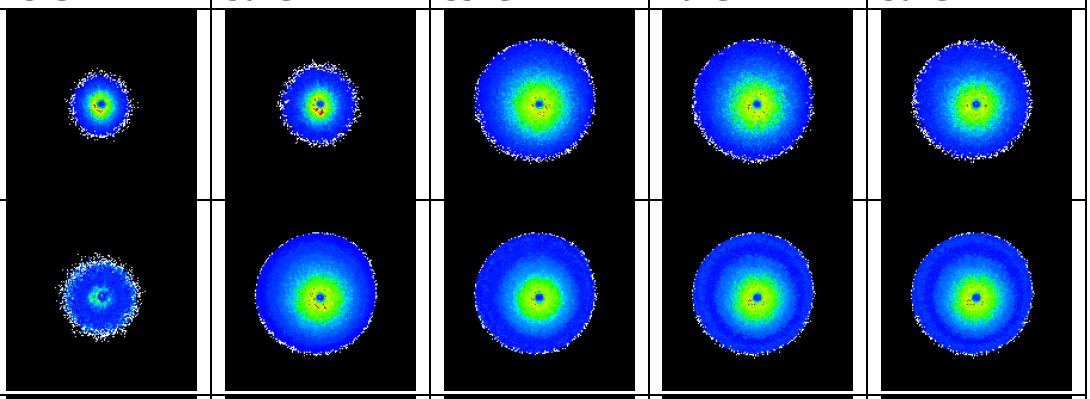				
MHEC-gP 5wt% 1 s^{-1}					
MHEC-gP 5wt% 10 s^{-1}	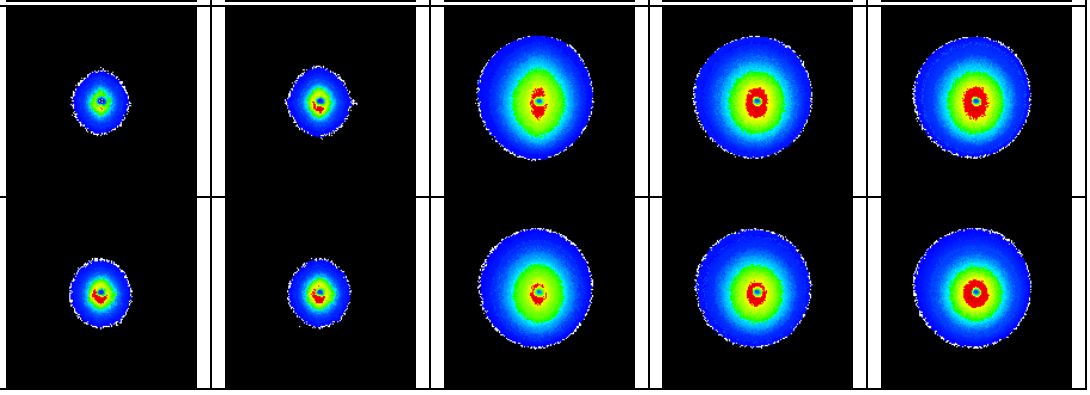				
MHEC-gP 5wt% 100 s^{-1}					

	25 °C	30 °C	35 °C	40 °C	50 °C
Min-MHEC-gP 1wt% 0 s^{-1}	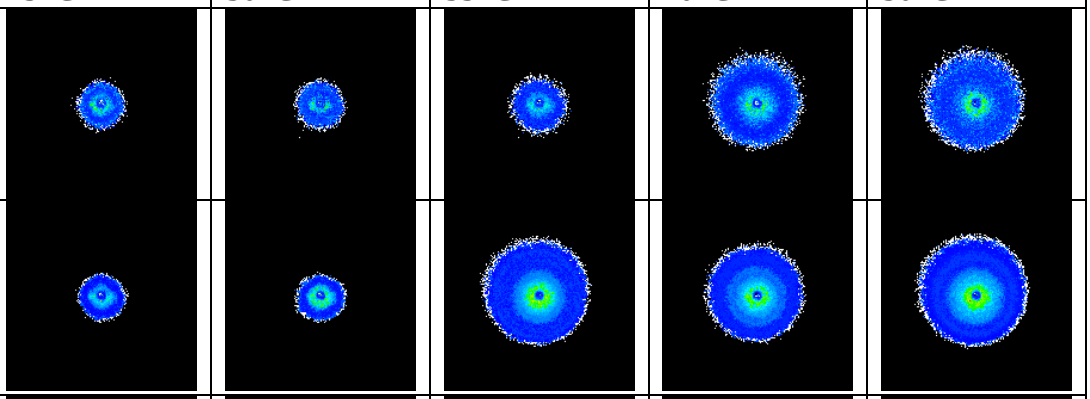				
Min-MHEC-gP 1wt% 1 s^{-1}					
Min-MHEC-gP 1wt% 10 s^{-1}					

Min-MHEC-gP 1wt% 100 s^{-1}	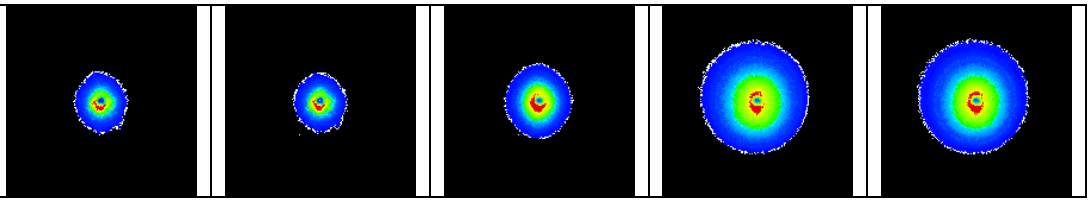

	25 °C	30 °C	33 °C	40 °C	50 °C
Min-MHEC-gP 3wt% 0 s^{-1}	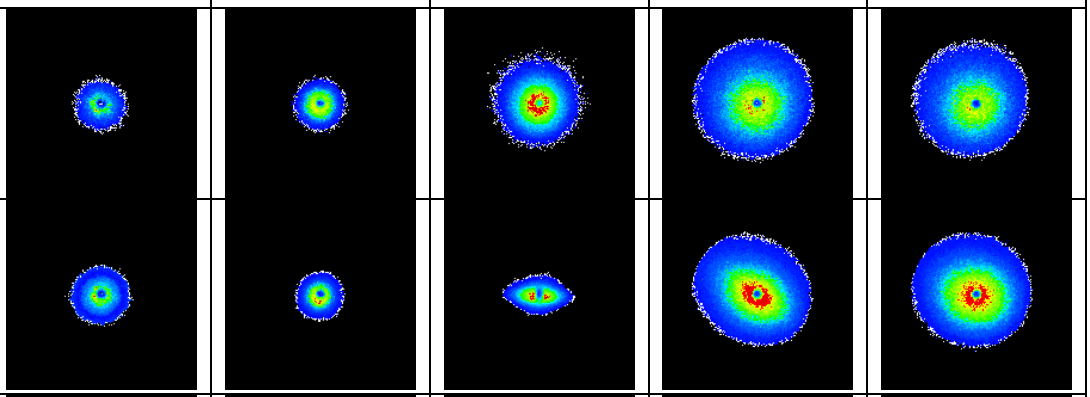				
Min-MHEC-gP 3wt% 1 s^{-1}					
Min-MHEC-gP 3wt% 10 s^{-1}	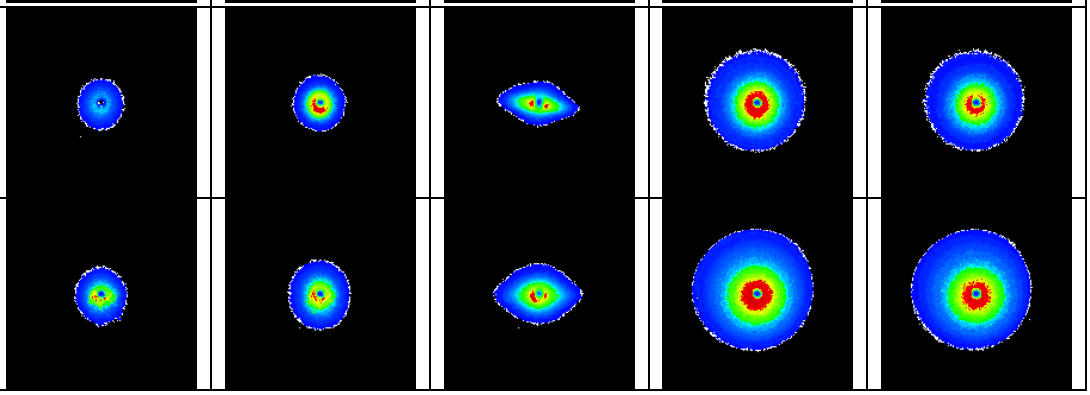				
Min-MHEC-gP 3wt% 100 s^{-1}					

	25 °C	30 °C	33 °C	40 °C	50 °C
Min-MHEC-gP 5wt% 0 s^{-1}	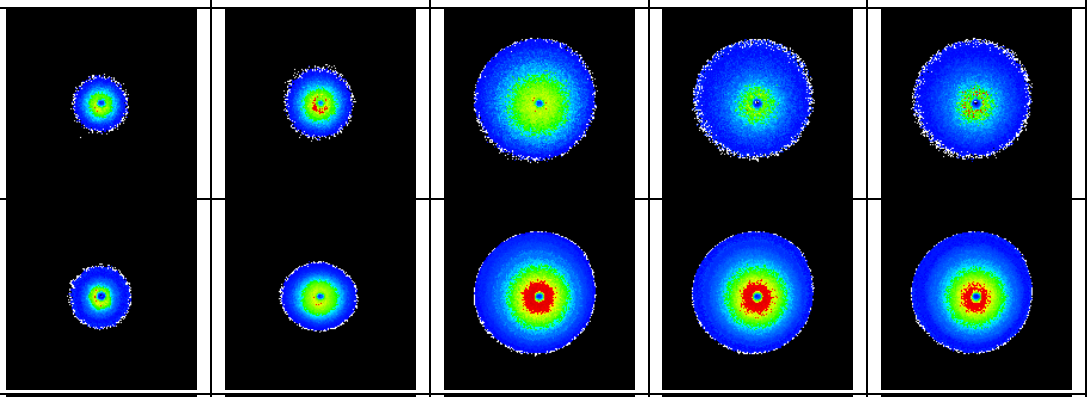				
Min-MHEC-gP 5wt% 1 s^{-1}					
Min-MHEC-gP 5wt% 10 s^{-1}	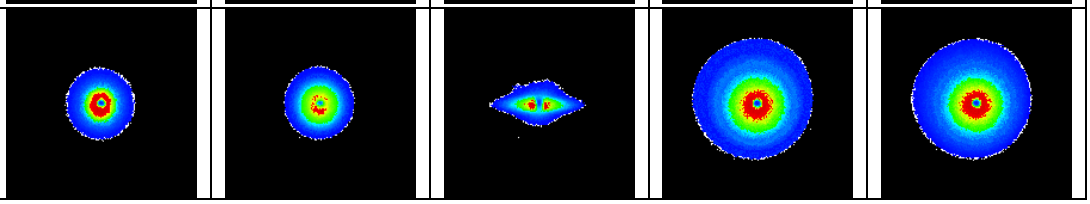				

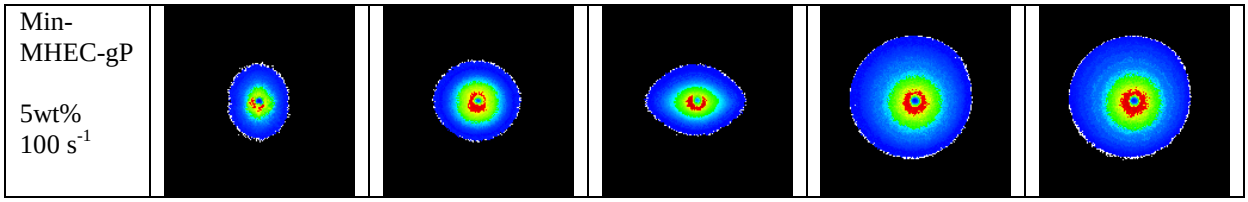

7. References

1) I. Dimitrov, B. Trzebicka, A. H. E. Mueller, A. Dworak, C. B. Tsvetanov, *Progress in Polymer Science*, 32, *1275*,(2007).

2) E. I. Tiktopulo, V. N. Uversky, V. B. Lushchik, S. I.Klenin, V. E. Bychkova, O. B. Ptitsyn, *Macromolecules*, 28, *7519*, (1995).

3) L. D.Taylor, L. D. Cerankowski, *J. Polym Sci Polym Chem Ed*, 13, *2551*,(1975).

4) S. Fujishige, K. Kubota, I. Ando, *J Phys Chem*, 93, *3311*, (1989).

5) K. Nagapudi, W. T. Brinkman, J. E.Leisen, L. Huang, R. A. McMillan, R. P. Apkarian, V. P.Conticello, E. L.Chaikof, *Macromolecules*, 35,*1730*, (2002).

6) A. Nagarsekar, J. Crissman, M. Crissman, F. Ferrari, J. Cappello, H. Ghandehari, *J Biomed Mater Res*, 62, *195*, (2002).

7) L. Ayres, K. Koch, P. H. H. M. Adams, H. Van, C. M. Jan, *Macromolecules*, 38, *1699*, (2005).

8) H. G. Schild, *Prog Polym Sci*, 17, *163*, (1992).

9) R. Pelton, *Adv Colloid Interface Sci*, 85, *1*, (2000).

10) E. S. Gil, S. M. Hudson, *Prog Polym Sci*, 29, *1173*, (2004).

11) A. Maleki, A.-L. Kjøniksen, B. Nyström, *J. Phys. Chem. B*, 109, *12329*, (2005).

12) Z. Liu, A. Maleki, K. Zhu, A.-L. Kjøniksen, B. Nyström, *Journal of Physical Chemistry B*, 112, *1082*, (2008).

13) N. Al-Manasir, A.-L. Kjøniksen, B. Nyström, *Journal of Applied Polymer Science*, 113(3), *1916*, (2009).

14) C. Vasile, C. Marinescu, R. Vornicu, G. Staikos, *Journal of Applied Polymer Science*, 87, *1383*, (2003).

15) S. B. Lee, D. I. Ha, S. K. Cho, S. J. Kim, Y. M. Lee, *Journal of Applied Polymer Science*, 92, *2612*, (2004).

16) R. Motokawa, K. Morishita, S. Koizumi, T. Nakahira, M. Annaka, *Macromolecules*, 38, *5748*, (2005).

17) M. D. C. Topp, P. J. Dijkstra, H. Talsma, J. Feijen, *Macromolecules* 30, *8518,* (1997).

18) K. Zhu, H. Jin, A.-L. Kjøniksen, B. Nyström, *Copolymer,Journal of Physical Chemistry B*, 111, *10862,* (2007).

19) K. Zhu, R. Pamies, A.-L. Kjøniksen, B. Nyström, *Langmuir*, 24, *14227*, (2008).

20) R. R. Schmidt, R. Pamies, A.-L. Kjøniksen, K. Zhu, J. G. H. Cifre, B. Nyström, J. G. de la Torre, *Journal of Physical Chemistry B*, 114, *8887*, (2010).

21) F. Meeussen, E. Nies, H. Berghmans, S. Verbrugghe, E. Goethals, F. Du Prez, *Polymer*, 41, *8597*,(2000).

22) H. Vihola, A. Laukkanen, L. Valtola, H. Tenhu, J. Hirvonen, *Biomaterials*, 26, *3055*, (2005).

23) H. Uyama, S. Kobayashi, *Chem Lett*, 1643, (1992).

24) A.-L. Kjøniksen, A. Laukkanen, C. Galant, K. D. Knudsen, H. Tenhu, B. Nystöm, *Macromolecules*, 38, *948*, (2005).

25) K. Kamide, *Cellulose and Cellulose Derivates Molecular Characterization and its Applications, 1st. ed.*, pp. 1-3, (2005), ISBN: 0-444-82254-2.

26) J. Wiley and Sons, *Encyclopedia of polymer science and engineering 2st ed.*, pp. 90-119, (1985), ISBN: 0-471-88789-7 (v. 3).

27) D.Klemm, B. Phillipp, T. Heinze, U. Heinze, W. Wagenknecht, *Comprehensive Cellulose Chemistry*, pp. 40-41, (1998), ISBN: 3-527-29413-9, (v. 1).

28) D. Klemn, H-P. Fink, et al., *Angew. Chem. Int. Ed.*, 44, *3358*, (2005).

29) J. Wiley and Sons, *Encyclopedia of polymer science and engineering 2st ed.*, pp. 124-125, (1985), ISBN: 0-471-88789-7, (v. 3)

30) A. M. Hillery, A. W. Lloyd, J. Swarbrick, *Drug delivery and targeting*, pp. 2,3,136-138, (2001), ISBN: 0-415-27197-5.

31) K. S. Deffeyes, P. Hubbert's, *The Impending World Oil Shortage*, Princeton University Press (2001).

32) *Scarcity and Growth Considering Oil and Energy: An Alternative Neo-Classical View, Reynold, D. B.*

33) K. K. Mohanty, *AlChE Journal*, 49, *2454*, (2003).

34) R. L. Hirsch, R. Bezdek, R. Wendling, *Peaking of world oil technology laboratory, U.S. Depertment of energy* (2005).

35) L. W. Lake, N. J. Englewood Cliffs, *Enhanced oil recovert*, Prentice Hall (1989).

36) R. K. Prud'homme, J. T. Uhl, J. P. Poinsatte, F. Halverson, SPEJ, *Society of Petroleum Engineers Journal* , 23, *804*, (1983).

37) T. A.Maxcy, G. P. Willhite, D. W. Green, K. Bowman-James, *Journal of Petroleum Science & Engineering*, 19, *253*, (1998) .

38) S. M. Vargas-Vasquez, L. B. Romero-Zeron, *Petroleum Science and Technology* , 26, *481*, (2008).

39) R. S.Yalow, S. A.Berson, *Journal of Clinical Investigation*, 39, *1157*, (1960).

40) L. G. Mendoza, P. McQuary, A. Mongan, R. Gangadharan, S. Brignac, M. Eggers, *BioTechniques*, 27, *778*, (1999).

41) M. E. Goldberg, L. Djavadi-Ohaniance, *Current Opinion in Immunology* , 5, *278*, (1993).

42) G. MacBeath, S. L.Schreiber, *Science*, 289, *1760*, (2000).

43) D. J.Stephens, V. J.Allan, *Science*, 300, *82*, (2003).

44) A. N. Shipway, E. Katz, I. Willner, *ChemPhysChem* , 1, *18*, (2000).

45) X. Chen, H. J. Schluesener, *Toxicology Letters*,176, *1*, (2008).

46) Niemeyer, Christof M., *Angewandte Chemie, International Edition* , 40, *4128*, (2001).

47) W. Shenton, S. A. Davis, S. Mann, *Advanced Materials*, 11, *449*, (1999).

48) A. A. Zofchak, J. Carson, J. Jorden, US patent application US2007/020272 A1

49) N. Al-Manasir, *Preparation and characterization of cross-linked polymeric nanoparticles for enhances oil recovery applications, Master thesis, Dep. Chem. UiO*, (2009).

50) N. Al-Manasir, A.-L. Kjøniksen, B. Nyström, *Journal of AppliedPolymer Science*, 113, *1916*, (2009).

51) N. Beheshti, G. T. M. Nguyen, A.-L. Kjøniksen, K. D. Knudsen, and B. Nyström, *Colloid surf. A: Physicochem Eng Asp*, 279. *40*, (2006).

52) S. Wan, M. Jiang, G. Zhang, *Macromolecules*, 40, *5552*, (2007).

53) A. S. Sarac. *Prog Polym Sci*, 24, *1149*, (1999).

54) R. Motokawa, K. Morishita, S. Koizumi, T. Nakahira, M. Annaka, *Macromolecules*, 38, *5748*, (2005)

55) S. M. Derkaoui, T. Avramoglou, C. Barbaud, D. Letourneur, *Biomacromolecules*, 9, *3033*, (2008)

56) T . Miyajima, T . Kitsuki, K . Kita, H . Kamitani, K . Yamaki, *US Patent* 5,891,450, April 6, (1999).

57) M. R. Antonio, *Polymer*, 39, *3115*, (1998).

58) N. Beheshti, K. Zhu, A.-L. Kjøniksen, B. Nyström, *Colloids and Surfaces A: Physicochem Eng Aspects*, 328, *79*, (2008).

59) M. Tsianou, A.-L. Kjøniksen, K. Thuresson, B. Nyström, *Macromolecules*, 32, *2974*, (1999).

60) N. Al-Manasir, K. Zhu, A.-L. Kjøniksen, K. D. Knudsen, G. Karlsson, B. Nyström, *J. Phys. Chem. B.*,113, *11115*, (2009).

61) A.-L. Kjøniksen, K. Zhu, G. Karlsson, B. Nyström, *Colloids and Surfaces A*, 333, *32*, (2009).